TECHNICAL REPORT H-74-6

LAKE ERIE INTERNATIONAL JETPORT MODEL FEASIBILITY INVESTIGATION

Report 17-4

NUMERICAL MODEL FEASIBILITY STUDY

by

Donald C. Raney, Donald L. Durham, H. Lee Butler

Hydraulics Laboratory
U. S. Army Engineer Waterways Experiment Station
P. O. Box 631, Vicksburg, Miss. 39180

April 1977

Report 4 of a Series

Prepared for Lake Erie Regional Transportation Authority
Cleveland, Ohio 44113

Under Task 17 of LERTA Second-Phase
Airport Feasibility Study

DEPARTMENT OF THE ARMY
WATERWAYS EXPERIMENT STATION, CORPS OF ENGINEERS
P. O. BOX 631
VICKSBURG, MISSISSIPPI 39180

IN REPLY REFER TO: WESAR

27 April 1977

Errata Sheet

No. 1

LAKE ERIE INTERNATIONAL JETPORT MODEL FEASIBILITY INVESTIGATION

NUMERICAL MODEL FEASIBILITY STUDY

Technical Report H-74-6

Report 17-4

April 1977

On the inside of the cover, in line 4 of the disclaimer, "Case Western Reserve University" should read "U. S. Army Engineer Waterways Experiment Station."

Unclassified

SECURITY CLASSIFICATION OF THIS PAGE *(When Data Entered)*

REPORT DOCUMENTATION PAGE

READ INSTRUCTIONS BEFORE COMPLETING FORM

1. REPORT NUMBER Report 17-4	2. GOVT ACCESSION NO.
3. RECIPIENT'S CATALOG NUMBER	
4. TITLE *(and Subtitle)* LAKE ERIE INTERNATIONAL JETPORT MODEL FEASIBILITY INVESTIGATION; NUMERICAL MODEL FEASIBILITY STUDY	5. TYPE OF REPORT & PERIOD COVERED Report 4 of a series
	6. PERFORMING ORG. REPORT NUMBER Technical Report H-74-6
7. AUTHOR(s) Donald C. Raney Donald L. Durham H. Lee Butler	8. CONTRACT OR GRANT NUMBER(s)
9. PERFORMING ORGANIZATION NAME AND ADDRESS U. S. Army Engineer Waterways Experiment Station Hydraulics Laboratory P. O. Box 631, Vicksburg, Miss. 39180	10. PROGRAM ELEMENT, PROJECT, TASK AREA & WORK UNIT NUMBERS
11. CONTROLLING OFFICE NAME AND ADDRESS Lake Erie Regional Transportation Authority 33 Public Square, Suite 1015 Cleveland, Ohio 44113	12. REPORT DATE April 1977
	13. NUMBER OF PAGES 151
14. MONITORING AGENCY NAME & ADDRESS*(if different from Controlling Office)*	15. SECURITY CLASS. *(of this report)* Unclassified
	15a. DECLASSIFICATION/DOWNGRADING SCHEDULE

16. DISTRIBUTION STATEMENT *(of this Report)*

Approved for public release; distribution unlimited.

17. DISTRIBUTION STATEMENT *(of the abstract entered in Block 20, if different from Report)*

18. SUPPLEMENTARY NOTES

19. KEY WORDS *(Continue on reverse side if necessary and identify by block number)*

Airports
Hydrodynamics
Lake Erie
Mathematical models

20. ABSTRACT *(Continue on reverse side if necessary and identify by block number)*

An integral part of the feasibility assessment of a proposed offshore jetport site near Cleveland, Ohio, is the investigation of the hydrodynamics of Lake Erie to aid in determining the effects of the structure on such phenomena as seiching, storm surge, and lake circulation. To assist in determining these effects, the feasibility of using numerical modeling techniques was investigated. Numerical models that appeared capable of predicting the extent and magnitude of hydrodynamic changes produced by the proposed jetport were reviewed. Based upon

(Continued)

DD FORM 1 JAN 73 1473 EDITION OF 1 NOV 65 IS OBSOLETE

Unclassified

SECURITY CLASSIFICATION OF THIS PAGE *(When Data Entered)*

20. ABSTRACT (Continued).

this investigation, a determination was made of the feasibility of applying numerical models to the problems of seiching, storm surge, and lake circulation in Lake Erie. The numerical model feasibility study was restricted to the consideration of existing state-of-the-art models. No extensive model development was undertaken in this feasibility study; however, areas where additional numerical development is required were identified. The theoretical limitations, verification, resolution capabilities, and accuracy of the model as well as the cost of application of the model were considered.

THE CONTENTS OF THIS REPORT ARE NOT TO BE USED FOR ADVERTISING, PUBLICATION, OR PROMOTIONAL PURPOSES. CITATION OF TRADE NAMES DOES NOT CONSTITUTE AN OFFICIAL ENDORSEMENT OR APPROVAL OF THE USE OF SUCH COMMERCIAL PRODUCTS.

PREFACE

This study was sponsored by the Lake Erie Regional Transportation Authority (LERTA), Cleveland, Ohio, as a part of the model feasibility investigation being conducted at the U. S. Army Engineer Waterways Experiment Station (WES). The WES investigation, Task 17 of the LERTA investigation, is a portion of the second-phase airport feasibility study undertaken by LERTA to evaluate proposed airport sites, one of which is in Lake Erie near Cleveland. The numerical model feasibility study is associated with the selection and preliminary design of the necessary numerical models for studying various phenomena considered pertinent to an offshore jetport site.

This report was prepared by Dr. Donald C. Raney, Dr. Donald L. Durham, and Mr. H. Lee Butler of the Wave Dynamics Division (WDD), Hydraulics Laboratory (HL), WES, under the general supervision of Dr. R. W. Whalin, Chief, WDD, and Mr. H. B. Simmons, Chief, HL. Dr. Raney is a Professor in the Aerospace and Mechanical Engineering Department, University of Alabama, and was assigned to WES under terms of the Intergovernmental Personnel Exchange Act during conduct of this study and preparation of the report.

The Directors of WES during the conduct of this investigation and the preparation and publication of this report were COL G. H. Hilt, CE, and COL J. L. Cannon, CE. Technical Director was Mr. F. R. Brown.

CONTENTS

CONVERSION FACTORS, METRIC (SI) TO U. S. CUSTOMARY AND
U. S. CUSTOMARY TO METRIC (SI) UNITS OF MEASUREMENT

Units of measurement used in this report can be converted as follows:

Multiply	By	To Obtain
Metric (SI) to U. S. Customary		
metres	3.280839	feet
kilometres	0.6213711	miles (U. S. statute)
metres per second	3.280839	feet per second
square centimetres per second	0.1550	square inches per second
Kelvins or Celsius degrees	9/5	Fahrenheit degrees*
U. S. Customary to Metric (SI)		
inches	2.54	centimetres
feet	0.3048	metres
miles (U. S. statute)	1.609344	kilometres
square feet	0.09290304	square metres
cubic feet	0.02831685	cubic metres
pounds (force) per square inch absolute	6894.757	pascals
feet per second	0.3048	metres per second
miles per hour (U. S. statute)	1.609344	kilometres per hour
degrees (angle)	0.01745329	radians
degrees Fahrenheit	5/9	Celsius degrees or kelvins**

* To obtain Fahrenheit (F) temperature readings from Celsius (C) readings, use the following formula: $F = 9/5(C) + 32$. To obtain Fahrenheit readings from Kelvins (K), use: $F = 9/5(K - 273.15) + 32$.

** To obtain Celsius (C) temperature readings from Fahrenheit (F) readings, use the following formula: $C = (5/9)(F - 32)$. To obtain Kelvin (K) readings, use: $K = (5/9)(F - 32) + 273.15$.

LAKE ERIE INTERNATIONAL JETPORT
MODEL FEASIBILITY INVESTIGATION

NUMERICAL MODEL FEASIBILITY AND SEICHE STUDY

PART I: INTRODUCTION

Background

1. The Lake Erie Regional Transportation Authority (LERTA) is conducting a feasibility and site selection study for a major hub airport in the Cleveland Service Area. One of the sites being evaluated is offshore in Lake Erie near Cleveland, Ohio. As a part of the feasibility analysis of an offshore site, the U. S. Army Engineer Waterways Experiment Station (WES) is conducting a model feasibility investigation. Objectives of the WES study[1] are:

a. Compilation of available data on wave activity (wind waves, seiches, and tides) and mass circulation in Lake Erie with particular emphasis on effects of these phenomena in and around Cleveland.

b. Selection and preliminary design of necessary hydraulic models for studying various phenomena considered pertinent to the jetport site.

c. Evaluation and preliminary application of analytical and/or numerical models of seiching and mass circulation in a lake to the jetport study.

The five study tasks in the WES investigation are:

a. Synthesis of available data primarily concerning wave climate, mass circulation, general shoreline characteristics, and general features of erosional problems.

b. Lake seiche analysis.

c. Wave diffraction and refraction analyses including qualitative effects on shore erosion.

d. Analytical mass circulation analysis.

e. Preliminary design of necessary hydraulic models.

This report is the fourth report in the series published under the general title "Lake Erie International Jetport Model Feasibility

Investigation." The results of study task b and a portion of study task d are presented. Under study task d only the initial selection of the numerical models to be applied is presented in this report. Detailed results from application of these numerical models will be presented in later reports.

Problem Definition

2. An integral part of the feasibility assessment of a proposed offshore jetport site near Cleveland Harbor is the investigation of the hydrodynamics of Lake Erie to aid in determining effects of the structure on such phenomena as seiching, storm surge, and lake circulation. To assist in determining these effects, the feasibility of using numerical modeling techniques was investigated. Numerical models that appeared capable of predicting the extent and magnitude of hydrodynamic changes produced by the proposed jetport were reviewed. Based upon this investigation of existing state-of-the-art numerical models, an assessment of the feasibility of applying numerical models to the problems of seiching, storm surge, and wind-driven circulation in Lake Erie is made. Any models selected for this purpose must provide sufficient resolution to allow the hydrodynamic changes induced by the jetport to be observable. This survey and evaluation could not cover all existing models or models under development; therefore, various models available from the literature and personal knowledge of the authors were considered at the time of this survey.

3. One phenomenon investigated during this study is seiching. Seiches are long-period oscillations of the lake surface about the mean level. These standing waves are formed after a wind blowing across the lake subsides and the setup of the water surface is no longer maintained by the wind stress. The free oscillations have periods that are dependent upon the horizontal and vertical dimensions of the lake, friction, and the number of nodes of the standing wave, that is, lines where deviation of the free surface from its undisturbed value is zero. Seiching affects both water level and mass circulation patterns. It was

necessary to investigate the periods, mode configurations, and velocity regimes for the free oscillations of Lake Erie both with and without the jetport structure. This investigation provides relative information for comparison of the effects of such a structure on the mode configurations and periods of the free oscillations of Lake Erie.

4. Another phenomenon sometimes associated with seiching is storm surge. Surge is a lake level fluctuation caused by the wind stress accompanying a moving storm system. A wind blowing over the lake exerts a horizontal force on the lake surface and induces a surface current in the general direction of the wind. These currents are impeded in shallow-water areas, thus causing the lake level to rise down wind and fall at the windward side. Terms used to describe these fluctuations are "set up" and "set down." The lake surface fluctuations and associated currents produced by moving storm systems are considered both with and without the jetport structure.

5. A third phenomenon of importance in this investigation is mass circulation in the lake. The main driving force producing mass circulation in Lake Erie is the winds.[1] The wind-generated currents can be separated into two categories: quasi-steady and time dependent. In a precise sense, there are no steady-state currents in the lake since the factors causing the currents are usually varying in time. However, there are periods when the wind is varying sufficiently slowly to permit a steady-state analysis to be approximately valid. A steady-state numerical model based on an extension of the shallow-lake theory of Welander[2] should be valid during the fall and winter months since the lake is well mixed during this period due to wind-driven turbulence and thermal convection.

6. When these well mixed conditions are not applicable, as in the summer months, a stratified model is required to investigate the mass circulation. A stratified model provides for a cooler bottom layer (hypolimnion) separated from the top layer (epilimnion) by a thin thermocline. Of particular interest is any effect of the jetport structure on location of the thermocline and the effect on hypolimnion and epilimnion circulation produced by typical summer wind conditions.

7. The numerical model feasibility study was restricted to the consideration of existing state-of-the-art models. No extensive model development was undertaken in this feasibility study; however, areas where additional numerical development are required were identified. The theoretical limitations, verification, and accuracy of the model as well as the cost of application of the model were considered.

PART II: SEICHE ANALYSIS

8. In this part of the report, an analytical and numerical study of the effects of a jetport in Lake Erie near Cleveland, Ohio, on seiches in the lake is presented. For the first five modes of free oscillations in Lake Erie, the mode configuration, period, and velocity regimes both with and without a jetport are calculated. These data are used as relative information for estimating the effects of a jetport structure on seiches in Lake Erie.

Mathematical Formulation

9. As previously defined, seiches are vertical oscillations of the water surface about the mean lake level. For a body of water with variable depth and with a maximum depth which is small compared with the wavelength of the oscillation, a boundary value problem for seiches in Lake Erie can be formulated from the long-wave equation:

$$\frac{\partial^2 \eta}{\partial t^2} = g \left[\frac{\partial}{\partial x} \left(h \frac{\partial \eta}{\partial x} \right) + \frac{\partial}{\partial y} \left(h \frac{\partial \eta}{\partial y} \right) \right] \tag{1}$$

where

$\eta(x,y,t)$ = surface displacement as a function of time and space*

t = time

g = acceleration due to gravity

$h(x,y)$ = water depth

x,y,z = Cartesian coordinates

The coordinate system is shown in Figure 1 in which the undisturbed free surface is the plane $z = 0$, where z is the vertical distance, the bottom is $z = -h(x,y)$, and the surface displacement is $z = \eta(x,y,t)$. For free oscillation in a basin, the surface displacement can be assumed to be harmonic in time.

---

* For convenience, symbols and unusual abbreviations are listed and defined in the Notation (Appendix A).

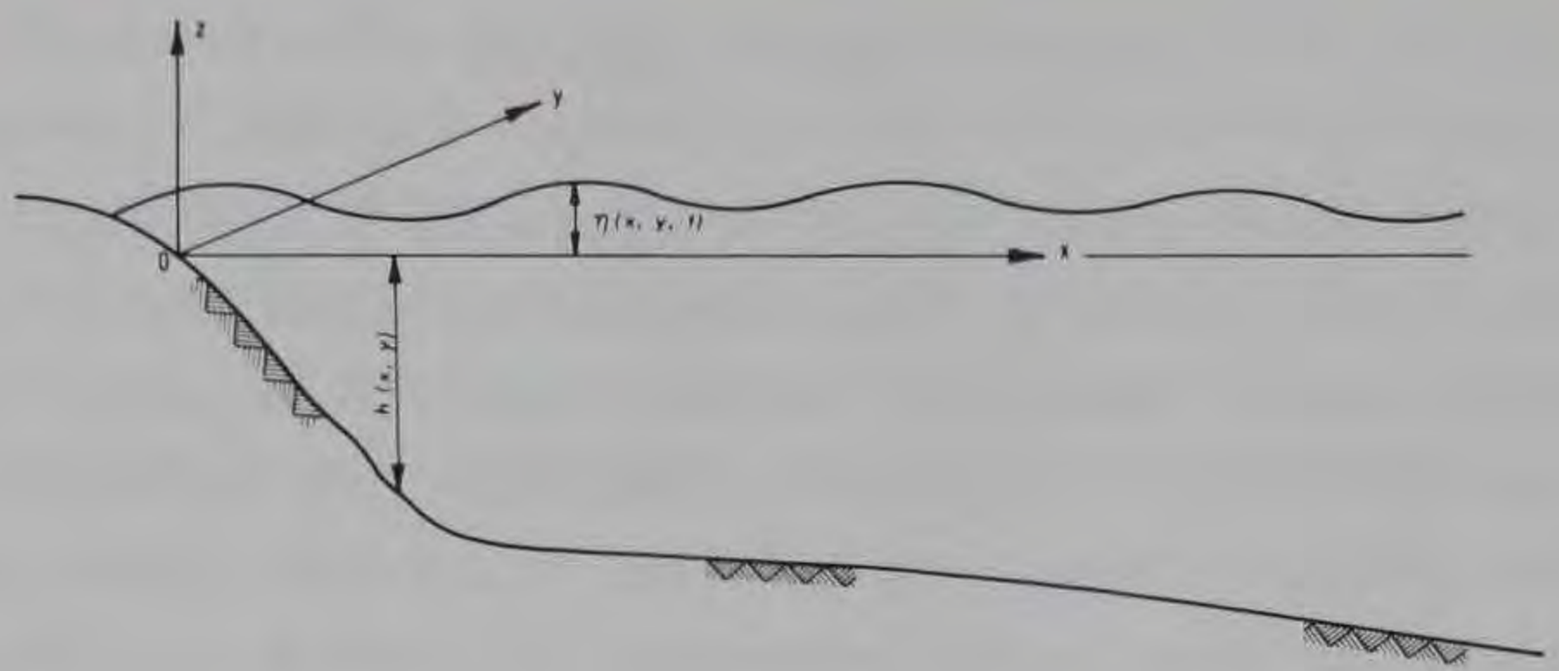

Figure 1. Coordinate system and surface profile

Thus, η can be represented as:

$$\eta(x,y,t) = \mathrm{Re}\left[\xi(x,y)\ \exp\ (-i\omega t)\right] \qquad (2)$$

where

Re = real number

ξ = wave amplitude

i = imaginary number

$\omega = 2\pi/T$ where T = period of oscillation

Based on Equations 1 and 2, the governing partial differential equation for free harmonic oscillations of a body of water becomes

$$\frac{\partial}{\partial x}\left\{h(x,y)\left[\frac{\partial \xi(x,y)}{\partial x}\right]\right\} + \frac{\partial}{\partial y}\left\{h(x,y)\left[\frac{\partial \xi(x,y)}{\partial y}\right]\right\} + \lambda^2 \xi(x,y) = 0 \qquad (3)$$

where λ is an eigenvalue expressed as $\lambda^2 = \omega^2/g$. The boundary condition for this problem is that the normal component of velocity at the basin boundary be equal to zero. Since Equation 3 (special form of the Helmholtz equation) is the equation for a standing wave, this boundary condition can be expressed as

$$\frac{\partial \xi}{\partial n} = 0 \qquad (4)$$

where n = unit normal to boundary. Therefore, Equations 3 and 4 are the partial differential equation and the boundary condition, respectively, for the boundary value problem of the free oscillations of a body of water.[3] The x and y components of velocity (u and v, respectively) can be obtained by integrating over a suitable time interval the equations of x and y momentum with the pressure gradient expressed as the gradient of the surface displacement. These components can be shown to have the following form:

$$u(x,y) = -\frac{g}{\omega}\left[\frac{\partial \xi(x,y)}{\partial x}\right]; \quad v(x,y) = -\frac{g}{\omega}\left[\frac{\partial \xi(x,y)}{\partial y}\right] \tag{5}$$

Thus, a solution to the boundary value problem for the surface displacement or the gradient of the surface displacement having been obtained, the velocity components can be calculated from Equation 5.

Numerical Scheme

Finite element method

10. The boundary value problem of Equations 3 and 4 can be solved analytically for basins of simple geometry and topography. However, for basins of complex geometry and variable topography such as Lake Erie, solutions to this problem must be obtained numerically. The numerical approach chosen to solve this boundary value problem as applied to Lake Erie is a variational approach using the finite element method (FEM).[4] The FEM is a discrete approximation procedure applicable whenever a variational principle can be formed.[5] This principle is expressed as an integral over the region under consideration which is discretized into small regions known as finite elements. Within each element the dependent variable (surface displacement) is approximated by a local Taylor series expansion. Since there are no constraints imposed on the shape of each element, the FEM can conveniently and easily solve boundary value problems involving irregularly shaped boundaries.

11. The variational formulation for the boundary value problem of

the free oscillations of a body of water consists of the functional integral

$$\chi = \iint_A \frac{1}{2} \left\{ h(x,y) \left[\frac{\partial \xi(x,y)}{\partial x} \right]^2 + h(x,y) \left[\frac{\partial \xi(x,y)}{\partial y} \right]^2 - \lambda^2 \xi^2(x,y) \right\} dx\, dy \qquad (6)$$

where A is the surface area of Lake Erie. For a stationary value of χ (maximum or minimum) with respect to $\xi(x,y)$, the Euler-Lagrange condition of the functional integral is identical with Equation 3. The identical boundary condition for Equation 4 is[6]

$$h \frac{\partial \xi}{\partial n} = 0 \qquad (7)$$

12. The solution of $\xi(x,y)$ for Equation 6 is found by applying the finite element techniques developed for what are known as constant strain triangles (CST). The FEM coding for the program was developed using linear element geometrics and interpolation functions that describe CST as outlined by Desai and Abel.[4] Dividing A into N subregions or elements, A^e where $e = 1 \ldots n$, the shape of an element can be defined by a number of nodes (vertices) that connect the element to other elements of the grid. Equation 6 can now be expressed at the element level as

$$\chi = \sum_{e=1}^{n} \iint_{A^e} \frac{1}{2} \left\{ \bar{h}^e \left[\frac{\partial \xi(x,y)}{\partial x} \right]^2 + \bar{h}^e \left[\frac{\partial \xi(x,y)}{\partial y} \right]^2 - \lambda^2 \xi^2(x,y) \right\} dx\, dy \qquad (8)$$

where $\bar{h}^e$ = the mean depth for each element. For a triangular-shaped element, $\xi(x,y)$ can be assumed to be approximated by a Taylor series expansion:

$$\xi(x,y) = \alpha_1 + \alpha_2 x + \alpha_3 y \qquad (9)$$

where α_1 , α_2 , and α_3 are unknown coefficients of the expansion. By defining the matrix vector $\{\xi\}^e$ as

$$\{\xi\}^e = \begin{bmatrix} \xi_i \\ \xi_j \\ \xi_k \end{bmatrix}$$

and the coordinates of the three nodes forming the elements as (x_i,y_i), (x_j,y_j), and (x_k,y_k) where i, j, and k are indices of these nodes, Equation 9 can then be expressed in matrix form for each element as:

$$\{\xi\}^e = \begin{bmatrix} 1x_iy_i \\ 1x_jy_j \\ 1x_ky_k \end{bmatrix} \begin{bmatrix} \alpha_1 \\ \alpha_2 \\ \alpha_3 \end{bmatrix}$$

By expressing the α matrix in terms of the node coordinates, a matrix [N] , which is known as the "interpolation" or "shape" function, can be defined as

$$[N] = \left[N_i, N_j, N_k\right]$$

where

$N_i = \left[(x_k y_j - x_j y_k) + (y_k - y_j)x + (x_j - x_k)y\right] \Big/ 2\Delta$ and Δ = area of the element A^e

N_j, N_k = similar expressions obtained by the cyclical permutation of i , j , and k

Hence $\xi(x,y)$ (Equation 9) can be expressed for any point within the element as

$$\xi(x,y) = [N]\{\xi\}^e \qquad (10)$$

Now, with ξ uniquely and continously defined throughout the region of A^e , the functional χ can be minimized or maximized with respect to

the nodal values of ξ . Substitution of Equation 10 into Equation 8 and setting the first variation of χ with respect to any nodal point m equal to zero gives

$$\frac{\partial \chi}{\partial \eta_m} = 0 = \sum_{e=1}^{n} \iint_{A^e} \frac{1}{2}\left(\frac{\partial}{\partial \eta_m}\right)\left[\bar{h}^e\left(\frac{\partial \{\xi\}^e}{\partial x}\right)^2 + \bar{h}^e\left(\frac{\partial \{\xi\}^e}{\partial y}\right)^2 - \lambda^2\left(\{\xi\}^e\right)^2\right] dx\, dy \qquad (11)$$

for $m = 1...M$, where M is the total number of node points. Equation 11 represents a system of M linear algebraic equations in terms of the M values of ξ_m of the nodal points, in which the values of ξ_m form the solution of Equation 3. The system of equations formed by Equation 11 can be expressed in general matrix format for the entire region of interest as

$$[K]\{\xi\} = \lambda^2[M]\{\xi\} \qquad (12)$$

where λ is the eigenvalue expressed as

$$\lambda^2 = \omega^2/g$$

and $[K]$ = element stiffness matrix

$[M]$ = lumped mass matrix

Details of the expression of individual terms of [K] and [M] matrices can be found in Reference 7. After assemblage of Equation 12, the boundary condition (Equation 7) is inserted at the appropriate nodal values.

13. Equation 12 is a form of an eigenvalue problem. Thus, for real, square matrices of order M there will be n independent real eigenvalues, λ_n , where $n = 1...M$, which satisfy Equation 12 and define the natural frequencies of the system. For each λ_n there will be an eigenvector or "mode" $\{\xi\}$ in which the relative magnitudes of nodal displacements are fixed but not their absolute values

(solution not unique). To solve this eigenvalue problem by direct matrix procedures requires the conversion of Equation 12 into the standard form

$$[H]\{Z_i\} = \lambda_i\{Z_i\} \ , \ i = 1,2,...M \tag{13}$$

or

$$[H][Z] = [\Lambda][Z]$$

where

$[H]$ = M × M square matrix of coefficients

$[Z]$ = modal matrix, where columns are eigenvectors $\{Z_i\}$ of $\{H\}$

$[\Lambda]$ = diagonal matrix of eigenvalues

Procedures for reducing Equation 12 to standard form (Equation 13) are presented in detail in References 7 and 8.

14. Once $\{\xi\}$ is obtained for a particular frequency (eigenvalue) of oscillation, the velocity components (Equation 5) may be obtained from the slope of ξ, which when expressed at the element level is

$$\begin{bmatrix} \frac{\partial \xi}{\partial x} \\ \\ \frac{\partial \xi}{\partial y} \end{bmatrix} = G\{\xi\}^e \tag{14}$$

where G is the element slope matrix. G is defined as:

$$G = \begin{bmatrix} \frac{\partial N_i}{\partial x} & \frac{\partial N_j}{\partial x} & \frac{\partial N_k}{\partial x} \\ \\ \frac{\partial N_i}{\partial y} & \frac{\partial N_j}{\partial y} & \frac{\partial N_k}{\partial y} \end{bmatrix} \tag{15}$$

Thus, $\{\xi\}^e$ having been calculated and the shape function $[N]$ known, the horizontal velocity at any point (x,y) within an element can be determined from Equations 14 and 15. For this study, the velocity was

evaluated at the centroid of each element.

15. The numerical calculations required for the finite element procedure were performed on a G-635 Honeywell computer with plotting performed on a Calcomp drum plotter. The inputs required by the finite element code are as follow:

a. The total number of elements and nodes.

b. The arrangement of nodes for each element.

c. The x,y coordinates of each node.

d. The depth at each node.

e. The boundary conditions.

f. The digitized natural boundary of the lake.

The basic outputs of the finite element code are as follow:

a. M natural frequencies (or eigenvalues) of the lake.

b. Normalized surface displacements at every node and centroid of each element for each natural frequency.

c. Normalized x and y velocity components at the centroid of each element for each natural frequency.

Thus, results for the local region of interest (Figure 2) consist of normalized surface elevations at each point labeled with an alpha N or alpha E and normalized velocity components at each point labeled with an alpha E .

Discretization of Lake Erie

16. The surface area of Lake Erie (Figure 3) was approximated by 238 elements with 264 total nodal points. It should be noted that many of the elements are quadrilateral in shape, and these elements were represented in the finite element code by four CST's.* A local region of interest near Cleveland, Ohio, is identified by a heavy lined boundary in Figure 3. This area is expanded as Figure 2 for element definition of shape with nodes and centroids for elements of particular interest being assigned numbers for future identification in interpreting the results. The choice of the element shapes in the vicinity of

---

* J. F. Abel, Memorandum for Record, U. S. Army Engineer Waterways Experiment Station, CE, Vicksburg, Miss.

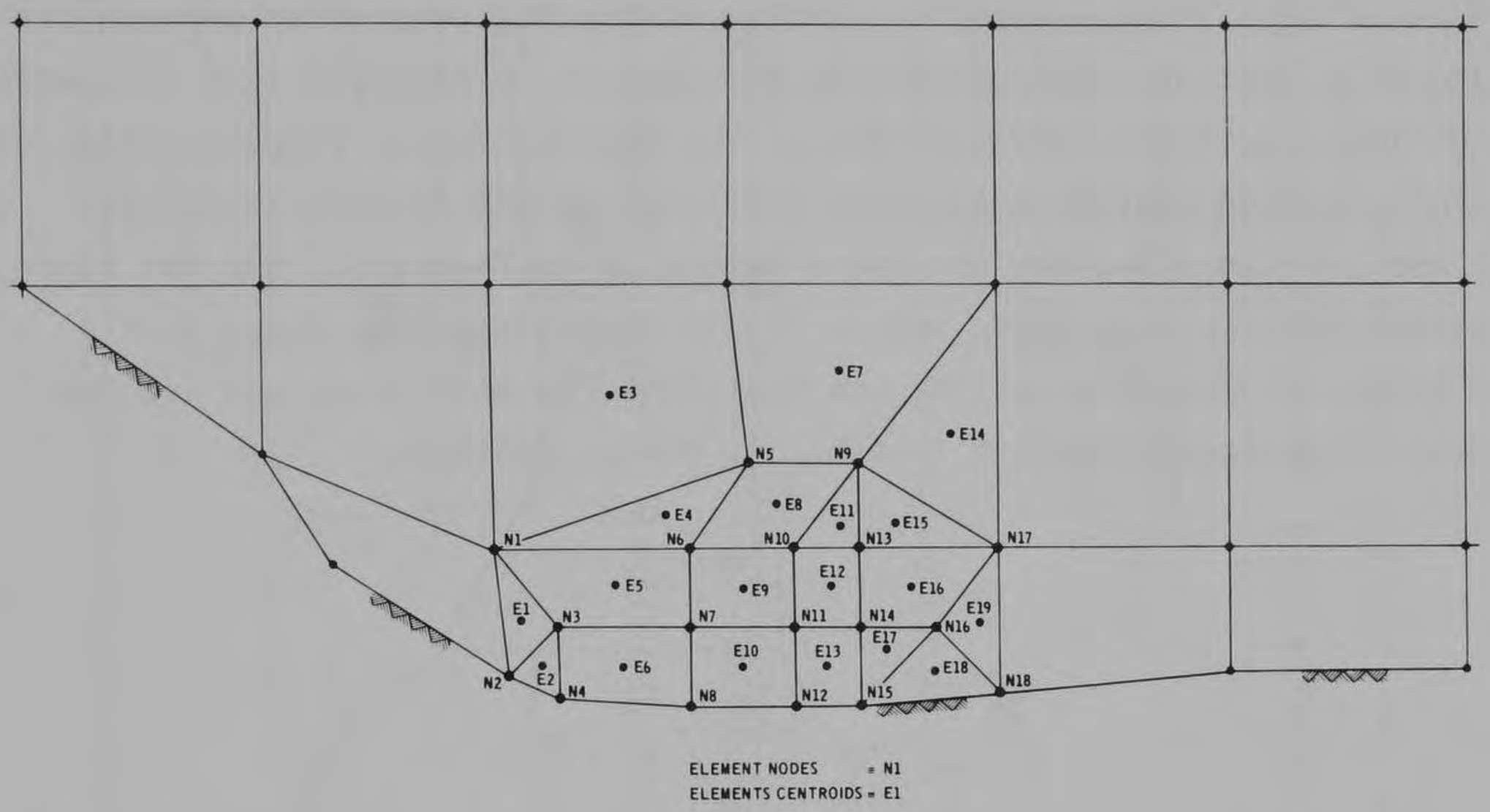

Figure 2. Finite element representation of local region of interest

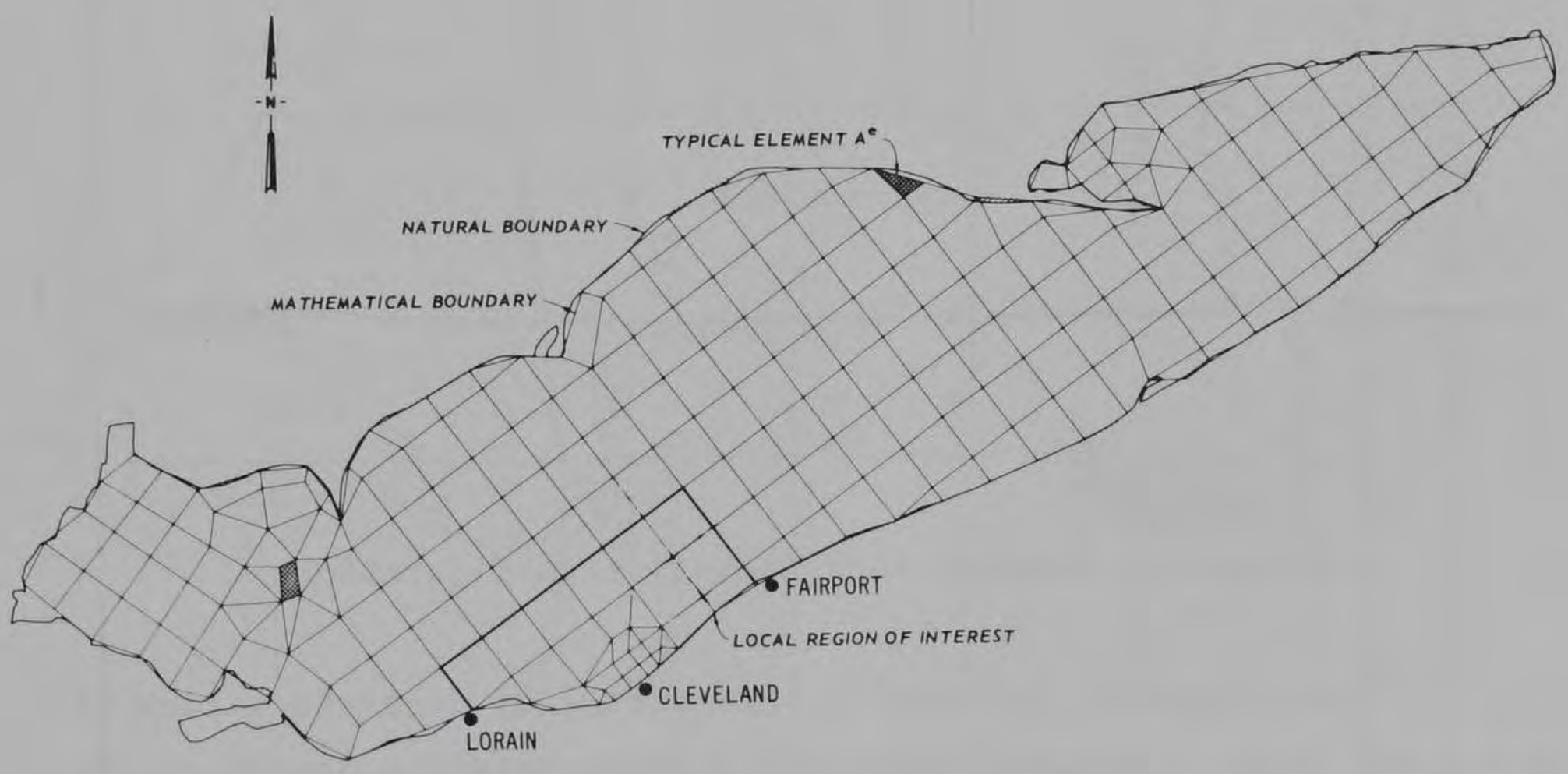

Figure 3. Finite element representation of Lake Erie

the proposed jetport site was dictated by the configurations of the offshore jetport island, its shoreward extension, and shore connection. Because their location and configuration had not been selected at the time of this study, tentative configurations for this study were chosen based on available prefeasibility information.* Figure 4 is a schematic of these tentative configurations. The finite element representation of these assumed configurations and locations of the jetport island are shown in Figure 5a, the shoreward extension in Figure 5b, and two shore connections in Figures 5c and d. It is emphasized that these four configurations and locations are tentative for this study and are subject to change as LERTA's feasibility study continues.

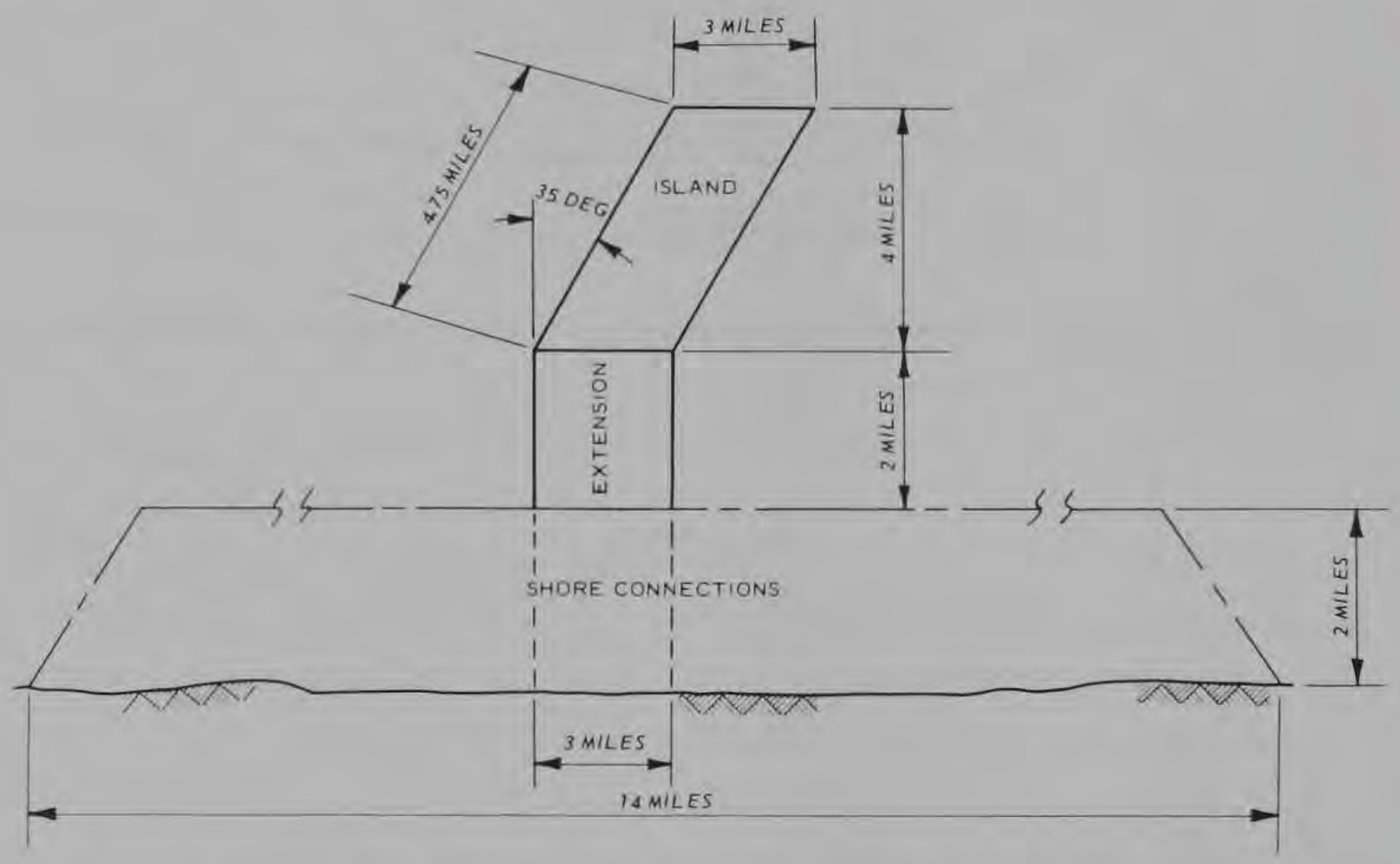

Figure 4. Schematic of tentative configurations

17. The depth of the lake is represented by discrete values at each nodal point. Figure 6 depicts the representative depths at the nodal points. These depths were taken from the U. S. Lake Survey

---

* "The Lake Erie International Jetport Project," Pre-Feasibility Technical Report, March 1971, Greater Cleveland Growth Association.

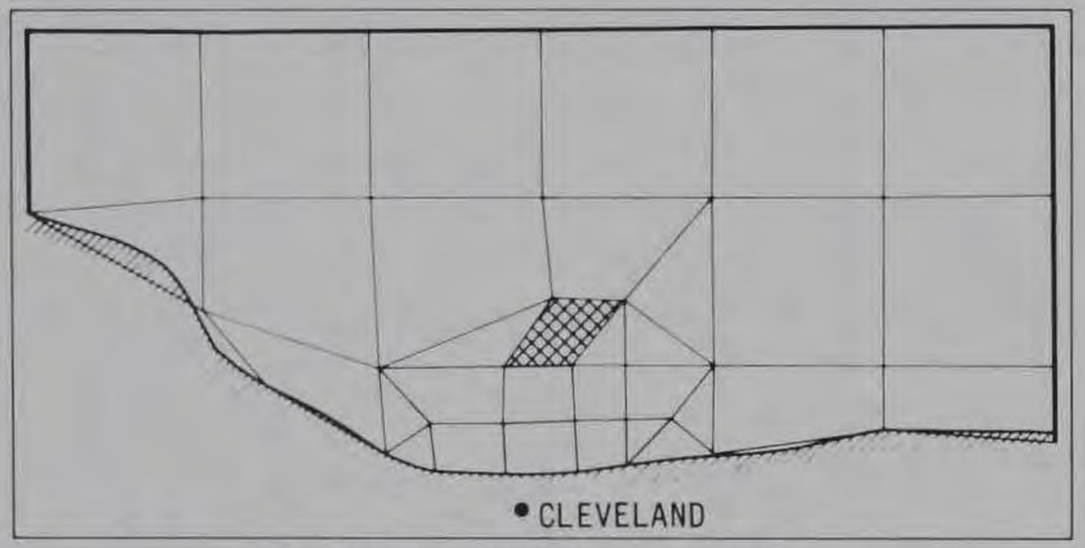

a. CONFIGURATION A: ISLAND

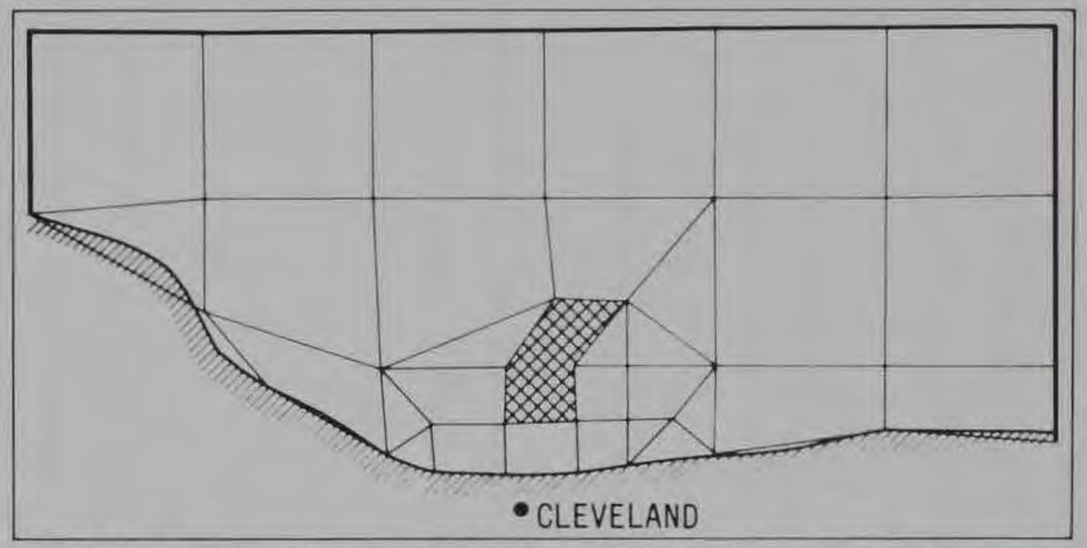

b. CONFIGURATION B: ISLAND WITH SHOREWARD EXTENSION

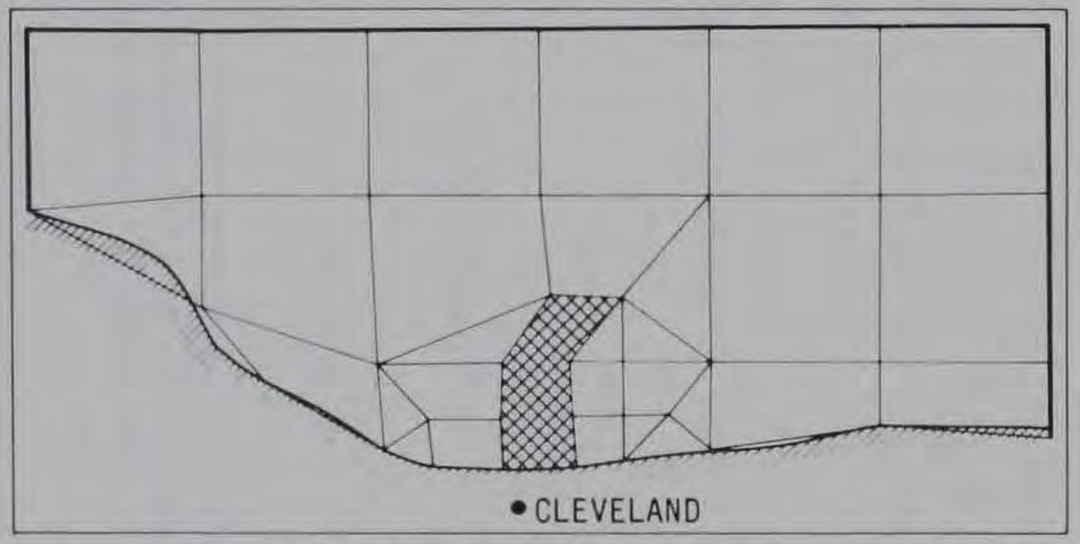

c. CONFIGURATION C: ISLAND WITH SHORE CONNECTION

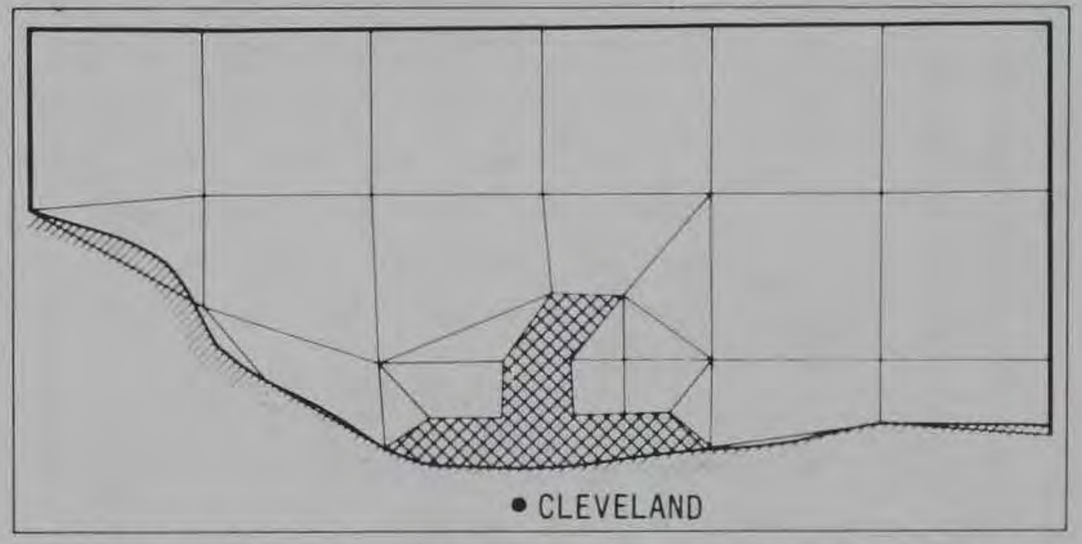

d. CONFIGURATION D: ISLAND WITH ALONGSHORE CONNECTION

Figure 5. Finite element representation for tentative configurations

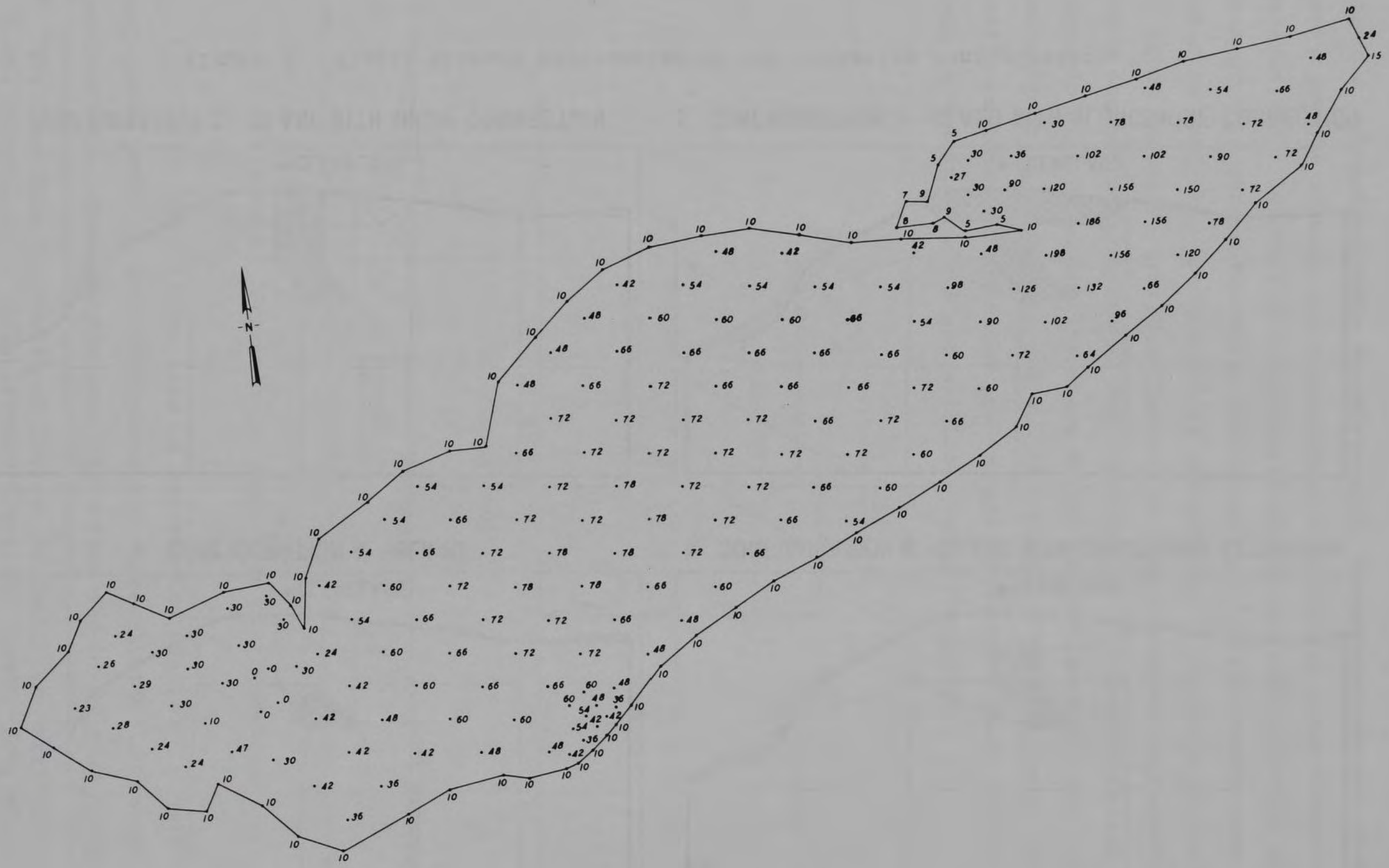

Figure 6. Representative depth field

Chart L.S.3 which is referenced to a low water datum of 570.5 ft.*

18. The volume, surface area, and mean depth for the discretized representation of Lake Erie are represented in the following tabulation.

Parameter	Observed	Computed
Volume, cu ft	16.8×10^{12}	16.43×10^{12}
Surface area, sq ft	27.6×10^{10}	27.07×10^{10}
Mean depth, ft	60.7	60.69

For comparison, the factual (observed) values of these parameters for Lake Erie are also listed. The computed values, in particular the mean depth, agree very well with the observed values.

Verification

19. To verify the application of the numerical procedure outlined in the previous sections to the investigation of the effects of a jetport on the natural oscillations of Lake Erie, the natural periods and corresponding normal modes of variation in surface elevations for the first five modes of oscillations were calculated for Lake Erie without the jetport structure. The calculated natural periods of the free oscillations are shown in the following tabulation.

Mode	Computed Periods, hr	Observed Periods, hr*
1	14.43	14.38
2	9.22	9.14
3	6.01	5.93
4	4.31	4.15
5	3.87	- -

* From Reference 9.

* A table of factors for converting metric (SI) units of measurement to U. S. customary units and U. S customary units to metric (SI) units is given on page 4.

Also tabulated are the observed periods for the free oscillations of Lake Erie as determined from spectra of records of lake levels by Platzman and Rao.[9] The discretized depths in this study, discussed in paragraph 17, were corrected to correspond to actual depths of the lake at time of observed oscillations by considering differences in the reference datum of Chart L.S.3 and mean lake level at times of observation. There is relatively good agreement between the observed periods and the periods computed by the finite element procedure. In addition to the comparison of periods, the computed amplitudes of the relative surface variation for the fundamental mode of seiching for 13 locations around the lake were compared with the observed values from Platzman and Rao.[10] The relative amplitudes around the lake from this seiche study are normalized amplitudes such that actual seiche amplitudes around the lake can be determined, if the seiche amplitude at one location is known, by multiplying the relative amplitudes by the known seiche amplitude. For example, actual seiche amplitudes around the lake for a 3-ft amplitude at Toledo can be estimated by multiplying this 3-ft amplitude by the relative amplitudes around the lake. For this case, the actual seiche amplitude of the first mode at Cleveland would be 3.0 times 0.27 or 0.8 ft. Table 1 shows this comparison, which exhibits good agreement around the lake. The maximum deviation between computed and observed relative amplitudes occurs near Port Clinton. This deviation may reflect the reliability of the observations at Port Clinton or, more probable, is associated with the numerical representation of the islands, topography, and shoreline in the eastern basin of the lake.

Model Results

20. For the full lake and nearshore region without a jetport, mode configurations of relative amplitudes and depth-averaged horizontal velocities are numerically computed for the first five modes (paragraph 19) or eigenvalues. Results of these computations for the full lake are presented in Figures 7-16. For each spatial location in the nearshore region, the depth-averaged horizontal velocity is defined as

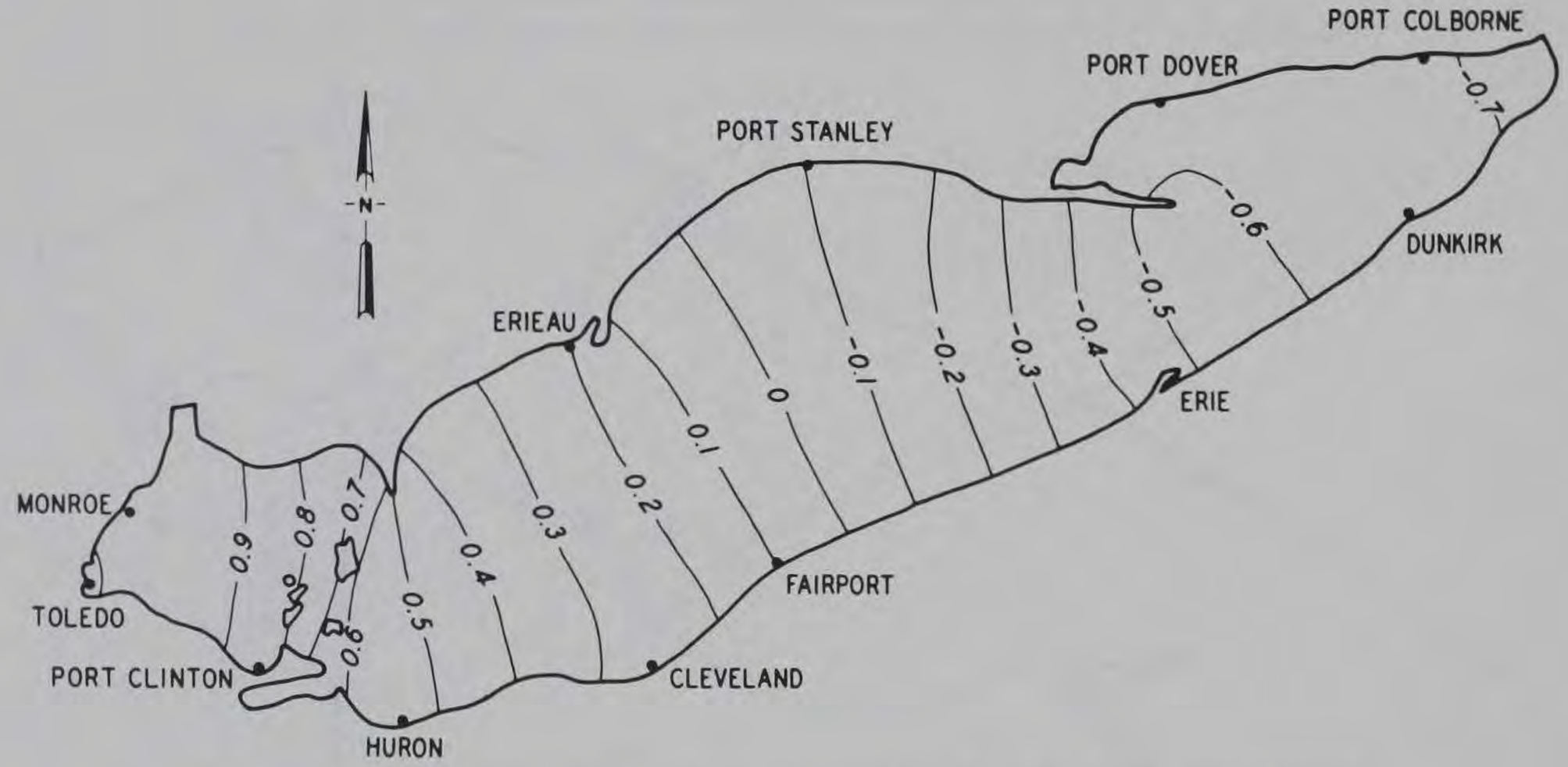

Figure 7. Mode shape of the first eigenvalue for the full lake without jetport (normalized to maximum elevation 1)

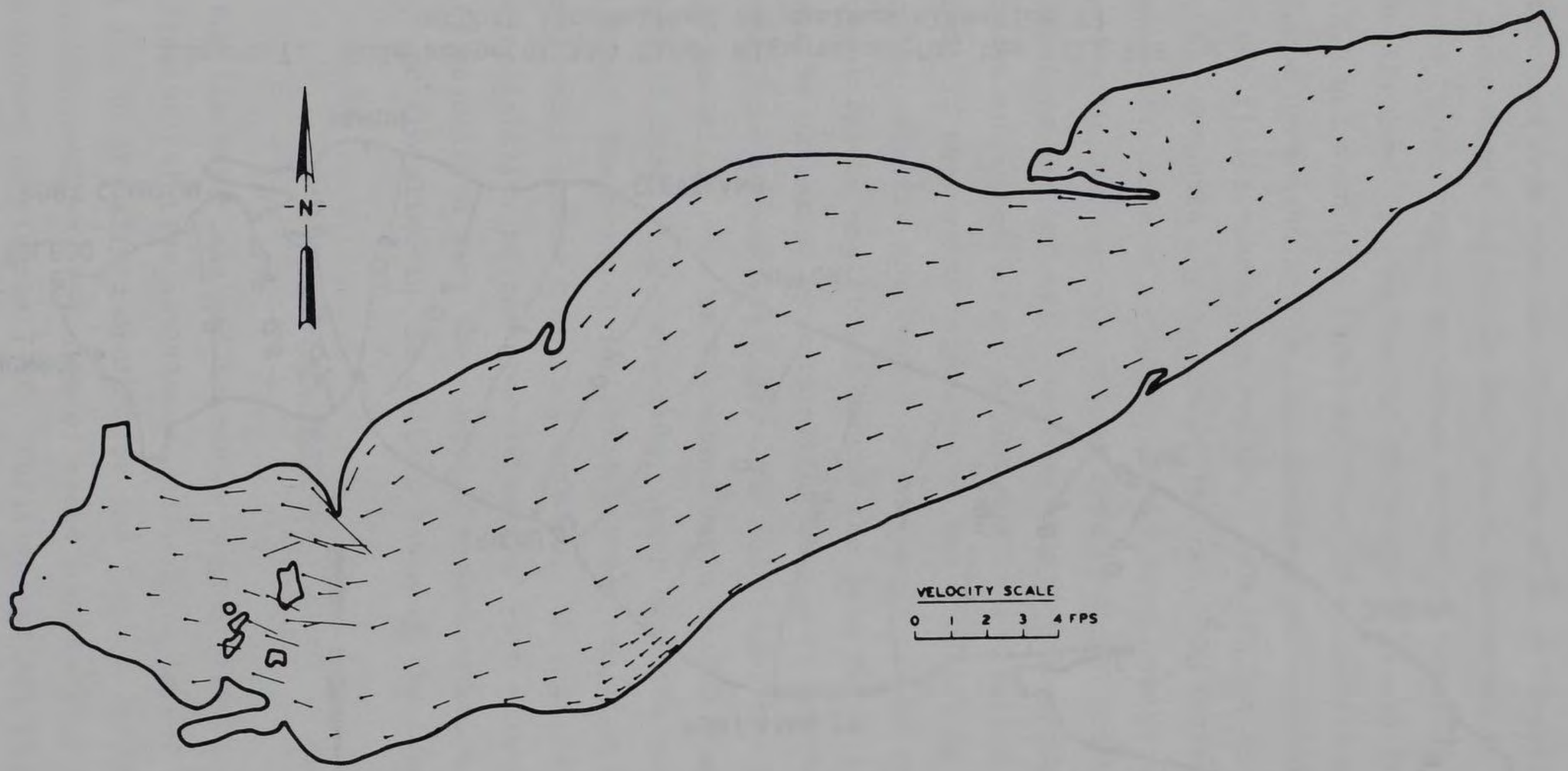

Figure 8. Normalized current of the first eigenvalue for the full lake without jetport (normalized to maximum elevation 1)

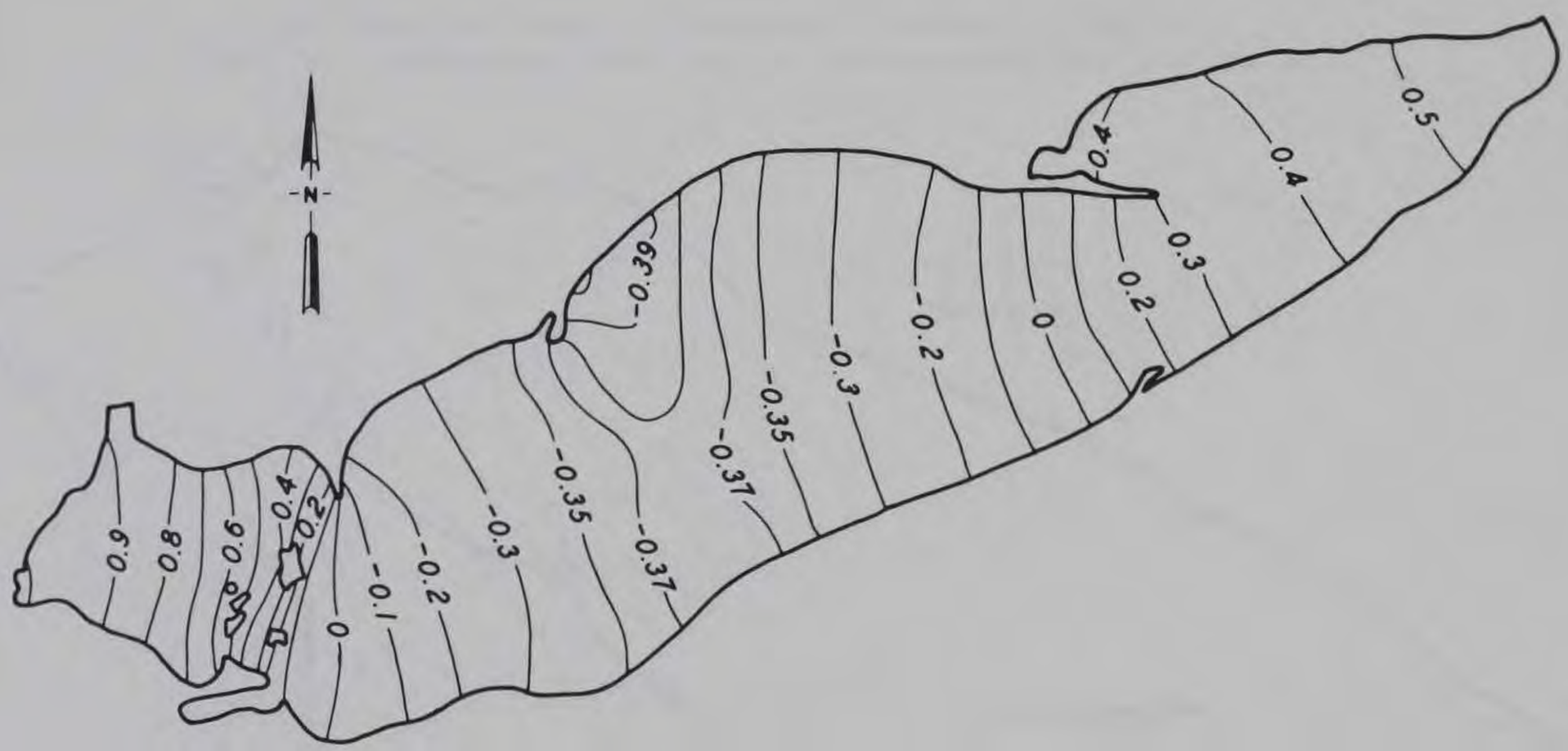

Figure 9. Mode shape of the second eigenvalue for the full lake without jetport (normalized to maximum elevation 1)

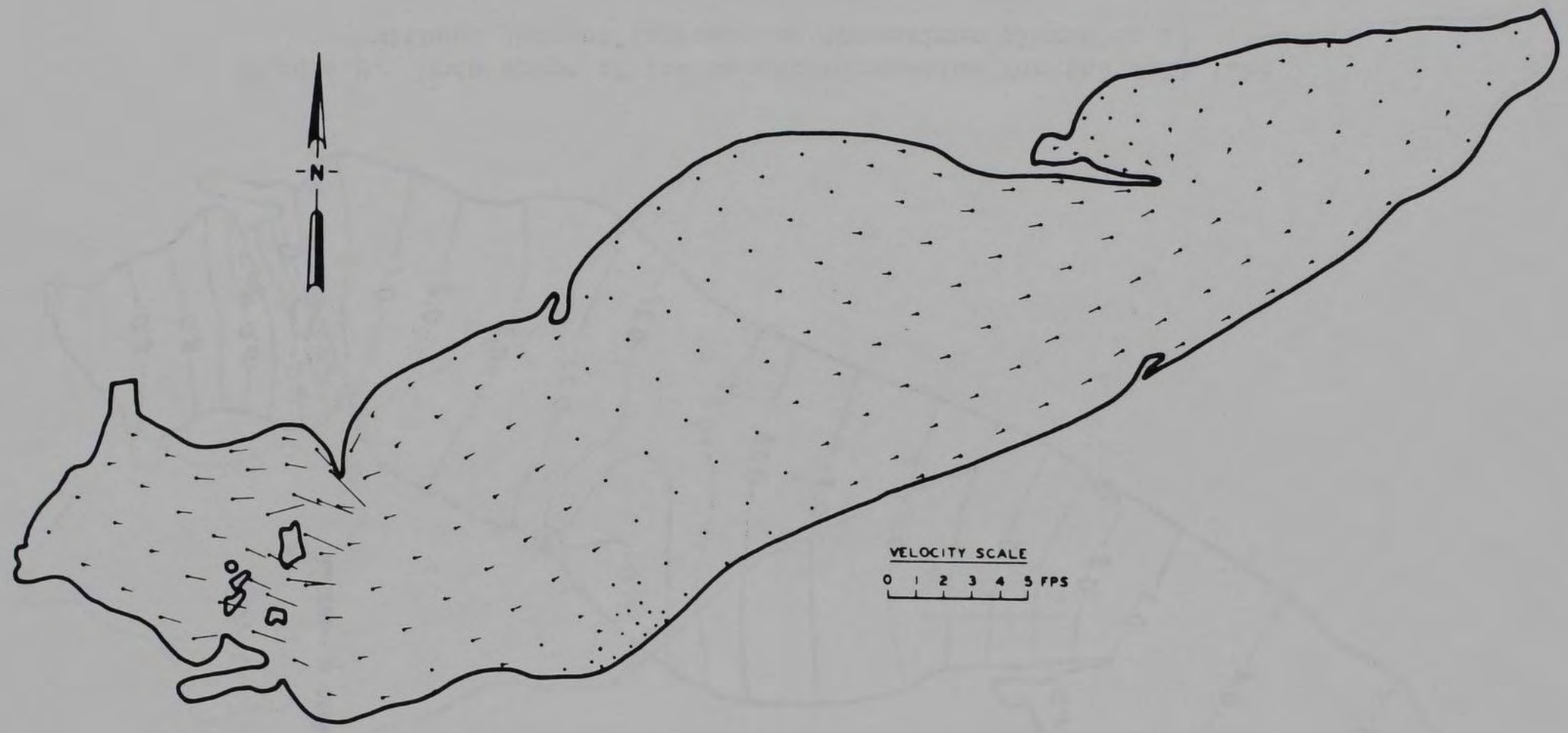

Figure 10. Normalized current of the second eigenvalue for the full lake without jetport (normalized to maximum elevation 1)

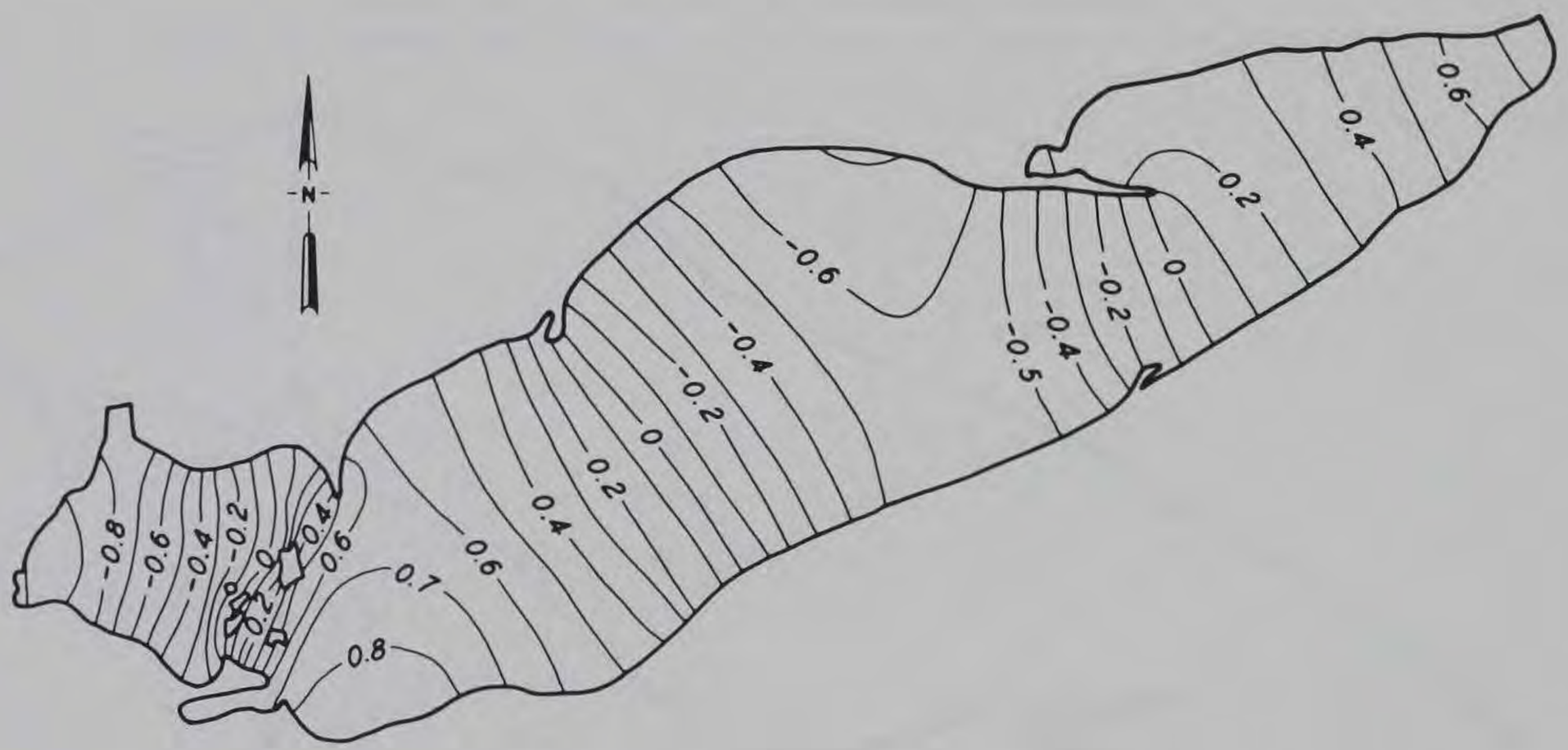

Figure 11. Mode shape of the third eigenvalue for the full lake without jetport (normalized to maximum elevation 1)

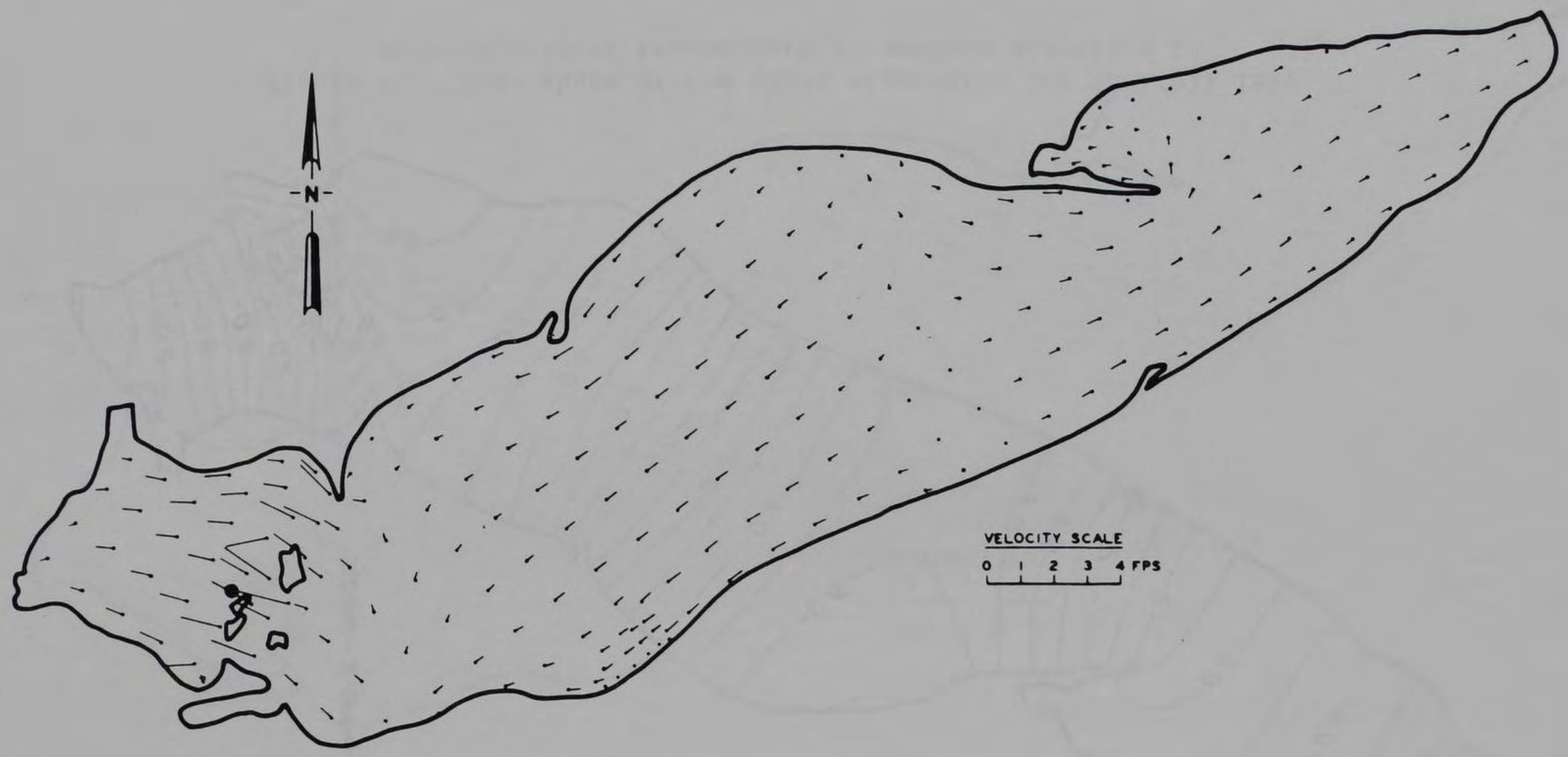

Figure 12. Normalized current of the third eigenvalue for the full lake without jetport (normalized to maximum elevation 1)

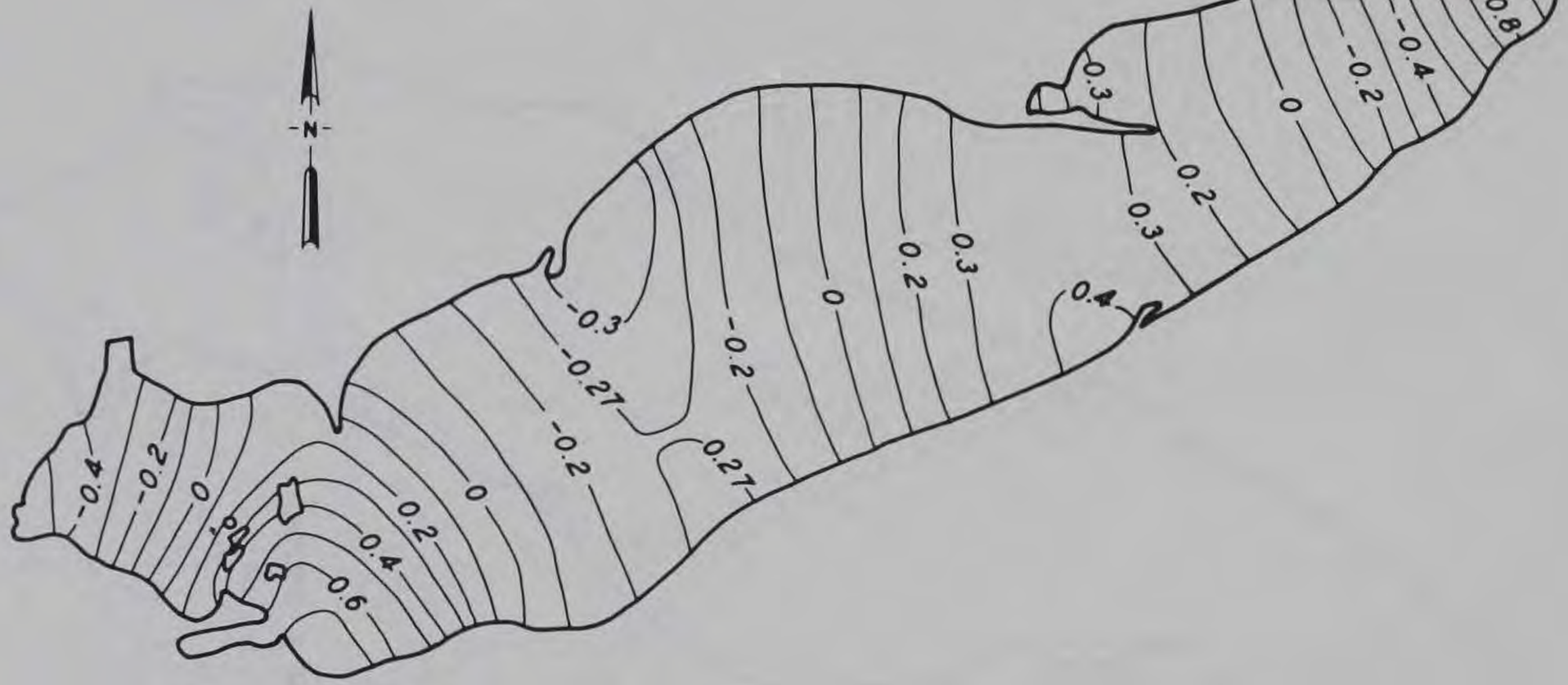

Figure 13. Mode shape of the fourth eigenvalue for the full lake without jetport (normalized to maximum elevation 1)

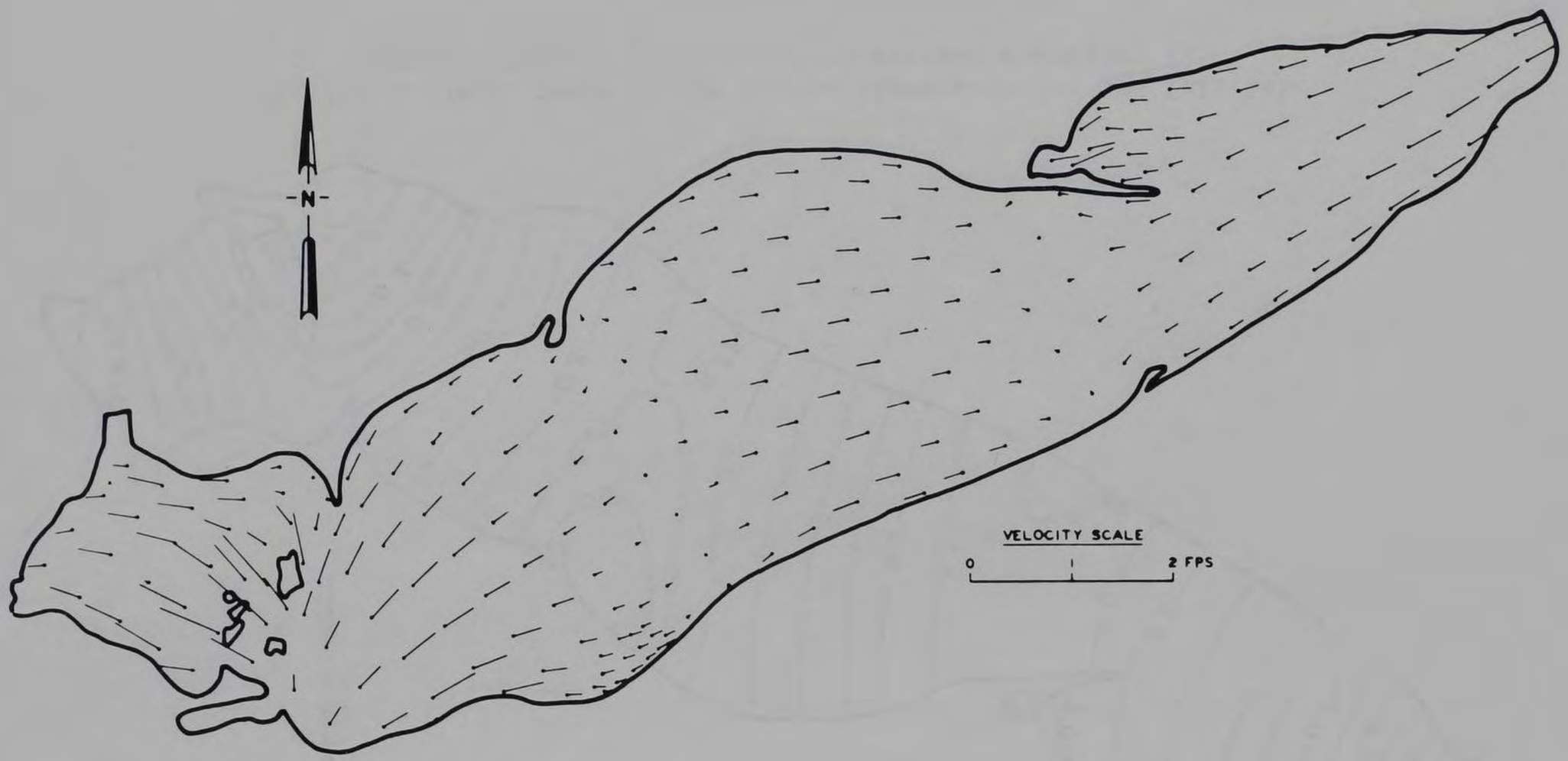

Figure 14. Normalized current of the fourth eigenvalue for the full lake without jetport (normalized to maximum elevation 1)

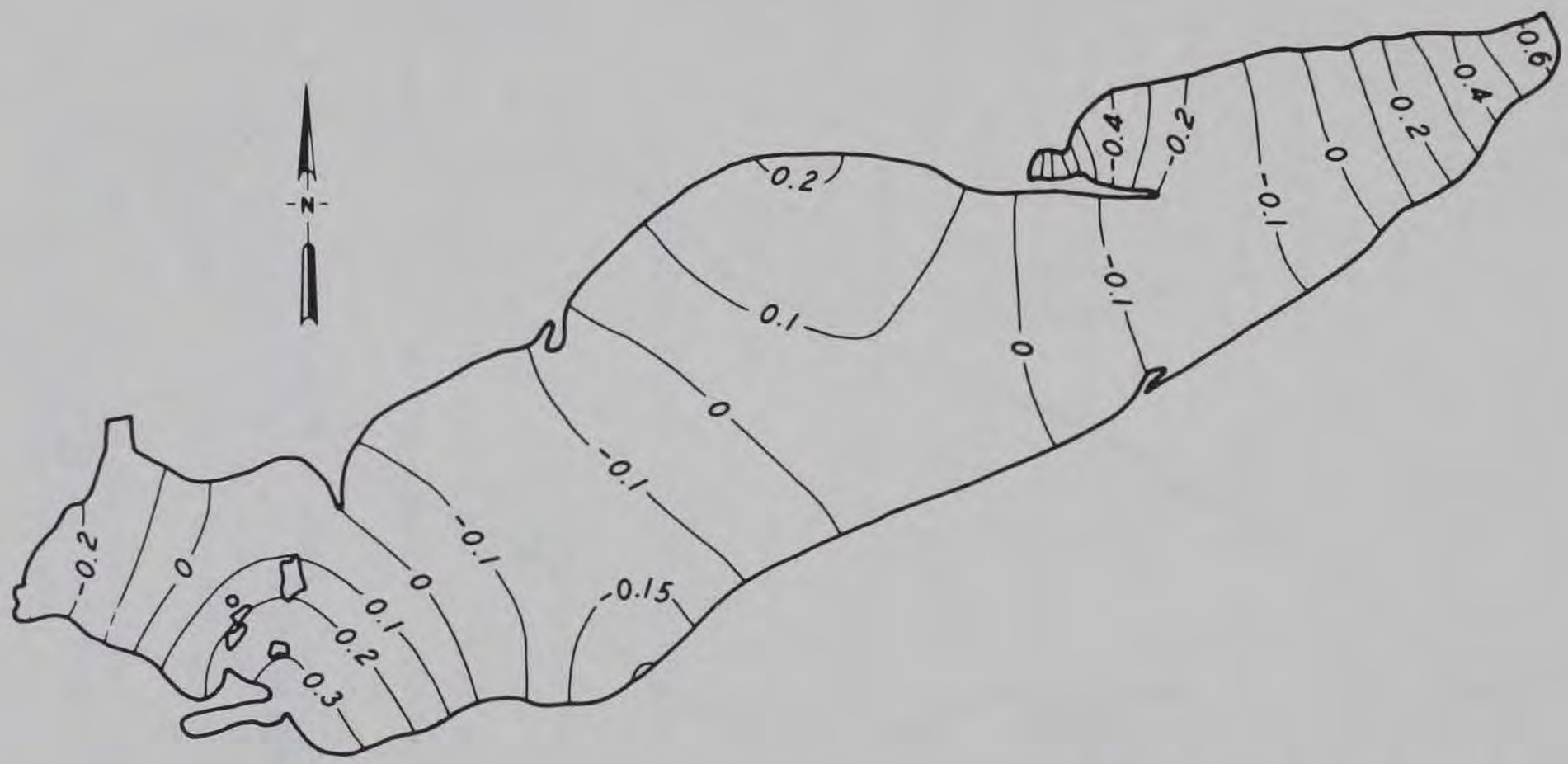

Figure 15. Mode shape of the fifth eigenvalue for the full lake without jetport (normalized to maximum elevation 1)

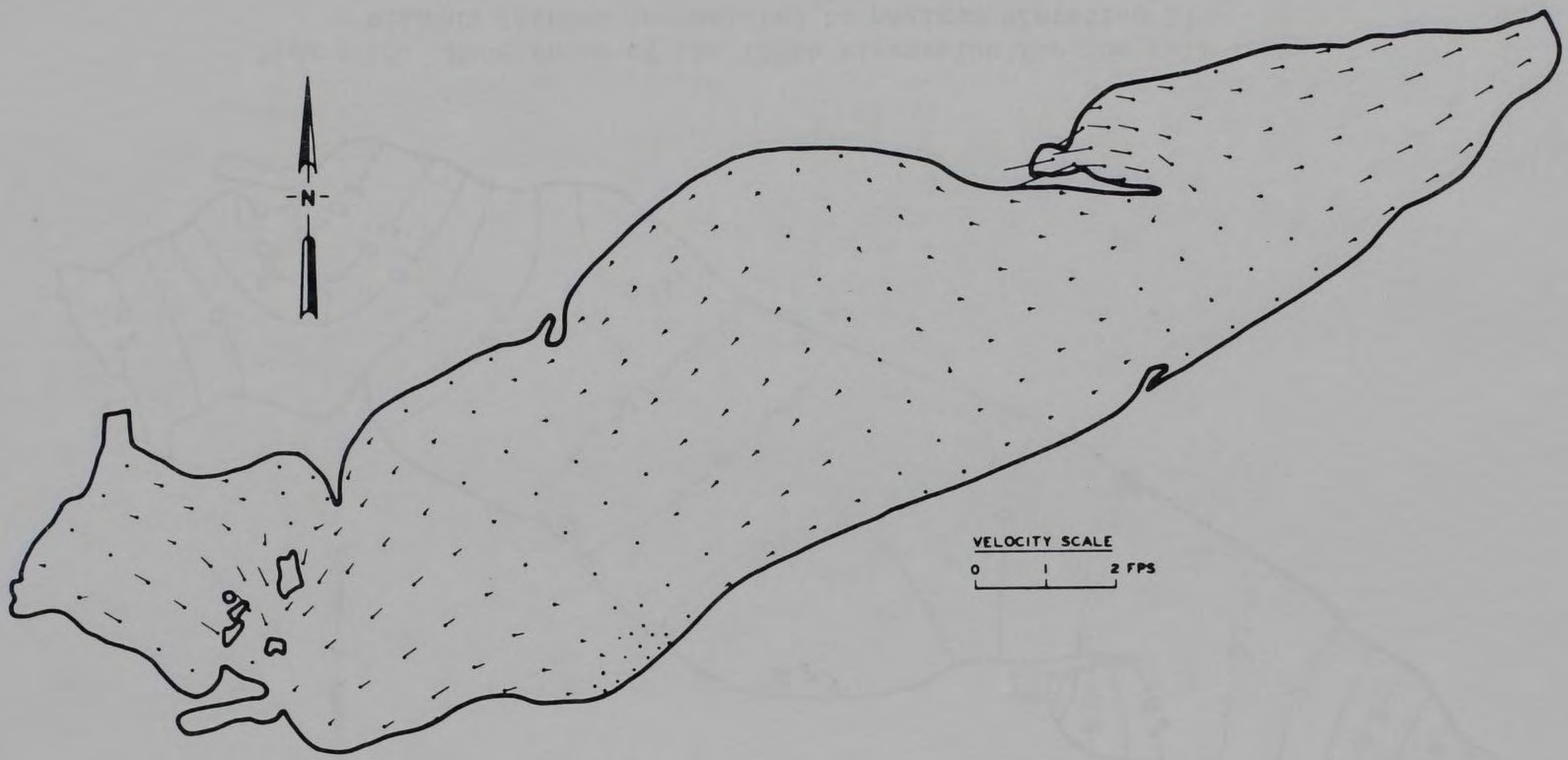

Figure 16. Normalized current of the fifth eigenvalue for the full lake without jetport (normalized to maximum elevation 1)

a velocity with constant direction and magnitude over the entire water column and whose constant direction and magnitude represent the averaged velocity over the entire water column. In addition, the magnitude of the depth-averaged horizontal velocity is a normalized variable like the relative seiche amplitude (refer to paragraph 19). The velocity magnitudes, which are computed in this study, are normalized to a maximum seiche amplitude of 1.0 ft. For the first mode (fundamental), the magnitude of the normalized velocity vectors in the Cleveland area must be multiplied by the actual seiche amplitude at Toledo to obtain the actual velocity magnitude. However, for comparison the relative magnitudes can be used without scaling. The nearshore results without a jetport for the first five modes of oscillation are presented in Figure 17. For four generalized configurations and locations (Figure 5) of the jetport, nearshore results of the relative amplitudes and depth-averaged horizontal velocities for the first five modes are presented in Figures 18-22. The calculated periods of the first five modes of free oscillations for different jetport configurations are presented in Table 2.

Conclusions of the Seiche Analysis

21. Based upon results of the numerical analysis of the effects of a jetport offshore near Cleveland, Ohio, on the free oscillations of Lake Erie, several conclusions are apparent. These conclusions hold for all five modes of free oscillation unless stated otherwise and are as follow:

a. Periods of the first five modes are relatively unchanged by any jetport configuration. There exist slight increases (2.5-5.0 min.) in the periods of the first three modes with the first mode exhibiting the largest increase of 4-5 min.

b. Changes in relative seiche amplitudes and horizontal velocity are confined within a distance of 4-6 miles from the four jetport configurations.

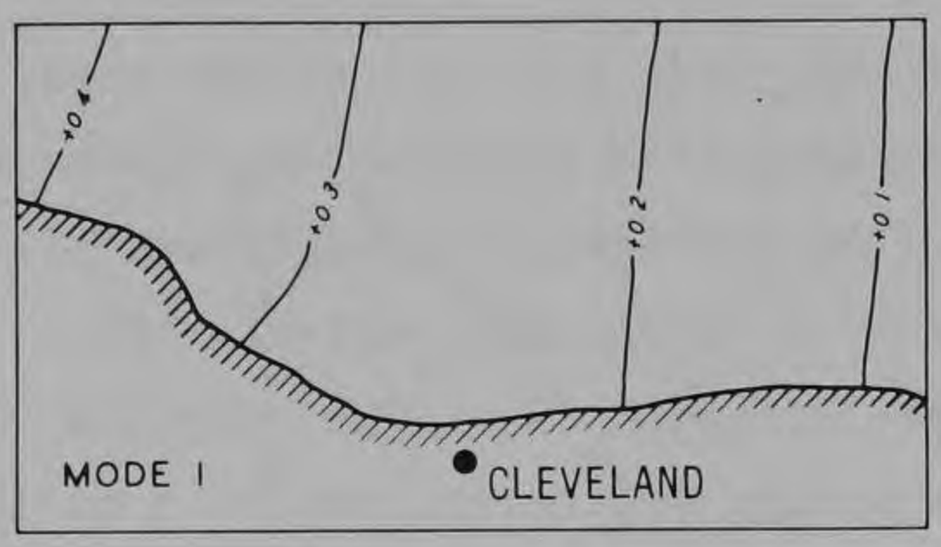

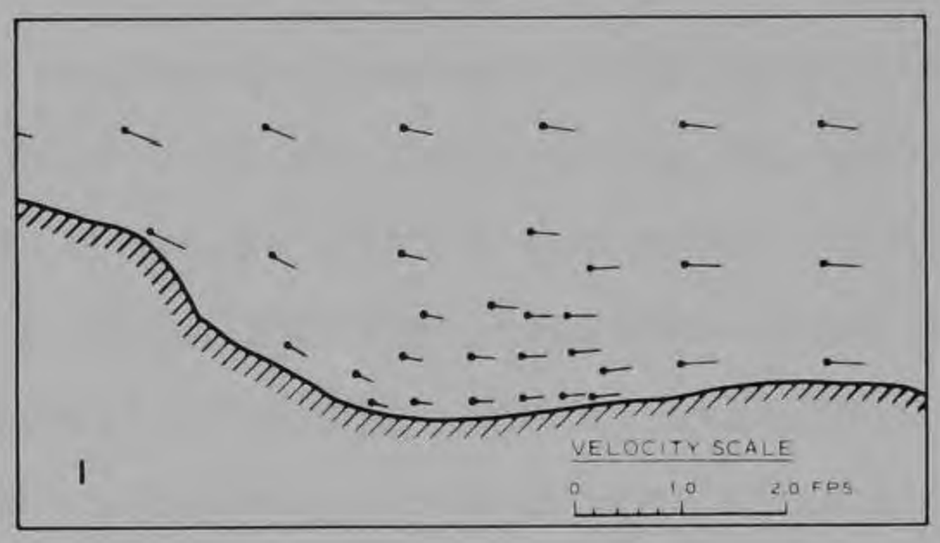

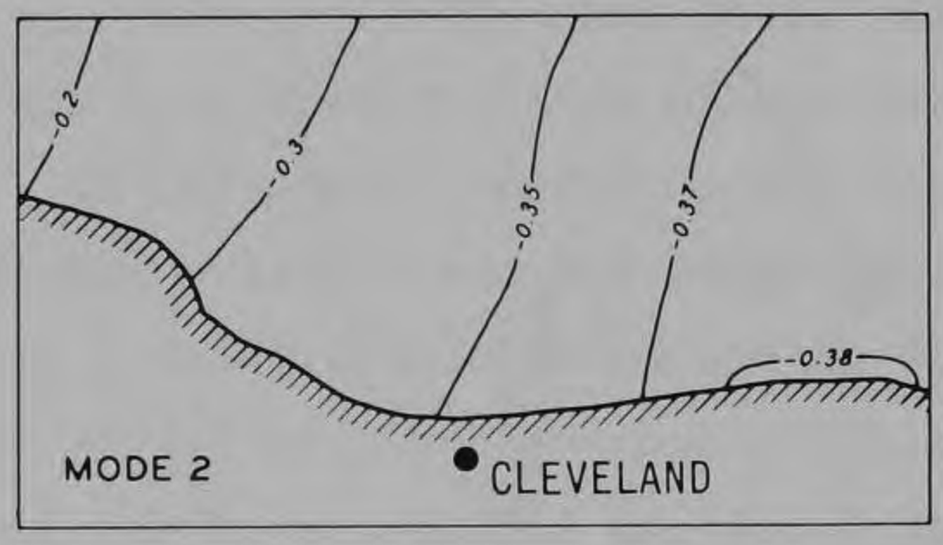

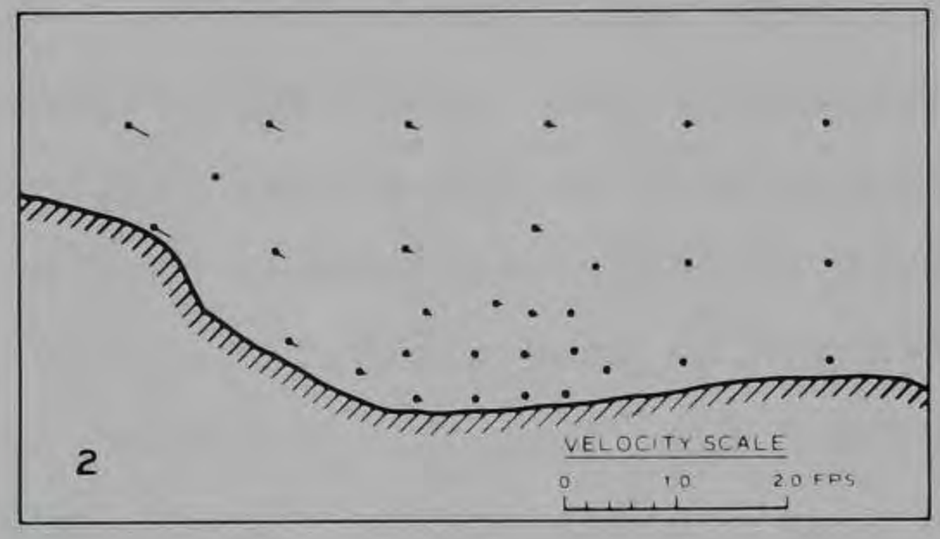

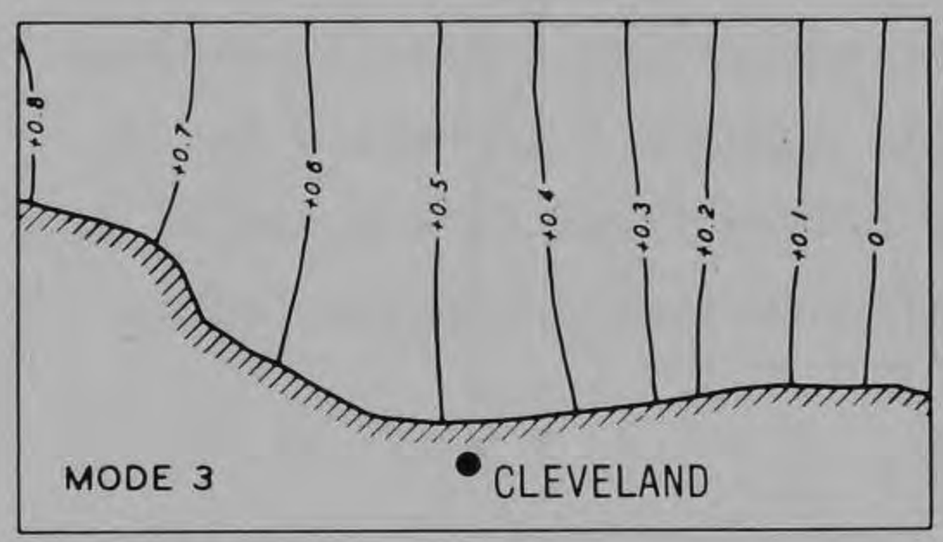

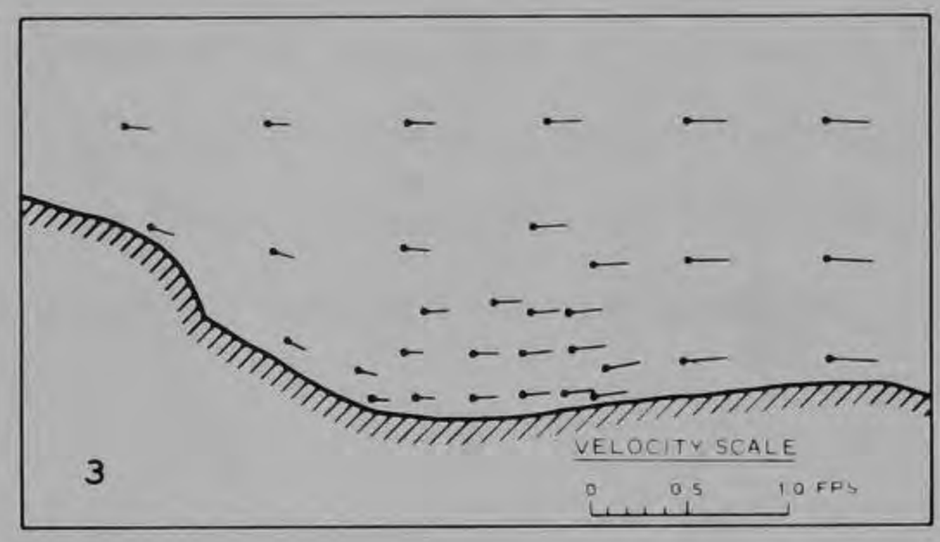

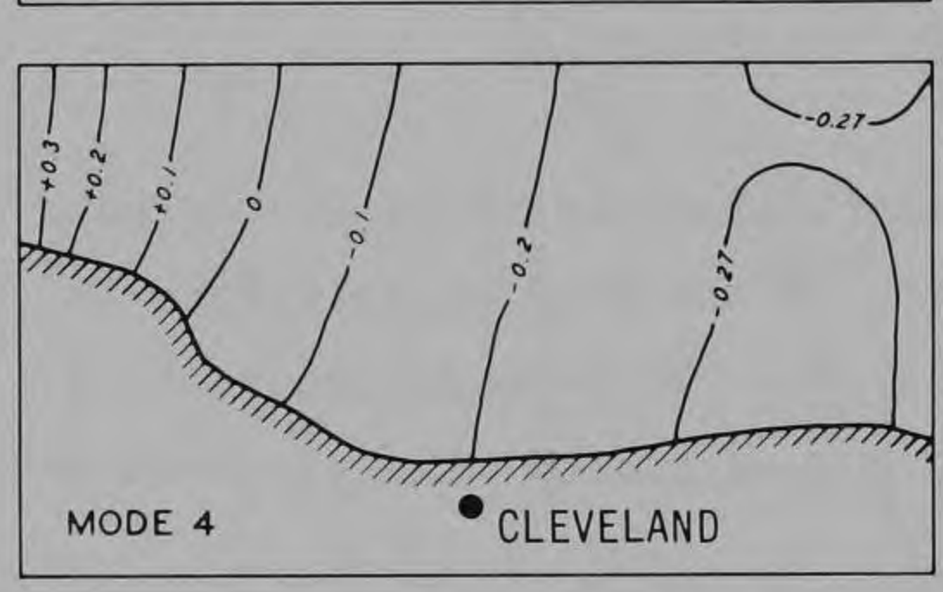

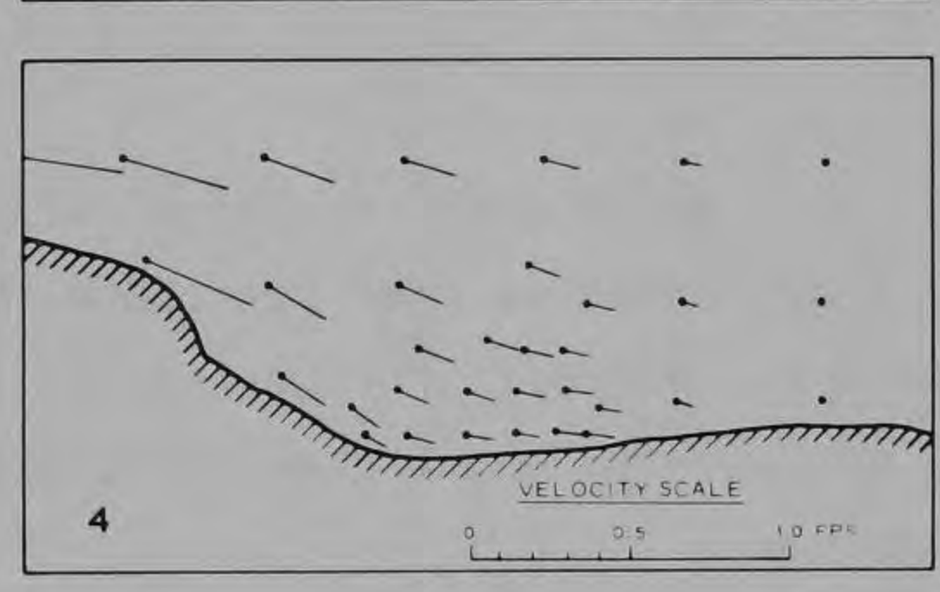

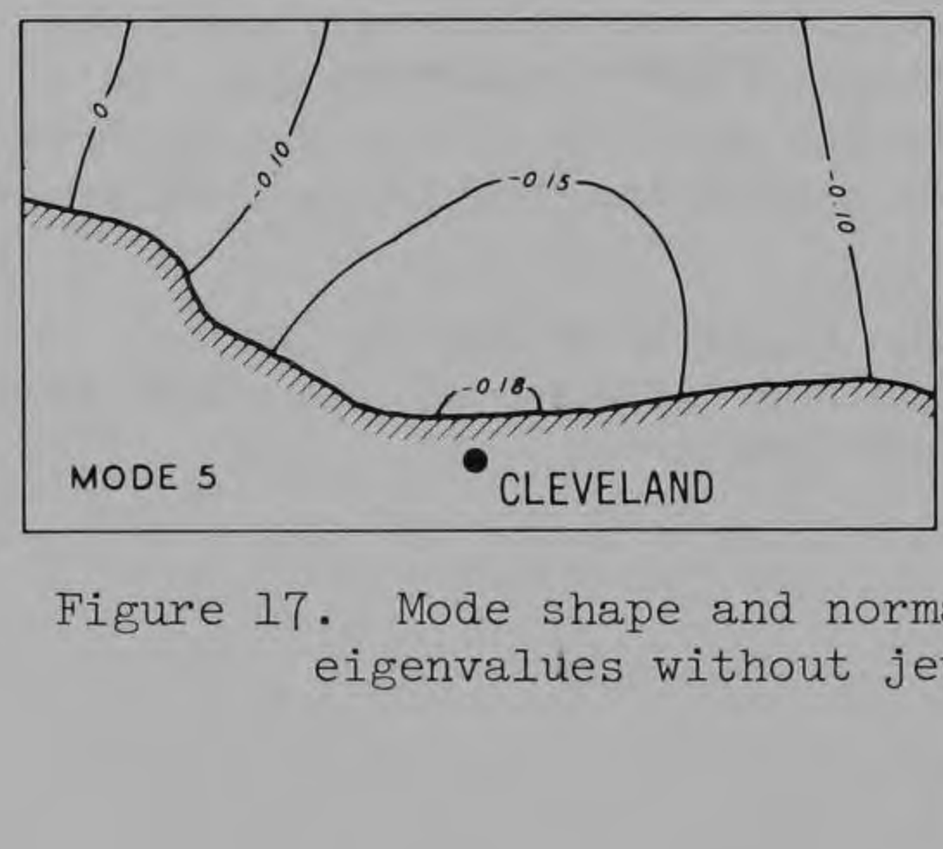

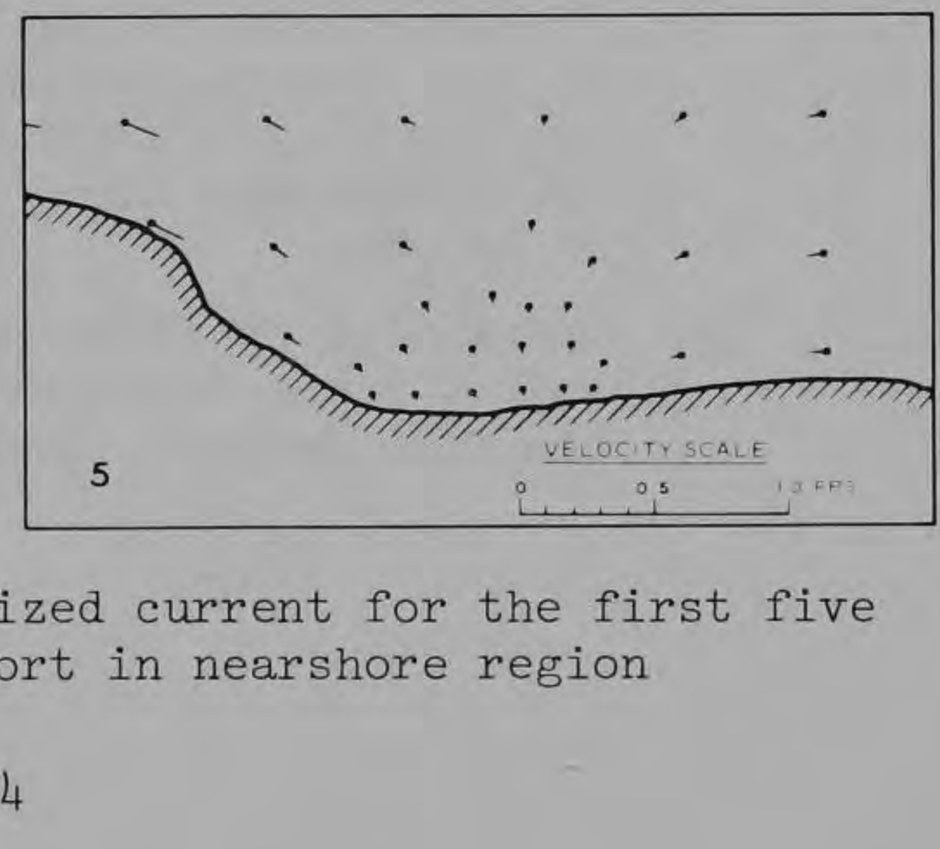

Figure 17. Mode shape and normalized current for the first five eigenvalues without jetport in nearshore region

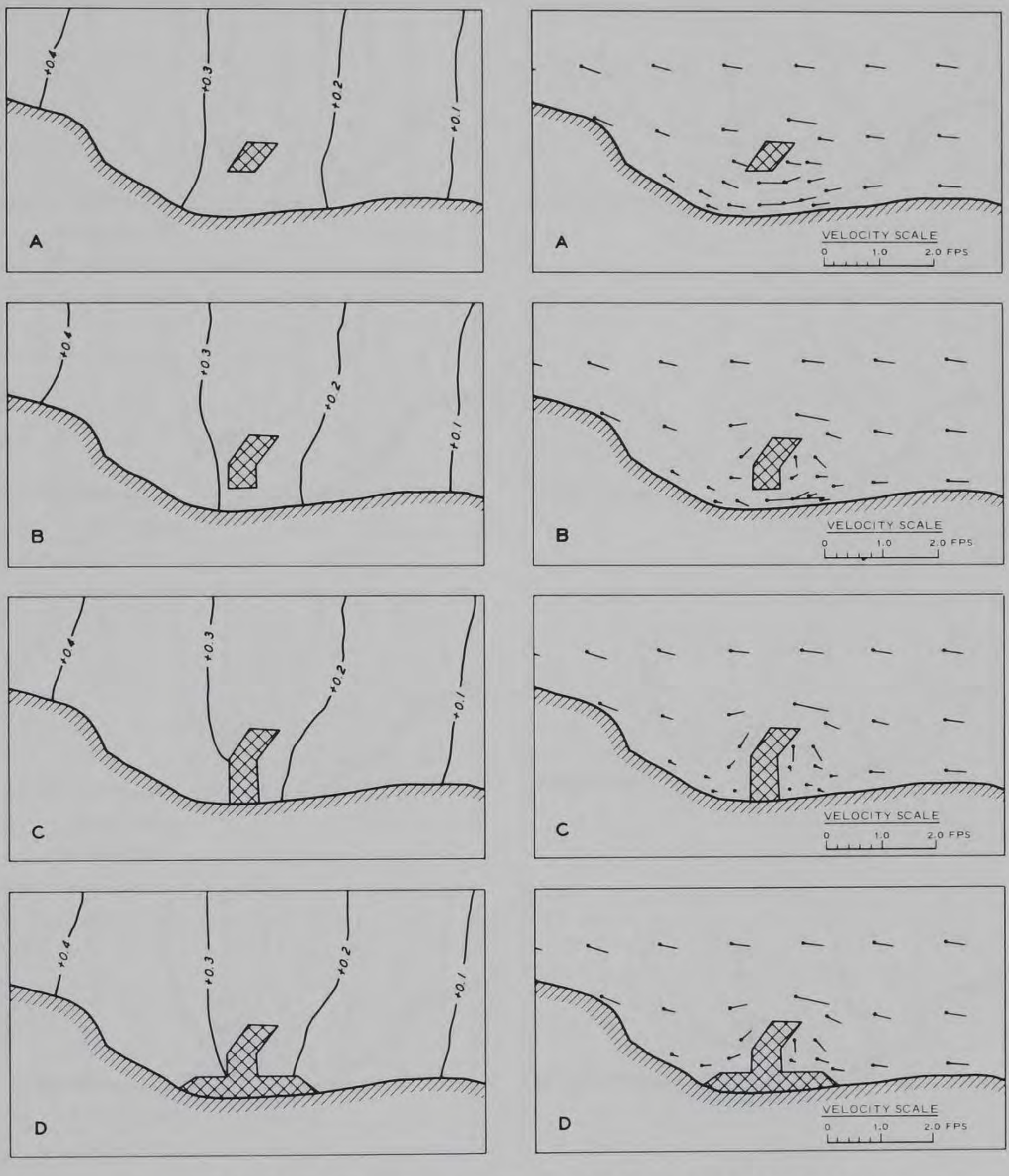

Figure 18. Mode shape and normalized current for first eigenvalue with different jetport configurations

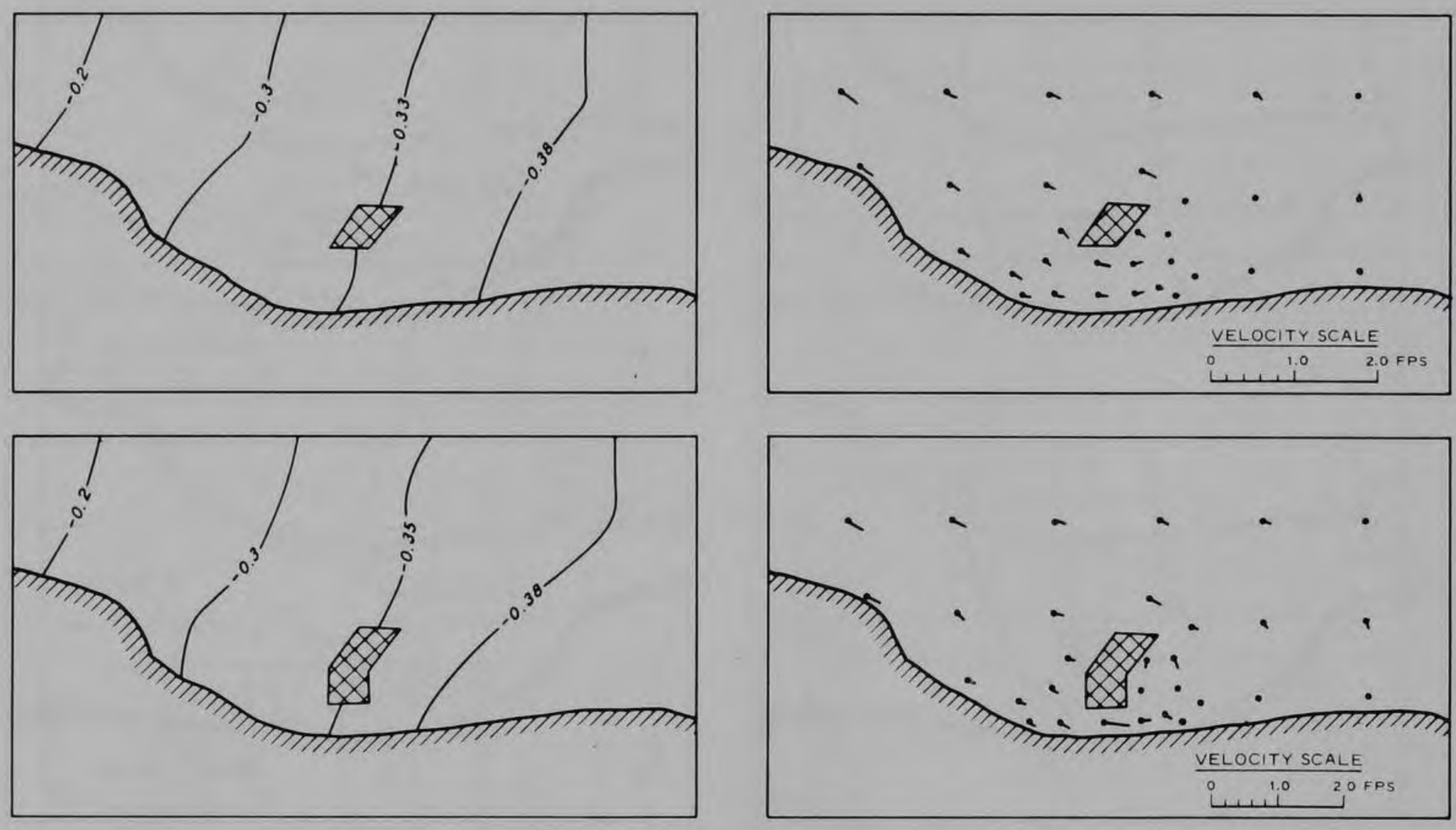

Figure 19. Mode shape and normalized current for second eigenvalue with different jetport configurations

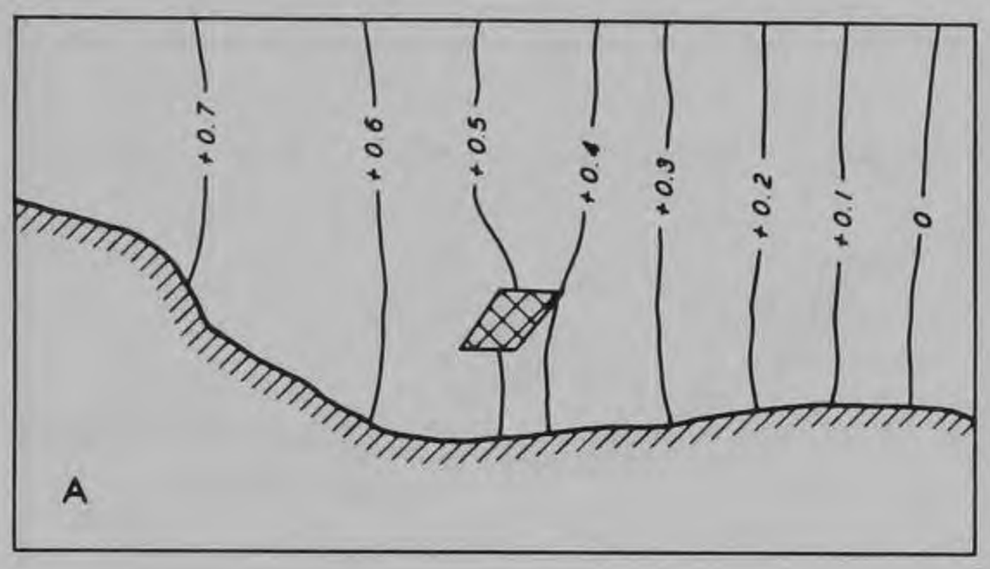

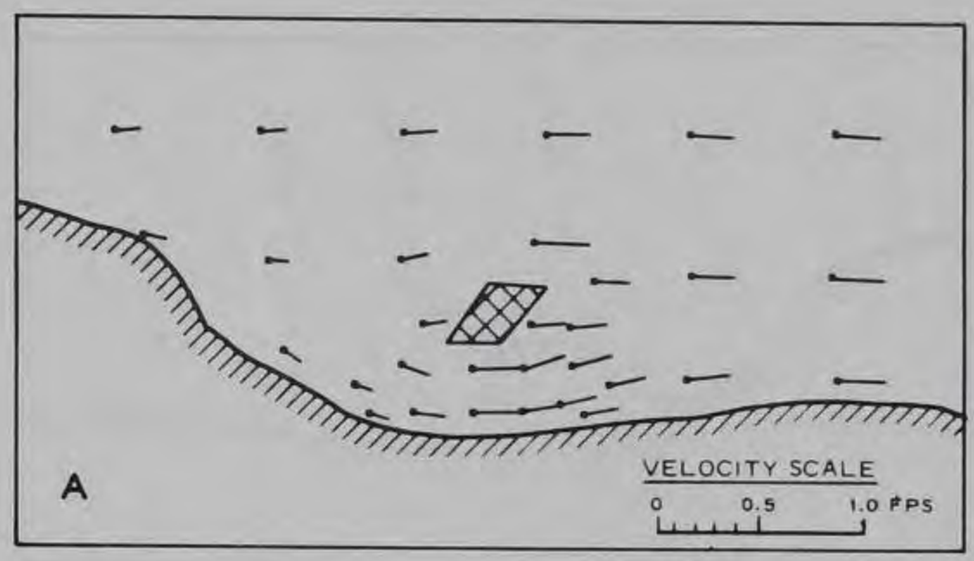

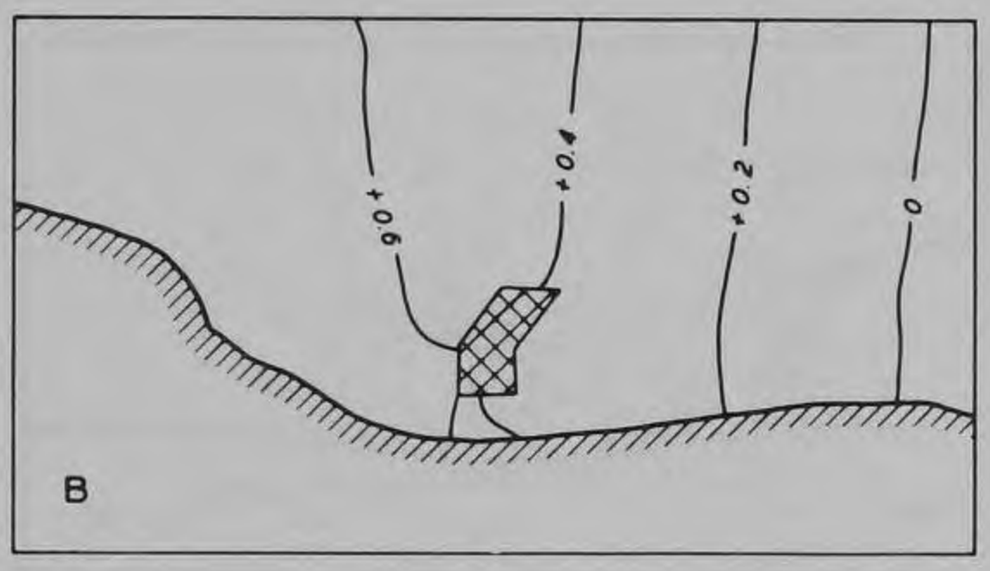

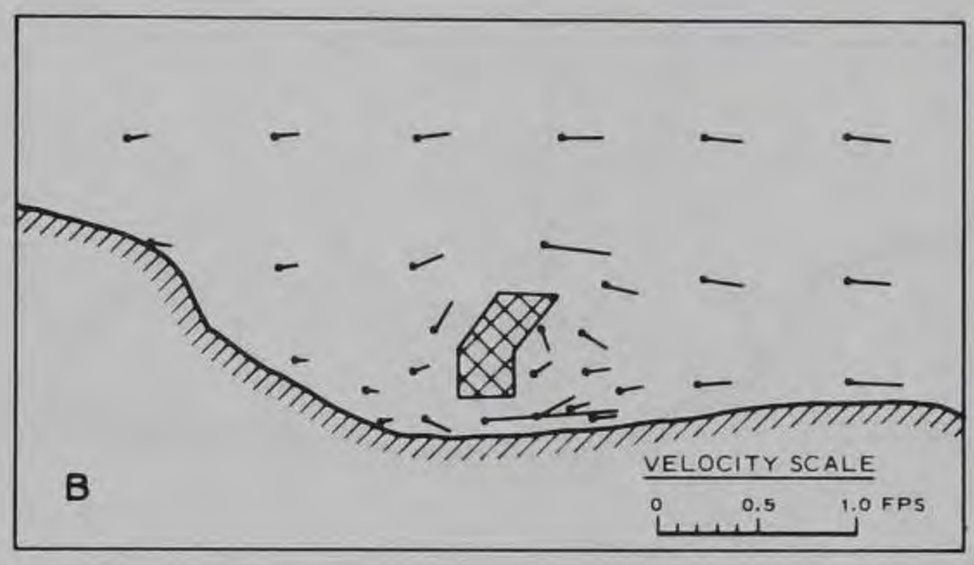

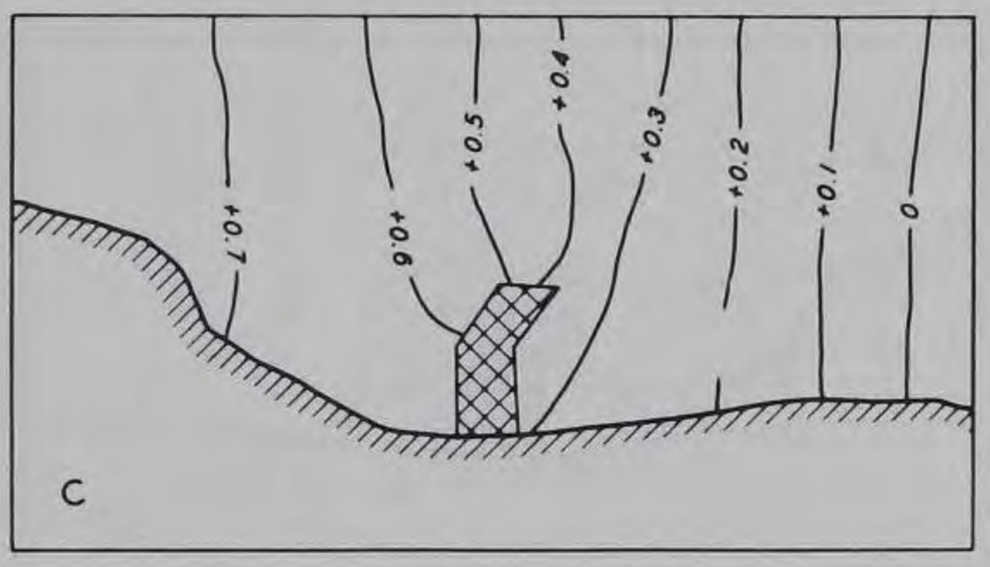

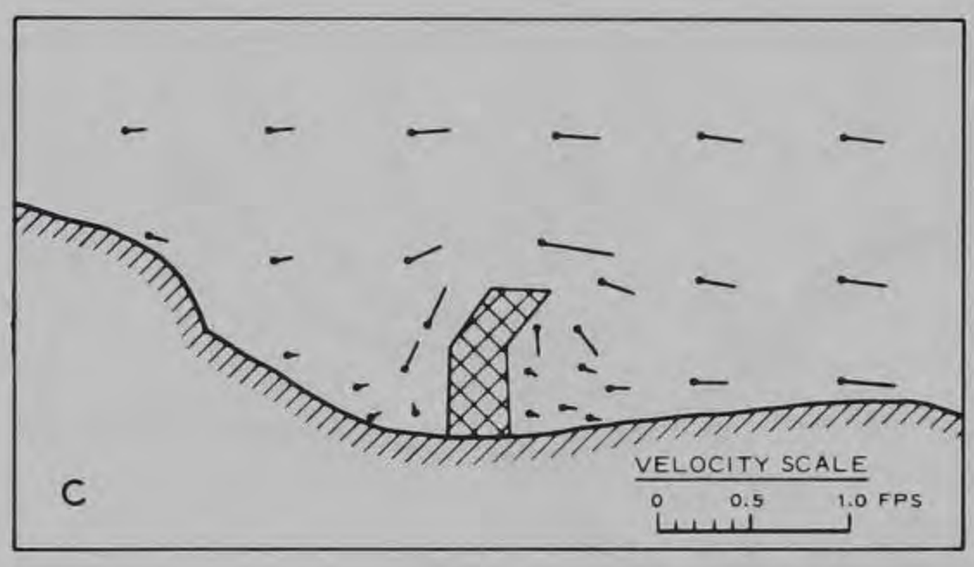

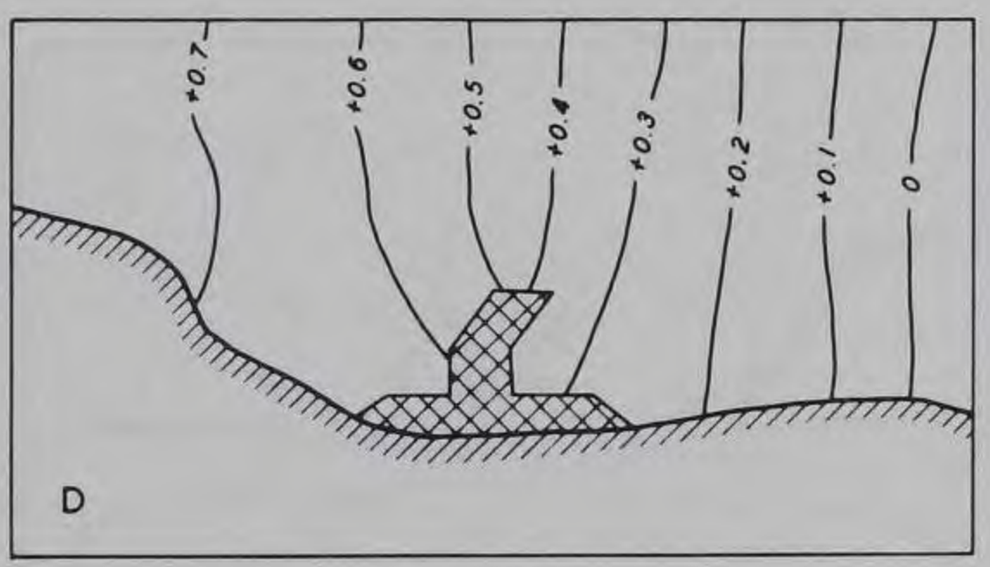

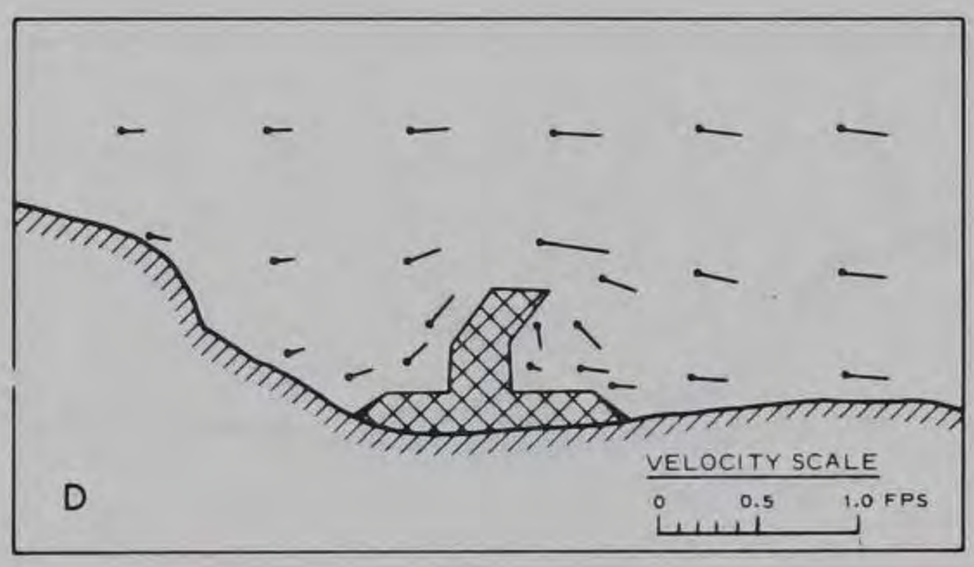

Figure 20. Mode shape and normalized current for third eigenvalue with different jetport configurations

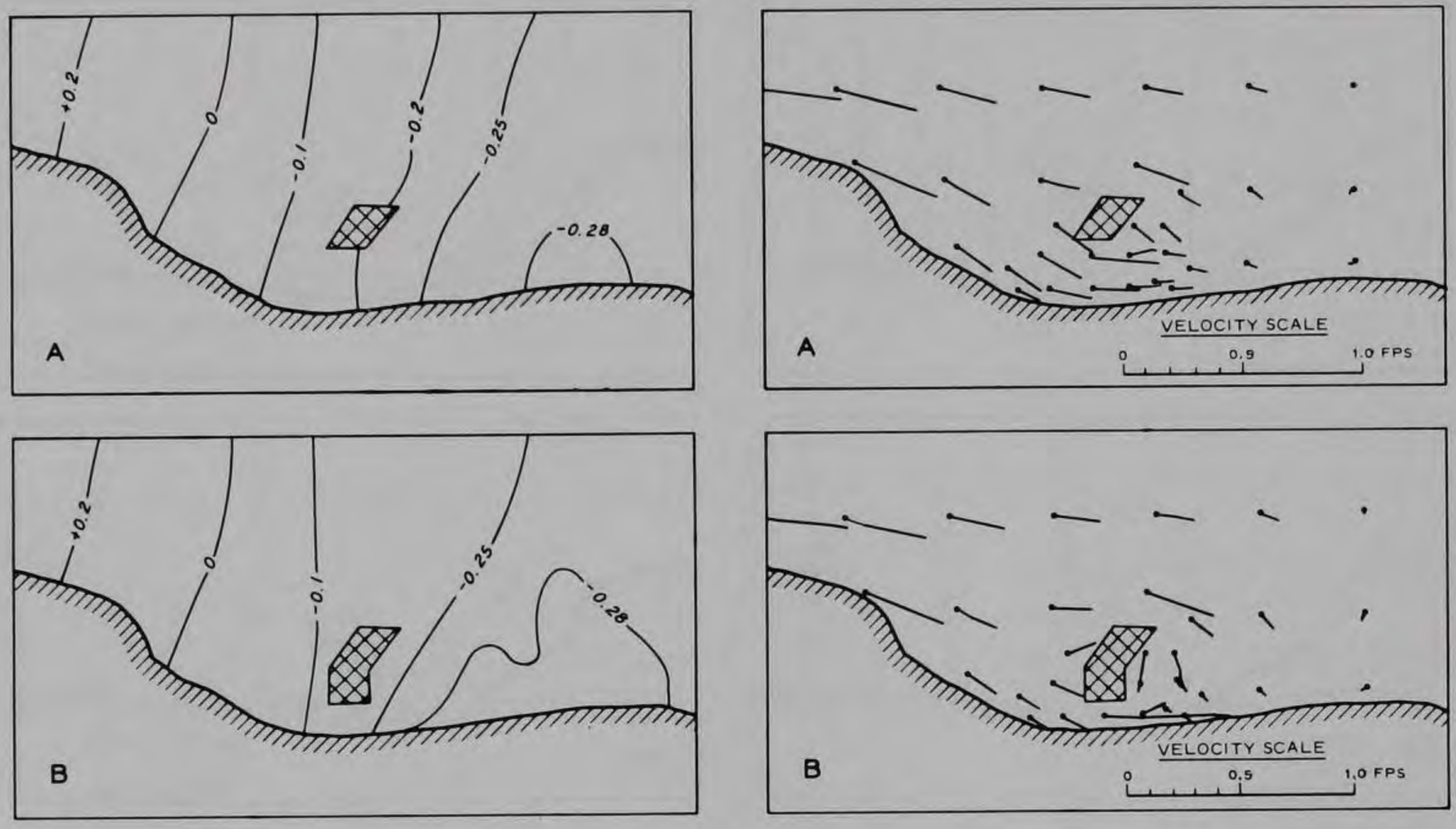

Figure 21. Mode shape and normalized current for fourth eigenvalue with different jetport configurations

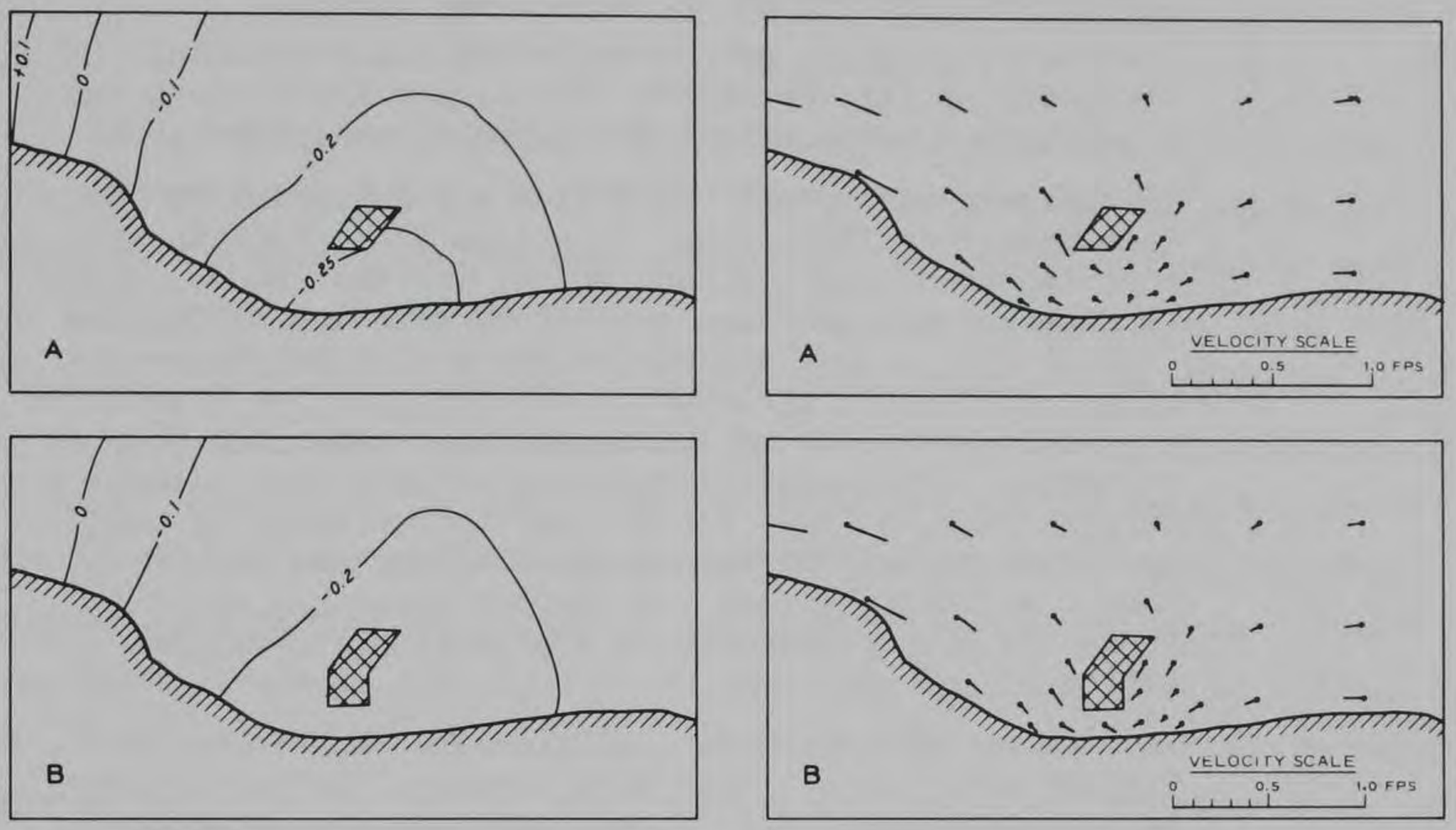

Figure 22. Mode shape and normalized current for fifth eigenvalue with different jetport configurations

c. Changes in relative seiche amplitude due to any of the four jetport configurations are equal to or less than 0.1 ft for a 1.0-ft maximum seiche amplitude or no greater than 10 percent change in seiche amplitudes.

d. Changes in relative seiche amplitude and horizontal gradients of this amplitude are largest for jetport configuration C and smallest for jetport configuration A.

e. The largest horizontal velocities are generated by the fundamental or first mode of oscillation, which is the most important and dominant mode. For this mode, jetport configuration A produces a relative velocity of 0.5 fps (relative to 1.0-ft maximum seiche amplitude) between shore and jetport structure, and configuration B produces a relative velocity of 1.0 fps between shore and jetport structure. The relative velocity in this area without a jetport is 0.25 fps. For the first four modes of oscillation, both configurations A and B increase the horizontal velocity between the jetport structure and the shoreline with configuration B producing the largest increases.

f. Recurrence intervals[1] for Buffalo-minus-Toledo setup (seiche wave height) have been computed for the 20-year period 1940-1959. Using these results, the expected frequency of occurrence and absolute values of seiche velocity for the fundamental mode were estimated for existing conditions and configurations A and B (between the jetport structure and the shoreline). These estimates are presented in the following tabulation.

Recurrence Interval, yr	Seiche Amplitude, ft	Velocity, fps		
		Existing	Plan A	Plan B
0.25	3	0.75	1.5	3.0
0.50	3.5	0.875	1.75	3.5
1.0	4	1.0	2.0	4.0
2	5	1.25	2.5	5.0
5	6	1.5	3.0	6.0
20	7	1.75	3.5	7.0

g. Jetport configurations C and D block the alongshore flow near the jetport configurations with configuration C producing the largest decrease in these horizontal velocities and creating areas near the shoreline with minimum or no circulation.

h. Of the four generalized jetport configurations used in this study, jetport configuration A has the least effect on seiche periods, relative seiche amplitudes, and relative horizontal velocities for the first five modes of free oscillation in Lake Erie.

22. This numerical study was conducted to evaluate quantitatively the effects of a jetport in Lake Erie near Cleveland, Ohio, on seiches (free oscillations) in the lake. The four jetport configurations used in this study are tentative and general in configuration and location; however, these configurations should provide results from which the effects of a specific configuration can be extrapolated. The conclusions of this study indicate that the nearshore effects of all jetport configurations are minimal for seiche periods and mode configurations. However, the horizontal velocity regime is most affected by the jetport configurations with the island configuration (configuration A) having the least effect on the velocity regime. These results for the velocity regime indicate that additional studies are needed to determine the nearshore effects of a jetport structure on the velocity regime for steady-state and time-dependent wind-driven circulation in Lake Erie.

PART III: TWO-DIMENSIONAL DEPTH-AVERAGED HYDRODYNAMIC MODELS

General Formulation

23. The generalized three-dimensional differential equations governing the motion of an infinitesimal fluid element are readily derived from basic considerations of mass and momentum. If the coordinate system shown in Figure 23 is used, the three-dimensional governing equations for an infinitesimal fluid element can be expressed in the form of momentum and continuity equations:[11]

Momentum equations

$$\frac{\partial u}{\partial t} + u\frac{\partial u}{\partial x} + v\frac{\partial u}{\partial y} + w\frac{\partial u}{\partial z} - fv = -\frac{1}{\rho}\frac{\partial p}{\partial x} + K\left(\frac{\partial^2 u}{\partial x^2} + \frac{\partial^2 u}{\partial y^2} + \frac{\partial^2 u}{\partial z^2}\right) \quad (16)$$

$$\frac{\partial v}{\partial t} + u\frac{\partial v}{\partial x} + v\frac{\partial v}{\partial y} + w\frac{\partial v}{\partial z} + fu = -\frac{1}{\rho}\frac{\partial p}{\partial y} + K\left(\frac{\partial^2 v}{\partial x^2} + \frac{\partial^2 v}{\partial y^2} + \frac{\partial^2 v}{\partial z^2}\right) \quad (17)$$

$$\frac{\partial w}{\partial t} + u\frac{\partial w}{\partial x} + v\frac{\partial w}{\partial z} + w\frac{\partial w}{\partial z} = -\frac{1}{\rho}\frac{\partial p}{\partial z} + K\left(\frac{\partial^2 w}{\partial x^2} + \frac{\partial^2 w}{\partial y^2} + \frac{\partial^2 w}{\partial z^2}\right) + g \quad (18)$$

Continuity equation

$$\frac{\partial \rho}{\partial t} + \frac{\partial}{\partial x}(\rho u) + \frac{\partial}{\partial y}(\rho v) + \frac{\partial}{\partial z}(\rho w) = 0 \quad (19)$$

where

w = velocity in z direction

f = Coriolis parameter

ρ = density

p = pressure

K = coefficient of eddy viscosity or diffusivity

In the momentum equations the first term is the local acceleration term, the next three terms are the convective or advective acceleration

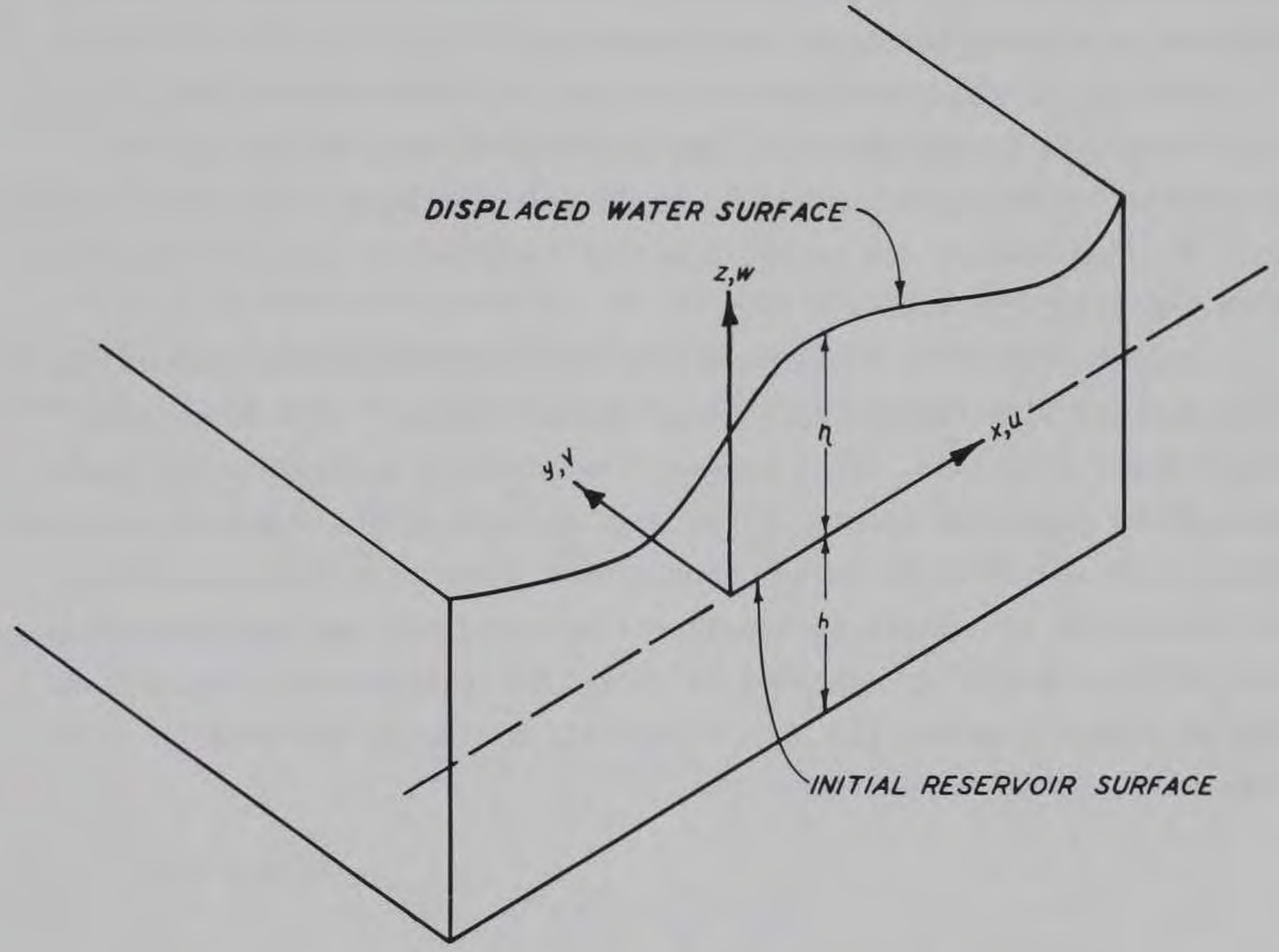

Figure 23. Coordinate system for problem formulation

terms, the next term is the Coriolis force term, followed by the pressure gradient term and the viscous stress or diffusion terms. The continuity equation is simply a statement of the conservation of mass.

24. Various simplifying conditions are applied to the three-dimensional equations to yield a two-dimensional system of equations that can be more readily treated by numerical techniques. If application is made only to problems consistent with restrictions imposed by the various simplifying assumptions, then valuable information can be derived from two-dimensional considerations.

25. A general procedure for reducing the three-dimensional equations to a two-dimensional, depth-averaged formulation will be presented. Most two-dimensional, depth-averaged models are very similar with the differences due to the specific formulation used for the friction and diffusion terms.

26. It is normal to simplify the continuity equation immediately when working with "basically incompressible fluids." The Boussinesq approximation is made, which assumes that density variations are small and can be neglected except in the gravity term of the momentum equation. Thus, even if the fluid is not considered as strictly incompressible, the variation in density is considered as small and the incompressible form of the continuity equation is used. Two-dimensional formulations almost always consider the flow to be well mixed and the density to be constant. Equation 19 reduces to:

$$\frac{\partial u}{\partial x} + \frac{\partial v}{\partial y} + \frac{\partial w}{\partial z} = 0 \qquad (20)$$

27. The vertical component of the local acceleration, advective acceleration, and velocity is assumed to have a negligible effect on the momentum equations. This reduces the momentum equation to:

$$\frac{\partial u}{\partial t} + u \frac{\partial u}{\partial x} + v \frac{\partial u}{\partial y} - fv = - \frac{1}{\rho} \frac{\partial p}{\partial x} + K \left(\frac{\partial^2 u}{\partial x^2} + \frac{\partial^2 u}{\partial y^2} + \frac{\partial^2 u}{\partial z^2} \right) \qquad (21)$$

$$\frac{\partial v}{\partial t} + u\frac{\partial v}{\partial x} + v\frac{\partial v}{\partial y} + fu = -\frac{1}{\rho}\frac{\partial p}{\partial y} + K\left(\frac{\partial^2 v}{\partial x^2} + \frac{\partial^2 v}{\partial y^2} + \frac{\partial^2 v}{\partial z^2}\right) \qquad (22)$$

$$-\frac{1}{\rho}\frac{\partial p}{\partial z} = g \qquad (23)$$

Equation 23 is now simply a statement of the hydrostatic variation of pressure if density is a constant. The hydrostatic pressure assumption is reasonable for shallow-water waves, i.e. long-period waves, where the pressure fluctuations due to a wave are transmitted virtually unattenuated from the surface to the bottom. For intermediate- or short-period waves the hydrostatic assumption may not be a good representation of the pressure.

28. Equations 20-23 are now in the appropriate forms for applying the depth averaging process. Integrating the continuity equation, Equation 20, in the z direction over the water depth gives

$$\int_{-h}^{\eta}\frac{\partial u}{\partial x}\,dz + \int_{-h}^{\eta}\frac{\partial v}{\partial y}\,dz + \int_{-h}^{\eta}\frac{\partial w}{\partial z}\,dz = 0$$

which in turn yields

$$\int_{-h}^{\eta}\frac{\partial u}{\partial x}\,dz + \int_{-h}^{\eta}\frac{\partial v}{\partial y}\,dz + w\Big|_{-h}^{\eta} = 0 \qquad (24)$$

At the water surface,

$$z = \eta(x,y,t)$$

must be a streamline. In other words,

$$\frac{d}{dt}\left[z - \eta(x,y,t)\right] = 0$$

which becomes

$$\frac{dz}{dt} - \left(\frac{\partial \eta}{\partial t} + u \frac{\partial \eta}{\partial x} + v \frac{\partial \eta}{\partial y}\right) = 0$$

or

$$w - \left(\frac{\partial \eta}{\partial t} + u \frac{\partial \eta}{\partial x} + v \frac{\partial \eta}{\partial y}\right) = 0$$

Therefore, the free-surface boundary condition is

$$w = \frac{\partial \eta}{\partial t} + u \frac{\partial \eta}{\partial x} + v \frac{\partial \eta}{\partial y} \quad \text{at} \quad z = \eta \tag{25}$$

If the so-called rigid lid assumption is made, then the boundary condition at the surface reduces to

$$w \equiv 0 \tag{26}$$

The boundary condition at the bottom, $z = -h$, is similar to that at the surface; however, since

$$\frac{\partial h}{\partial t} \equiv 0$$

the boundary condition reduces to

$$w = -\left(u \frac{\partial h}{\partial x} + v \frac{\partial h}{\partial y}\right) \quad \text{at} \quad z = -h \tag{27}$$

Substituting Equations 25 and 27 into 24 yields

$$\int_{-h}^{\eta} \frac{\partial u}{\partial x} dz + \int_{-h}^{\eta} \frac{\partial v}{\partial y} dz + \left(\frac{\partial \eta}{\partial t} + u \frac{\partial u}{\partial x} + v \frac{\partial \eta}{\partial y}\right)_{z=\eta} + \left(u \frac{\partial h}{\partial x} + v \frac{\partial h}{\partial y}\right)_{z=h} = 0 \tag{28}$$

Using differentiation of an integral involving a parameter in the limits of the integral,

$$\frac{\partial}{\partial x}\int_{-h(x,y)}^{\eta(x,y)} u\,dz = u\Big|_{z=\eta}\frac{\partial \eta}{\partial x} + u\Big|_{z=-h}\frac{\partial h}{\partial x} + \int_{-h}^{\eta}\frac{\partial u}{\partial x}\,dz$$

or

$$\int_{-h}^{\eta}\frac{\partial u}{\partial x}\,dz = \frac{\partial}{\partial x}\int_{-h}^{u} u\,dz - u\Big|_{z=\eta}\frac{\partial h}{\partial x} - u\Big|_{z=-h}\frac{\partial h}{\partial x} \qquad (29)$$

In a similar manner

$$\int_{-h}^{\eta}\frac{\partial v}{\partial y}\,dz = \frac{\partial}{\partial y}\int_{-h}^{\eta} v\,dz - v\Big|_{z=\eta}\frac{\partial \eta}{\partial y} - u\Big|_{z=-h}\frac{\partial h}{\partial y} \qquad (30)$$

Substituting Equations 29 and 30 into 28 and cancelling terms gives

$$\frac{\partial}{\partial x}\int_{-h}^{\eta} u\,dz + \frac{\partial}{\partial y}\int_{-h}^{\eta} v\,dz = -\frac{\partial \eta}{\partial t} \qquad (31)$$

The u and v components of velocity are assumed to be of the form

$$u(x,y,z,t) = U(x,y,t)[1 + u'(z)]$$

$$v(x,y,z,t) = V(x,y,t)[1 + v'(z)]$$

where

$$\int_{-h}^{\eta} u'(z)\,dz = 0$$

$$\int_{-h}^{\eta} v'(z)\,dz = 0$$

and

U = x-component of depth-averaged horizontal velocity

u' = depth-dependent perturbation in horizontal velocity in x direction

V = y-component of depth-averaged, horizontal velocity

v' = depth-dependent perturbation in horizontal velocity in y direction

If $U(x,y,t)$ and $V(x,y,t)$ are depth-averaged velocities given by

$$U = \frac{1}{h + \eta} \int_{-h}^{\eta} u \, dz \tag{32}$$

and

$$V = \frac{1}{h + \eta} \int_{-h}^{\eta} v \, dz \tag{33}$$

then the continuity equation reduces to

$$\frac{\partial}{\partial x} [(h + \eta)V] + \frac{\partial}{\partial y} [(h + \eta)V] = - \frac{\partial \eta}{\partial t} \tag{34}$$

29. From the simplified momentum equation in the z direction, Equation 23,

$$- \frac{1}{\rho} \frac{\partial p}{\partial x} = g$$

Integrating from the water surface to an arbitrary depth z gives

$$\int_{z}^{\eta} dp = - \int_{z}^{\eta} \rho g \, dz$$

and

$$p|_z - p|_\eta = -\rho g(\eta - z)$$

or

$$p|_z = \rho g(\eta - z) + p|_\eta \tag{35}$$

Also, it follows that

$$\frac{\partial p}{\partial x} = \rho g \frac{\partial \eta}{\partial x} + \frac{\partial p}{\partial x}\Big|_\eta$$

and

$$\frac{\partial p}{\partial y} = \rho g \frac{\partial \eta}{\partial y} + \frac{\partial p}{\partial y}\Big|_\eta$$

The terms $\partial p/\partial x|_\eta$ and $\partial p/\partial y|_\eta$ represent the variation of atmospheric pressure with horizontal distance at the free surface. These terms are normally neglected, and the pressure gradient is given by

$$\frac{\partial p}{\partial x} = \rho g \frac{\partial \eta}{\partial x} \tag{36}$$

and

$$\frac{\partial p}{\partial y} = \rho g \frac{\partial \eta}{\partial y} \tag{37}$$

30. The momentum equation in the x direction can now be integrated over the depth after substituting from Equation 36 for the pressure gradient.

$$\int_{-h}^{\eta} \frac{\partial u}{\partial t} dz + \int_{-h}^{\eta} u \frac{\partial u}{\partial x} dz + \int_{-h}^{\eta} v \frac{\partial u}{\partial y} dz - \int_{-h}^{\eta} fv \, dz = -\int_{-h}^{\eta} g \frac{\partial \eta}{\partial x} dz$$

$$+ K \int_{-h}^{\eta} \left(\frac{\partial^2 u}{\partial x^2} + \frac{\partial^2 u}{\partial y^2} + \frac{\partial^2 u}{\partial z^2} \right) dz \tag{38}$$

Considering the individual terms in this equation and performing the indicated integration gives

$$\int_{-h}^{\eta} \frac{\partial u}{\partial t}\, dz = \int_{-h}^{\eta} \frac{\partial}{\partial t} \left\{U[1 + u'(z)]\right\} dz = (h + \eta) \frac{\partial U}{\partial t}$$

$$\int_{-h}^{\eta} u \frac{\partial u}{\partial x}\, dz = \int_{-h}^{\eta} U[1 + u'(z)] \frac{\partial U}{\partial x}\, dz = U \frac{\partial U}{\partial x} (h + \eta)$$

$$\int_{-h}^{\eta} v \frac{\partial u}{\partial y}\, dz = \int_{-h}^{\eta} V[1 + u'(z)] \frac{\partial U}{\partial y}\, dz = V \frac{\partial U}{\partial y} (h + \eta)$$

$$\int_{-h}^{\eta} fv\, dz = f \int_{-h}^{\eta} V[1 + v'(z)]\, dz = fV (h + \eta)$$

$$\int_{-h}^{\eta} K \frac{\partial^2 u}{\partial x^2}\, dz = \int_{-h}^{\eta} K \frac{\partial^2}{\partial x^2} [U(1 + u'(z)]\, dz = K \frac{\partial^2 U}{\partial x^2} (h + \eta)$$

$$\int_{-h}^{\eta} K \frac{\partial^2 u}{\partial y^2}\, dz = K \frac{\partial^2 U}{\partial y^2} (h + \eta)$$

$$\int_{-h}^{\eta} K \frac{\partial^2 U}{\partial z^2}\, dz = \int_{-h}^{\eta} \frac{\partial}{\partial z}\left(K \frac{\partial U}{\partial z}\right) dz = \int_{-h}^{\eta} \frac{\partial}{\partial z}(\tau_x)\, dz$$

$$= \int_{-h}^{\eta} d\tau_x = \tau_x\Big|_{\eta} - \tau_x\Big|_{-h}$$

where τ_x is stress in the x direction. Therefore, the basic momentum equation in the x direction becomes

$$\frac{\partial U}{\partial t} + U \frac{\partial U}{\partial x} + V \frac{\partial U}{\partial y} = - g \frac{\partial \eta}{\partial x} + fV + \frac{\tau_{wx}}{\rho(h + \eta)} - \frac{\tau_{Bx}}{\rho(h + \eta)}$$

$$+ K\left(\frac{\partial^2 U}{\partial x^2} + \frac{\partial^2 U}{\partial y^2}\right) \qquad (39)$$

where

τ_{wx} = the x-component of wind stress at the water surface

τ_{Bx} = the x-component of bottom friction

31. In a similar manner the momentum equation in the y direction becomes

$$\frac{\partial V}{\partial t} + U \frac{\partial V}{\partial x} + V \frac{\partial V}{\partial y} = - g \frac{\partial \eta}{\partial y} - fU + \frac{\tau_{wy}}{\rho(h + \eta)} - \frac{\tau_{By}}{\rho(h + \eta)}$$

$$+ K\left(\frac{\partial^2 V}{\partial x^2} + \frac{\partial^2 V}{\partial y^2}\right) \qquad (40)$$

where

τ_{wy} = the y-component of wind stress at the water surface

τ_{By} = the y-component of bottom friction.

32. Equations 34, 39, and 40 form the basis for most two-dimensional, depth-averaged models. These equations can be formulated in terms of finite difference equations for solution. It should be noted that while the equations are formulated in terms of two-dimensional horizontal velocity components, a pseudo-three-dimensional effect is present since actual depths are input to the model.

Discussion of Specific Models

33. The two-dimensional depth-averaged formulation was shown to reduce to the system of equations represented by Equations 34, 39, and 40. These differential equations must be discretized and formulated in terms of finite difference equations for solution by numerical techniques.[12] The finite difference representation of the differential equations is not unique; it can be formulated in terms of backward differences, forward differences, central differences, or some combination of these difference schemes. The problem also can be formulated such that it is explicit, implicit, or implicit-explicit in time. Each method of formulation does offer advantages and disadvantages, although some formulation schemes have been shown to be completely unsatisfactory. In general, the explicit techniques are simpler to formulate and require less computer time for a given size time step. The explicit schemes, however, have stability criteria that normally require a smaller step size than the comparable calculation using an implicit scheme.

34. Basically the two-dimensional depth-averaged models are used for two different types of problems. In the first case the determination of circulation patterns is the primary objective with wind or tides being the predominant forcing function. The second type of application is used mainly to calculate the displacement of the free surface during storm surge. Experience has shown that the importance of the various terms in the governing equations and the boundary conditions vary with the application. For example, the nonlinear advective terms and horizontal diffusion terms are normally neglected in the

storm surge models while they may be very important in circulation models, particularly near the shore.

35. Several specific two-dimensional depth-averaged models will now be discussed. The departure of each model from the basic formulation of the problem will be outlined. Applications and verification of the model will be discussed along with the general conclusions of the authors. The models discussed are representative of the many two-dimensional models available.

Model of T. J. Simons

36. The two-dimensional numerical model by T. J. Simons[13] is a straightforward application of the two-dimensional, depth-averaged equations. The model is formulated, however, in terms of volumetric flow rate per unit width (foot) rather than average velocities.

$$(P,Q) = \int_{-h}^{\eta} (u,v)\, dz \tag{41}$$

where P and Q are volumetric flows in x and y directions, respectively. The depth-averaged velocities can be obtained by averaging the volume transport over depth.

$$(U,V) = \frac{(P,Q)}{h + \eta} \tag{42}$$

37. The equations used in the model to calculate volume transport are as follows:

$$\frac{\partial p}{\partial t} + P \frac{\partial p}{\partial x} + Q \frac{\partial p}{\partial y} = - gh \frac{\partial \eta}{\partial x} + fQ + \frac{\tau_{wx}}{\rho} - \frac{\tau_{Bx}}{\rho} + A \left(\frac{\partial^2 P}{\partial x^2} + \frac{\partial^2 P}{\partial y^2} \right) \tag{43}$$

$$\frac{\partial Q}{\partial t} + P \frac{\partial Q}{\partial x} + Q \frac{\partial Q}{\partial y} = - gh \frac{\partial \eta}{\partial y} - fP + \frac{\tau_{wy}}{\rho} - \frac{\tau_{By}}{\rho} + A \left(\frac{\partial^2 Q}{\partial x^2} + \frac{\partial^2 Q}{\partial y^2} \right) \tag{44}$$

$$\frac{\partial \eta}{\partial t} = - \frac{\partial P}{\partial x} - \frac{\partial Q}{\partial y} \tag{45}$$

These equations are completely consistent with Equations 34, 39, and 40.

38. Simons expresses the bottom stress in terms of a bottom friction coefficient and the components of volume transport.

$$\frac{\tau_{Bx}}{\rho} = BP \tag{46}$$

$$\frac{\tau_{By}}{\rho} = BQ \tag{47}$$

The bottom stress coefficient is considered to be represented by the following simple relationships:

a. $B = a/h$ where $a \approx 0.01$ cm/sec

b. $B = b/h^2$ where $b \approx 100$ cm^2/sec

c. $B = c|P,Q|/h^2$ where $c \approx 0.0025$

39. The external forces during circulation are the surface pressure and the wind stress. In these calculations the surface pressure is set equal to zero. The surface wind stress is related to the wind velocity; however, this relationship is not considered in this model. Instead, more or less typical wind stress fields are specified. The wind stress fields are taken to simulate the general behavior of the wind following the passage of an atmospheric front. The winds tend to increase sharply for a relatively short period of time and thereafter vary more slowly. At the same time the wind field will move across the lake in the general direction of the wind stress itself. Idealizing this situation, a semi-infinite stress band moving with a constant translation speed V_s and having a linear increase of intensity of wind stress over a period of time T_s and a constant intensity after time T_s is used in the model.

40. The system of equations is solved using central differences and an implicit scheme. A space-staggered lattice is used on which velocity, water level displacement, and water depth are described at different locations within a grid cell.

41. The primary application of the model is to predict circulation patterns in lakes. The model has been applied to Lake Ontario both with and without the nonlinear advective terms in the equation. A 5-km rectangular grid was used, and circulation patterns are shown at various times during the passage of a hypothetical wind field.

42. Based upon numerical experimentation with the various parameters in the model, the following conclusions as to the effects of these parameters are presented:

a. The actual effect of the nonlinear terms does not seem to justify the tremendous increase in computational effort.

b. The nonlinear effects are completely obscured by the effects of bottom topography, bottom friction, and horizontal diffusion.

c. Increased efforts should be directed at increasing horizontal resolution and improving numerical treatment of the boundaries.

d. The actual formulation used for the bottom stress coefficient does not have a great effect on the circulation pattern as long as a reasonable formulation is used.

e. The smoothing effect of the horizontal diffusion term is considerable.

f. The vertically integrated or averaged velocities produced by the model are not indicative of the actual velocities found in a lake. In general, the volume transport model tends to underestimate the magnitude of the surface velocities, the time variation of the flow, and the Coriolis force effect.

g. A three-dimensional or layered model is needed for velocity distributions in a lake.

Model of George W. Platzman

43. The primary application of the model by Platzman[14] is to predict surface displacement during storm surge on lakes. The formulation of the problem is in term of volume transport rather than average velocity. The basic equations are essentially identical with those by Simons, Equations 43-45, except that the nonlinear advective terms and the horizontal diffusion terms are neglected.

44. While the equations used by Platzman are similar to those used by Simons, the wind stress and bottom friction terms are handled

differently. Coefficients that are functions of the Ekman number are introduced in such a manner that the solution for steady-state transport reduces to the analytical solution obtained by Ekman[15] for surface slope transport and wind transport. Basically, the bottom friction is related to the transport, and wind stress is related to the square of the wind speed; however, the various parameters are expressed as a function of the Ekman number.

45. The system of equations is solved using central differences in time and space and a space-staggered lattice upon which velocities, water level displacements, and water depths are described at different locations within a grid cell. The model provides for a time and spatial variation of wind stress by input of actual wind data.

46. The model is applied to nine actual extreme storm surge conditions on Lake Erie with wind stress information based upon hourly surface wind observations at six weather stations located on the periphery of the lake. The wind field on the lake varies with time and position and is based upon a weighted average of the wind data from the six weather stations. Computed lake-level configurations have been compared with observed data for the nine extreme storm surge conditions considered.

47. The following conclusions on the applicability of the model for storm surge analysis are presented:

a. The computed wind setup values agree well with observed values.

b. Perhaps the most conspicuous defect of the computations is failure to predict the free oscillations of the lake after the passing of the storm.

c. Improvements in the model would probably result from more careful consideration of the effect of differences in anemometer exposure for the various wind stations used in the analysis.

Model of J. J. Leendertse

48. The primary application of the model by Leendertse[16] is for circulation patterns for tidal flows in bays and estuaries. The basic governing equations are identical with Equations 34, 39, and 40. The horizontal diffusion terms are neglected; while wind stress is included

in the formulation, tidal elevations are the primary forcing function. The bottom stress term is considered proportional to the squared velocity and is formulated in terms of the Chezy coefficient, C, as follows:

$$\tau_{Bx} = \rho g U \sqrt{\frac{U^2 + v^2}{C^2}} \tag{48}$$

$$\tau_{By} = \rho g V \sqrt{\frac{u^2 + v^2}{C^2}} \tag{49}$$

The wind stress is formulated in the normal manner in terms of the square of the wind speed.

49. An explicit-implicit scheme is used to solve the system of equations using a space-staggered grid arrangement where velocities, surface displacement, and depths are defined at different locations in the grid system. This model has been applied to the North Sea, Jamaica Bay, Tokyo Bay and other large bodies of water. The general conclusions regarding the model are as follows:

a. For applications to bays, harbors, inlets, etc., where tidal elevations are the predominant forcing function and where a significant volume transport occurs, the depth-averaged circulation patterns appear to give reasonable results.

b. The model can also be used to model water waves generated by nuclear explosions, tsunami waves, and other long-period wave motion.

50. This model has no direct applicability to the problem of wind-driven circulation or storm surge on Lake Erie. The implicit-explicit numerical scheme used to solve the system of difference equations was of primary interest in this model. This basic numerical procedure has several desirable features that might prove beneficial if the procedure were applied to a model of Lake Erie. This particular solution scheme was investigated since it had not been used previously in a lake model.

Model of Frank D. Masch

51. The model by Masch[17] is primarily intended for application to estuaries where significant tidal flats exist. The basic equations are

formulated in terms of volume transport and are essentially identical to Equations 43-45. The bottom friction term is expressed in terms of the Manning friction factor, $\bar{n}$:

$$\frac{\tau_{Bx}}{\rho} = \frac{g\bar{n}^2 P}{2.21h^{7/3}} \sqrt{P^2 + Q^2} \tag{50}$$

$$\frac{\tau_{By}}{\rho} = \frac{g\bar{n}^2 Q}{2.21h^{7/3}} \sqrt{P^2 + Q^2} \tag{51}$$

Horizontal diffusion is neglected. This model is basically an extension of the Reid-Bodine model.[18]

52. The model contains provisions for flooding of tidal flats, such obstructions to flow as weirs or breakwaters, and other phenomena somewhat peculiar to tidal flows in estuaries. Several computational boundaries can be represented in the model indicating ocean boundaries, river inflows, or artificial boundaries established in the estuary for computational convenience. This model has been applied to several locations including Matagorda Bay and Galveston Bay, Texas, and Masonboro Inlet, North Carolina. As a result of these applications, it was concluded that:

a. Surface displacements and volume transport due to tidal forces can be predicted reasonably well with the model.

b. Flooding of tidal flats, underwater obstructions, breakwaters, and similar obstruction to flow can be included in the model if step sizes are small enough for the necessary spatial resolution.

53. This model has no direct application to the problem of wind-driven circulation or storm surge on Lake Erie. This model was investigated because of the detailed treatment of numerical procedures for treating breakwaters, weirs, underwater obstructions, flows from streams into the region being considered, flooding regions, and other hydrodynamic features. These phenomena have not been treated in detail in previous lake models, and their use may be necessary in modeling a

jetport in Lake Erie and its effect on circulation, particularly in Cleveland Harbor.

Model of David F. Paskausky

54. The model by Paskausky[19] has its origin in the three-dimensional equations of hydrodynamics; however, the development of the model differs significantly from the models discussed previously. The primary application of the model is for storm surge; however, the volume transport per unit width (foot) is the model output. A rigid lid assumption is made at the water surface.

55. The development of this model initially follows the basic formulation of the two-dimensional depth-averaged model. Consider Equations 20-23, which are the simplified three-dimensional differential equations prior to vertical integration over the water depth. Differentiation of Equation 21 by $-\partial/\partial y$ and Equation 22 by $\partial/\partial x$ introduction of the vorticity component $\hat{\zeta}$ and shear stress components τ_x and τ_y

$$\hat{\zeta} = \frac{\partial v}{\partial x} - \frac{\partial u}{\partial y}\ ,\quad \tau_x = K\frac{\partial u}{\partial z}\ ,\quad \tau_y = K\frac{\partial v}{\partial z}$$

and addition of the two equations yield the vorticity equation:

$$\overbrace{\frac{\partial \hat{\zeta}}{\partial t} + (f + \hat{\zeta})\left(\frac{\partial u}{\partial x} + \frac{\partial v}{\partial y}\right)}^{\bar{A}} + \overbrace{\left(u\frac{\partial \hat{\zeta}}{\partial x} + v\frac{\partial \hat{\zeta}}{\partial y}\right)}^{\bar{B}} + \overbrace{\left(\frac{\partial f}{\partial y}v\right)}^{\bar{C}}$$

$$+ \overbrace{\frac{\partial v}{\partial z}\frac{\partial w}{\partial x} - \frac{\partial u}{\partial z}\frac{\partial w}{\partial y} + W\frac{\partial \hat{\zeta}}{\partial z}}^{\bar{D}} = \overbrace{K\left(\frac{\partial^2 \hat{\zeta}}{\partial x^2} + \frac{\partial^2 \hat{\zeta}}{\partial y^2}\right)}^{\bar{E}}$$

$$\overbrace{- \frac{\partial}{\partial z}\left(\frac{\partial \tau_y}{\partial x} - \frac{\partial \tau_x}{\partial y}\right)}^{\bar{F}} \qquad (52)$$

In Equation 52, $\bar{A}$ is the topographic term, $\bar{B}$ is the horizontal advection term, $\bar{C}$ is the planetary vorticity term, $\bar{D}$ is the vertical advection term, $\bar{E}$ is the lateral friction term, and $\bar{F}$ is the net torque per unit volume exerted on the top and bottom of a water parcel.

The vertical advection term vanishes for a well mixed, constant-density application.

56. By combining terms and ignoring the vertical advection term, Equation 52 can be written in the form:

$$\frac{\partial \hat{\zeta}}{\partial t} + \vec{\nabla}_h \cdot (f + \hat{\zeta})\, \vec{V}_h = K_h\, \nabla_h^2\, \hat{\zeta} - \frac{\partial}{\partial z} (\text{curl } \tau) \qquad (53)$$

where

$$\vec{\Delta}_h = \vec{i}\,(\partial/\partial x) + \vec{j}\,(\partial/\partial y)$$

$$\vec{V}_h = \vec{i}u + \vec{j}v$$

$$\nabla_h^2 = (\partial^2/\partial x^2) + (\partial^2/\partial y^2)$$

$$\text{curl } \tau = (\partial \tau_y/\partial x) - (\partial \tau_x/\partial y)$$

in which $\vec{i}$ is unit vector in the x direction and $\vec{j}$ is unit vector in the y direction. Equation 53 is now integrated over the depth, D, to obtain a two-dimensional depth-averaged model.

$$\int_o^D \frac{\partial \hat{\zeta}}{\partial t}\, dz + \int_o^D \vec{\nabla}_h \cdot (f + \hat{\zeta})\, \vec{V}_h\, dz = K_h \int_o^D \nabla_h^2\, \hat{\zeta}\, dz - \int_o^D \frac{\partial}{\partial z} (\text{curl } \tau)\, dz \qquad (54)$$

Considering the individual terms in the equation for the well mixed, constant-density condition and assuming the bottom friction stress equal to the mass flux multiplied by a bottom friction coefficient σ gives

$$\int_o^D \frac{\partial \hat{\zeta}}{\partial t}\, dz = \frac{\partial \hat{\zeta}}{\partial t} \int_o^D dz = D\, \frac{\partial \hat{\zeta}}{\partial t}$$

$$\int_0^D \vec{\nabla}_h \cdot (f + \hat{\zeta})\, \vec{V}_h \, dz = \vec{\nabla}_h \cdot \int_0^D (f + \hat{\zeta})\, \vec{V}_h \, dz - \left[(f + \hat{\zeta})\, \vec{V}_h\right]\Big|_D \cdot \nabla_h D$$

$$= \vec{\nabla}_h \cdot \left[(f + \hat{\zeta})\, \vec{V}_h \int_0^D dz\right] - \left[(f + \hat{\zeta})\, \vec{V}_h\Big|_D \cdot \nabla_h D\right]$$

$$= \vec{\nabla}_h \cdot \left[(f + \hat{\zeta})\, \vec{V}_h D\right] - \left[(f + \hat{\zeta})\, \vec{V}_h\Big|_D \cdot \vec{\nabla}_h D\right]$$

$$= D\nabla_h \cdot \left[(f + \hat{\zeta})\, \vec{V}_h\right]$$

$$K_h \int_0^D \nabla_h^2 \hat{\zeta}\, dz = \left[K_h \nabla^2 \hat{\zeta}\right] D$$

$$\int_0^D \frac{\partial}{\partial z} (\text{curl } \tau)\, dz = \text{curl } \tau \Big|_0^D = \text{curl } \tau\Big|_D - \text{curl } \tau\Big|_0$$

$$= \left(\frac{\partial \tau_y}{\partial x} - \frac{\partial \tau_x}{\partial y}\right)\Bigg|_D - \text{curl } \tau\Big|_0$$

$$= \frac{\partial}{\partial x} (vD\bar{\sigma}) - \frac{\partial}{\partial y} (uD\bar{\sigma}) - \text{curl } \tau\Big|_0$$

$$= D\bar{\sigma} \left(\frac{\partial V}{\partial x} - \frac{\partial U}{\partial y}\right) - \text{curl } \tau\Big|_0$$

$$= D\bar{\sigma}\zeta - \text{curl } \tau\Big|_0$$

Where K_h is the horizontal diffusion coefficient, Equation 54 reduced to

$$\frac{\partial \hat{\zeta}}{\partial t} + \vec{\nabla}_h \cdot (f + \hat{\zeta}) \vec{V}_h = K_h \nabla_h^2 \hat{\zeta} - \bar{\sigma} \hat{\zeta} - \frac{1}{D} \text{curl } \tau \Big|_0 \qquad (55)$$

An Ekman boundary layer approximation for the bottom friction coefficient is used at the sea bed:

$$\bar{\sigma} = \left(\frac{0.5 K_v f}{D} \right)^{1/2}$$

where K_v is the vertical diffusion coefficient.

57. Integrating the continuity equation (Equation 45) across the depth yields

$$\int_0^D \left(\frac{\partial u}{\partial x} + \frac{\partial v}{\partial y} + \frac{\partial w}{\partial z} \right) dz = D \frac{\partial u}{\partial x} + D \frac{\partial v}{\partial y} + w \Big|_0^D = 0$$

Using the "rigid lid" boundary condition (Equation 26) at the free surface and the bottom boundary condition (Equation 27) reduces to

$$\frac{\partial}{\partial x} (Du) + \frac{\partial}{\partial y} (Dv) = 0 \qquad (56)$$

A volume transport stream function ψ exists, such that

$$\frac{\partial \psi}{\partial x} = - Dv \quad , \quad \frac{\partial \psi}{\partial y} = Du \qquad (57)$$

In terms of ψ the vorticity component $\hat{\zeta}$ is given by

$$\hat{\zeta} = \frac{\partial v}{\partial x} - \frac{\partial u}{\partial y}$$

$$\hat{\zeta} = \frac{\partial}{\partial x} \left(\frac{1}{D} \frac{\partial \psi}{\partial x} \right) + \frac{\partial}{\partial y} \left(\frac{1}{D} \frac{\partial \psi}{\partial y} \right) \qquad (58)$$

Use of Equation 58 with a knowledge of $\hat{\zeta}$ from Equation 55 allows evaluation of ψ by relaxation subject to appropriate boundary conditions. The velocity field can then be calculated from Equation 57.

58. The model has been applied to Lake Ontario for a simplified storm condition passing along the long axis of the lake. The velocity conditions in the lake are calculated at various times during the passage of the storm. The model has also been applied to Lake Erie during the passage of storm Agnes.[20]

59. While the results from this model are qualitatively interesting, certain of its assumptions are subject to question. The volume transport, which is integrated over the depth of the lake, and hence the surface elevations may be reasonably correct; however, these values cannot be related to prototype velocity values in the lake, which are highly depth dependent. The applicability of the rigid lid assumption made in this model is questionable for storm surge.

Limitations of the Models

60. From the literature survey of the various two-dimensional hydrodynamic models available and based upon the experience at WES with some of these models, the applicability and limitations of these models become fairly apparent:

a. Two-dimensional models will probably yield reasonable results in lakes for storm surge (free surface displacement) if a free surface rather than a rigid lid boundary condition is used at the lake surface. Free surface displacement is basically a function of the total mass transport, and two-dimensional models appear reasonably capable of representing this phenomenon.

b. Two-dimensional models will not yield results for depth-dependent, wind-driven lake currents, which are representative of the currents existing in the lake.

c. Two-dimensional models probably yield reasonable values for both surface displacements and currents in estuaries and bays if large salinity variations are not present.

61. The first and second conclusions appear in conflict at first inspection. This apparent conflict can be resolved by considering the

difference in surface elevations required to produce a specified velocity. Very small changes in surface elevation can produce significant velocities. Thus, the two-dimensional mathematical model can predict values of surface displacement in reasonable agreement with experimental data if the total mass transport is approximately correct. At the same time very poor representations of the actual currents in the lake are produced by the models due to the complex depth-dependent velocities existing in the lake. In most freshwater lakes the throughflow is small, and wind is the major current-producing forcing function. The current pattern is extremely depth dependent, varying in direction from surface to bottom by essentially 180 deg. A depth-integrated velocity such as produced by the two-dimensional models will generally yield a very small average velocity proportional to the lake throughflow and completely fail to indicate the very complex depth-dependent velocities existing in the lake.

62. Since the two-dimensional models have no provisions for a return flow along the bottom of the lake, they must establish return flow regions in the lake itself when wind is the primary forcing function. The depth-averaged flows predicted by the two-dimensional models will tend to be in the wind direction in the shallow areas of the lake with a return flow in the deeper portions. This flow further distorts the current pattern obtained from the two-dimensional model from those actually existing in the lake.

63. Because conditions in estuaries and bays normally are more consistent with the basic assumptions used in the derivation of two-dimensional models, the results are in better agreement with prototype conditions. For estuaries and bays, the primary forcing function is the tide, and significant mass transport does occur. The velocity distribution over the depth is generally in approximately the same direction and of the same order of magnitude. A depth-averaged velocity therefore has some physical meaning in the estuary or bay, and numerical velocity results compare more favorably than was the case in lakes.

PART IV: THREE-DIMENSIONAL HYDRODYNAMIC MODELS

General Formulation

64. The three-dimensional hydrodynamic models have only recently been developed to the state where application to complex geometries with reasonable resolution appears possible. The delay in developing three-dimensional models can be attributed to the unavailability of extremely large, fast computers as well as to formulation difficulties. As previously indicated, the depth-averaged two-dimensional models have been extensively applied to the hydrodynamics of lakes and oceans. The two-dimensional models have provided valuable quantitative information for certain types of problems; however, for many other problems the two-dimensional models yield, at best, qualitative results. Certainly the many pressing problems associated with pollutant and sediment transport require the details of the three-dimensional velocity profile in the lake, and such information cannot be obtained from the depth-integrated two-dimensional system of equations. The shortcomings of the depth-averaged models are most apparent when the bottom shear stress is considered. In the two-dimensional models the shear stress is normally related to the net horizontal mass flux. However, for major portions of a lake, the flow at the bottom may be a return flow that is not in the direction of the net mass flux.

65. The three-dimensional models can be broadly classified into the following categories:

a. Constant-density, steady-flow models

b. Constant-density, unsteady-flow models

c. Variable-density, unsteady-flow models

Within each category the models can vary considerably depending upon the assumptions that are imposed. Some of the assumptions are common to most of the models; others pertain to a specific model. A variable-density, steady-flow result can be obtained from model c and is not listed separately since no basically different formulation has been developed for problems of this type. The constant-density, steady-flow

models can be formulated more simply than the constant-density, unsteady-flow models.

66. The three-dimensional governing equations for an infinitesimal fluid element have been given previously in Equations 16-19. The basic equations for the three-dimensional models are obtained from these equations subject to certain assumptions that are common to most models.

67. The Boussinesq approximation is normally made. This approximation assumes that density variations are small and can be neglected except in the gravity term of the momentum equation. Thus, even if the fluid is not strictly treated as incompressible, the continuity equation is reduced to the incompressible form. In addition, for most existing models, the vertical component of the local and advective acceleration is assumed to have a negligible effect on the vertical momentum equation. This assumption reduces the vertical momentum equation to the equation for hydrostatic pressure variation in a compressible fluid.

68. The basic equations from which the development of most three-dimensional models proceed are therefore given by

$$\frac{\partial u}{\partial t} + u\frac{\partial u}{\partial x} + v\frac{\partial u}{\partial y} + w\frac{\partial u}{\partial z} - fv = -\frac{1}{\rho}\frac{\partial p}{\partial x} + K\left(\frac{\partial^2 u}{\partial x^2} + \frac{\partial^2 u}{\partial y^2} + \frac{\partial^2 u}{\partial z^2}\right) \quad (59)$$

$$\frac{\partial v}{\partial t} + u\frac{\partial v}{\partial x} + v\frac{\partial v}{\partial y} + w\frac{\partial w}{\partial z} + fu = -\frac{1}{\rho}\frac{\partial p}{\partial y} + K\left(\frac{\partial^2 v}{\partial x^2} + \frac{\partial^2 v}{\partial y^2} + \frac{\partial^2 v}{\partial z^2}\right) \quad (60)$$

$$-\frac{1}{\rho}\frac{\partial p}{\partial z} = g \quad (61)$$

$$\frac{\partial u}{\partial x} + \frac{\partial v}{\partial y} + \frac{\partial w}{\partial z} = 0 \quad (62)$$

In addition to these equations, an energy equation, a constitutive equation for the density and diffusion equations for substances of interest, may be required, depending upon the particular problem formulation. The K used in the momentum equation is generally a

combination of the molecular viscosity and the eddy viscosity. In practice, however, the molecular viscosity is often neglected since it is much smaller than the eddy viscosity for lake applications.

Discussion of Specific Models

69. The three-dimensional models vary considerably in their method of development; therefore, no general formulation of the model governing equations, such as was possible in the two-dimensional equation, will be attempted. Instead, specific models illustrating the various model categories will be considered in sufficient detail to indicate the formulation procedure as well as the strengths and weaknesses of the individual models. In general, the application of three-dimensional models to actual lake geometries is still in its infancy. Considerable work is still required in this area, and many of the questions concerning the accuracy of the various models can be resolved only when prototype data of the required quality and quantity become available.

Three-dimensional, steady-state, constant-density model of R. T. Gedney and W. Lick

70. This model[21, 22] is based upon the shallow-lake theory developed by Welander. The model can account for irregular boundaries and variable bottom topography; it is, however, restricted to constant density and steady flow. The primary application of the model is for calculation of three-dimensional steady-state velocities when the lake is in an unstratified condition. A rigid lid assumption is imposed at the surface of the lake to filter out gravity waves.

71. The basic model is capable of describing flows in a lake where the depth is comparable to or less than the Ekman layer (shallow lake) as well as in a deep lake. Several assumptions result in simplification of the governing equations when they are applied to shallow-lake conditions. The model is three-dimensional; however, the computer time requirements are reasonably small. This small requirement is possible since the finite difference numerical portion of the model is

actually two-dimensional with the variation in flow parameters along the vertical or third dimension being obtained from a closed-form analytical solution.

72. The basic starting equations for the model are those listed in Equations 59-62. These equations are, however, considerably simplified by assumptions consistent with the intended application to shallow lakes:

a. The lake is considered to be homogeneous, resulting in the density being considered as a constant even in the gravity term in the vertical momentum equation. This assumption of homogenity in Lake Erie is found to be valid approximately from about the middle of fall to the beginning of summer.

b. The nonlinear inertial forces are assumed to be small in comparison with the Coriolis force and are neglected in the momentum equations. The Rossby number is a measure of the ratio of the nonlinear inertia forces to the Coriolis force and is defined by $R_o = U_R/fL$, where U_R is a characteristic velocity in the lake, f is the Coriolis parameter, and L is a characteristic horizontal scale. A calculation using values characteristic of Lake Erie shows that except in localized regions where the horizontal length scale is smaller than 50 km, the nonlinear inertia terms will be relatively unimportant. These terms reduce the governing equation to a linear system; however, the solutions obtained from the model near islands and in shallow shore regions should be applied with caution.

c. The effects of the horizontal internal friction of the fluid are ignored, which eliminates the terms involving the horizontal eddy viscosity. The horizontal Ekman number E_H is a measure of the relative importance of the horizontal diffusion terms by comparison with the Coriolis force and is defined by $E_H = A_H/fL^2$ where A_H is the horizontal eddy diffusion coefficient. Typical values for Lake Erie indicate that E_H is small and can be ignored except in the boundary layer near the shoreline. The boundary layer near the shore is normally smaller, however, than the typical grid size used in the calculations.

d. The pressure is assumed to be hydrostatic as a result of neglecting vertical acceleration and velocity terms. This standard assumption for most numerical models is probably justified except near the shoreline where significant vertical velocities and accelerations can be

present as a result of bringing to rest the velocity component normal to the shore.

e. The turbulence in the lake is modeled by a constant vertical eddy diffusivity. This assumption is almost certainly invalid; however, lack of reliable information makes this assumption necessary since a satisfactory model for the vertical eddy diffusivity is not available.

73. The displacement of the lake surface is assumed to be small in comparison with the depth of the lake. This assumption allows the complete linearization of the problem, since the surface boundary conditions are now applied at the undisturbed water surface rather than the instantaneous surface.

74. Under the assumptions listed, the governing equations are reduced to the linear system:

Continuity Equation

$$\frac{\partial u}{\partial x} + \frac{\partial v}{\partial y} + \frac{\partial w}{\partial z} = 0 \tag{63}$$

Momentum Equations

$$\frac{\partial u}{\partial t} - fv = -\frac{1}{\rho}\frac{\partial p}{\partial x} + A_v \frac{\partial^2 u}{\partial z^2} \tag{64}$$

$$\frac{\partial v}{\partial t} + fu = -\frac{1}{\rho}\frac{\partial p}{\partial y} + A_v \frac{\partial^2 v}{\partial z^2} \tag{65}$$

$$\frac{\partial p}{\partial z} = -\rho g \tag{66}$$

where A_v is the vertical eddy diffusion coefficient. The boundary conditions are as follows:

$$u,v,w = 0 \quad \text{at } z = -h(x,y) \tag{67}$$

$$\left.\begin{aligned} \rho A_v \frac{\partial u}{\partial z} &= \tau_{wx} \\ \rho A_v \frac{\partial v}{\partial z} &= \tau_{wy} \\ w &= 0 \end{aligned}\right\} \quad \text{at } z = 0 \tag{68}$$

$$p = p_o(x,y) \quad \text{at } z = \zeta(x,y)$$

75. The model is made nondimensional by introducing the dimensionless variables:

$$x^* = \frac{x}{L} \ , \ y^* = \frac{y}{L} \ , \ Z^* = \frac{z}{H_m}$$

$$u^* = \frac{u}{U_R} \ , \ v^* = \frac{v}{U_R} \ , \ w^* = \frac{w}{w_R}$$

$$p^* = \frac{p}{\rho g H_m} \ , \ \zeta^* = \frac{\zeta}{\zeta_R} \ , \ t^* = \frac{t}{t_R}$$

$$\tau_x^* = \frac{\tau_{wx}}{\tau_R} \ , \ \tau_y^* = \frac{\tau_{wy}}{\tau_R} \ , \ U_R = \frac{\tau_{wR}}{\rho f o H m}$$

$$\zeta_R = \frac{\tau_{wRL}}{\rho g H_m} \ , \ D = \pi \sqrt{\frac{2A_v}{\rho f o}}$$

where

L = characteristic length in the horizontal direction

H = characteristic length in the vertical direction

U_R = characteristic velocity

ζ_R = reference surface displacement

D = frictional depth

τ_{wR} = reference wind shear stress

W_R = reference vertical velocity

t_R = reference time value

f_o = Coriolis parameters evaluated at mean latitude of Lake Erie

H_m = mean depth

The nondimensional form of the governing equations becomes

$$\frac{\partial u}{\partial x} + \frac{\partial v}{\partial y} + \frac{\partial w}{\partial z} = 0 \tag{69}$$

$$\frac{\partial u}{\partial t} - v = - \frac{\partial p}{\partial x} + E_V \frac{\partial^2 u}{\partial z^2} \tag{70}$$

$$\frac{\partial v}{\partial t} + u = - \frac{\partial p}{\partial y} + E_V \frac{\partial^2 v}{\partial z^2} \tag{71}$$

$$\frac{\partial p}{\partial z} = - 1 \tag{72}$$

where $E_V = A_v/fH^2$ is the vertical Ekman number and the asterisks have been dropped for convenience of notation.

76. Equation 61 can be integrated over the vertical to give

$$\int_o^p \frac{\partial p}{\partial z}\, dz = - \int_o^z dz$$

$$p - p_o = -z$$

$$p = p_o(x,y) - z \tag{73}$$

This equation gives a one-to-one correspondence between pressure and surface elevation; thus, pressure can be eliminated from the governing equations. Normally the variation of $p_o(x,y)$ with (x,y) is small enough to be neglected, Thus,

$$\frac{\partial p}{\partial x} = \frac{\partial \zeta}{\partial x} \quad \text{and} \quad \frac{\partial p}{\partial y} = \frac{\partial \zeta}{\partial y} \tag{74}$$

Using this equation, the momentum equations in the horizontal are written as

$$\frac{\partial u}{\partial t} - v = - \frac{\partial \zeta}{\partial x} + E_V \frac{\partial^2 u}{\partial z^2} \tag{75}$$

$$\frac{\partial v}{\partial t} + u = - \frac{\partial \zeta}{\partial y} + E_V \frac{\partial^2 v}{\partial z^2} \tag{76}$$

and the vertical momentum equation is eliminated.

77. The model is to be applied to steady-state current patterns; therefore, the time dependency in the governing equations is eliminated. Thus, basic governing equations for the model are as follows:

$$E_V \frac{\partial^2 u}{\partial z^2} + v = \frac{\partial \zeta}{\partial x} \tag{77}$$

$$E_V \frac{\partial^2 v}{\partial z^2} - u = \frac{\partial \zeta}{\partial y} \tag{78}$$

and

$$\frac{\partial u}{\partial x} + \frac{\partial v}{\partial y} + \frac{\partial w}{\partial z} = 0 \tag{79}$$

The nondimensionalized boundary conditions are as follows:

$$\left.\begin{aligned} \tau_{wx} &= \frac{1}{2\lambda^2} \frac{\partial u}{\partial z} \\ \tau_{wy} &= \frac{1}{2\lambda^2} \frac{\partial v}{\partial z} \end{aligned}\right\} \text{at} \quad z = 0 \tag{80}$$

$$w = 0$$

$$u = v = w = 0 \quad \text{at} \quad z = -h(x,y)$$

where λ, a constant which is proportional to the ratio of water depth to frictional depth, is given by $\lambda \equiv \pi H/D$.

78. Equations 77 and 78 can be combined into a single equation by defining the complex quantities:

$$\tau_w = \tau_{wx} + i\,\tau_{wy}$$

$$\frac{\partial \zeta}{\partial n} = \frac{\partial \zeta}{\partial x} + i\,\frac{\partial \zeta}{\partial y} \tag{81}$$

and a complex variable representing horizontal velocity Γ given by

$\Gamma \equiv u + iv$

The complex equation for Γ is then given by:

$$\frac{\partial^2 \Gamma}{\partial z^2} - \frac{i\lambda^2 \Gamma}{2} = \frac{\lambda^2}{2}\,\frac{\partial \zeta}{\partial n} \tag{82}$$

The boundary conditions are

$$\tau_w = \frac{2}{\lambda^2}\,\frac{\partial \Gamma}{\partial z} \quad \text{at} \quad z = 0$$

$$w = 0 \quad \text{at} \quad z = 0 \tag{83}$$

$$w = 0 \quad \text{at} \quad z = -h(x,y)$$

and

$$\Gamma = 0 \quad \text{at} \quad z = -h(x,y)$$

This second-order differential equation involving the single arbitrary parameter λ can be solved subject to the boundary conditions to yield

$$\Gamma = u + iv = -i \frac{\partial \zeta}{\partial n} \left(\frac{\cosh \lambda' z}{\cosh \lambda' h} - 1 \right) + \frac{\tau_w \lambda}{2\bar{\omega}} \frac{\sinh [\lambda'(h + z)]}{\cosh (\lambda' h)} \qquad (84)$$

where

$\bar{\omega} = (1 + i)/2$

ζ = surface displacement as a function of x and y

$\lambda' = \bar{\omega} \lambda$

$h = H/H_m$ dimensionless depth

Z = dimensionless coordinate

This equation represents a closed form solution for u and v if $\partial\zeta/\partial n$ and τ_w are known; however, the surface displacement gradient is not generally known. A method must first be obtained for evaluating this quantity prior to evaluating u and v .

79. The horizontal mass flux can be found by

$$M_T = M_x + iM_y = \int_{-h}^{0} \Gamma \, dz = \tau_w a + h \frac{\partial \zeta}{\partial n} b$$

where a and b are functions only of the local depth and M_x and M_y are the x and y components, respectively, of horizontal mass flux.

80. The continuity equation can be integrated vertically to yield

$$\int_{-h}^{0} \left(\frac{\partial u}{\partial x} + \frac{\partial v}{\partial y} + \frac{\partial w}{\partial z} \right) dz = \frac{\partial}{\partial x} \int_{-h}^{0} u \, dz + \frac{\partial}{\partial y} \int_{-h}^{0} v \, dz + w \Big|_{w(-h)}^{w(0)} = 0$$

But $w = 0$ at $z = 0$ and $z = -h$; therefore,

$$\frac{\partial}{\partial x} \int_{-h}^{0} u \, dz + \frac{\partial}{\partial y} \int_{-h}^{0} v \, dz \equiv \frac{\partial}{\partial x} (M_x) + \frac{\partial}{\partial y} (M_y) = 0 \qquad (85)$$

Introducing the mass flux stream function $\psi(x,y)$ gives

$$M_x = \frac{\partial \psi}{\partial y} \quad , \quad M_y = - \frac{\partial \psi}{\partial x} \tag{86}$$

then

$$M_x + iM_y = \frac{\partial \psi}{\partial y} - i \frac{\partial \psi}{\partial x}$$

$$= \tau_w a + h \frac{\partial \zeta}{\partial n} b$$

$$= \tau_w a + h \left(\frac{\partial \zeta}{\partial x} + i \frac{\partial \zeta}{\partial y} \right) b$$

Rewriting $a = c + id$ and $b = e + if$ where c, d, e, and f are real functions of local depth gives the following expression for the surface gradient:

$$\frac{\partial \zeta}{\partial x} = \frac{e}{h(e^2 + f^2)} \frac{\partial \psi}{\partial y} - \frac{f}{h(e^2 + f^2)} \frac{\partial \psi}{\partial x} - \frac{\tau_{wx}}{h} \left(\frac{ce + df}{e^2 + f^2} \right) - \frac{\tau_{wy}}{h} \left(\frac{cf - de}{e^2 + f^2} \right) \tag{87}$$

$$\frac{\partial \zeta}{\partial y} = \frac{-f}{h(e^2 + f^2)} \frac{\partial \psi}{\partial y} - \frac{e}{h(e^2 + f^2)} \frac{\partial \psi}{\partial x} + \frac{\tau_{wx}}{h} \left(\frac{fc - de}{e^2 + f^2} \right) - \frac{\tau_{wy}}{h} \left(\frac{c^2 + df}{e^2 + f^2} \right) \tag{88}$$

The surface gradients are linear functions of the stream function gradient and the wind shear. These equations allow the surface gradients to be calculated if the wind stress and stream function are known. Substituting back into the expression for the complex velocity allows u and v to be calculated.

81. In order to have a complete solution for the problem the stream function must be determined. Equations 87 and 88 can be combined and the surface displacement ζ eliminated by taking the $\partial/\partial y$ of the first equation, $- \partial/\partial x$ of the second equation and then adding the two equations:

$$\nabla^2\psi + \left(c_1 \frac{\partial \bar{h}}{\partial x} - c_2 \frac{\partial \bar{h}}{\partial y}\right)\frac{\partial \psi}{\partial x} + \left(c_2 \frac{\partial \bar{h}}{\partial x} + c_1 \frac{\partial \bar{h}}{\partial y}\right)\frac{\partial \psi}{\partial y} = c_3\left(\frac{\partial \tau_{wx}}{\partial x} + \frac{\partial \tau_{wy}}{\partial y}\right)$$

$$- c_4\left(\frac{\partial \tau_{wy}}{\partial x} - \frac{\partial \tau_{wx}}{\partial y}\right) - c_5\left(\tau_{wx}\frac{\partial \bar{h}}{\partial x} + \tau_{wy}\frac{\partial \bar{h}}{\partial y}\right)$$

$$- c_6\left(\tau_{wy}\frac{\partial \bar{h}}{\partial x} - \tau_{wx}\frac{\partial \bar{h}}{\partial y}\right) \quad (89)$$

where $\bar{h} = \lambda h$ and c_1, c_2, c_3, c_4, c_5, and c_6 are functions of $\bar{h}$. This governing equation for the stream function is a linear, elliptic equation and can be solved using the boundary condition that the normal mass flux at the shore is zero or equal to the river inflow or outflow.

82. It should be noted that the stream function formulation is independent of the vertical coordinate and is thus numerically a two-dimensional problem. In addition, it should be kept in mind that the stream function formulation does involve the vertical eddy diffusivity, which is basically a function of the wind speed.

83. The stream function equation is solved numerically by replacing the differential equation by a finite difference representation. This substitution allows the value of the stream function at each discrete point in the numerical grid to be solved in terms of the values at neighboring points and coefficients that are functions of the local topography and wind stress conditions. The resulting set of simultaneous equations is of the form

$$[A][\psi] = [C]$$

where $[A]$ is a square matrix whose order is equal to the number N of the interior grid points, $[\psi]$ is the vector column matrix for the stream function, and $[C]$ is the vector column matrix containing the nonhomogeneous portion of the difference equations. The matrix $[A]$ is sparse and is solved using successive overrelaxation by points (SOR) and by single-line overrelaxation (SLOR).

84. Islands in the lake create a multiply connected domain. They can be included, however, by requiring that the value of ψ on each island be specified in such a manner that the surface displacement is continuous around the island. This treatment increases the computational time; however, islands can be included satisfactorily. Because of the linearity of the problem, linear interpolation can be used to facilitate obtaining solutions for various wind conditions.

85. Once the stream function has been obtained, Equations 87 and 88 are used to evaluate the local slope of the lake surface. Once this information is known, Equation 84 allows the local vertical profile of horizontal velocity to be evaluated.

86. The model was initially applied to some simple geometries for which analytical solutions were available to allow the effect of various parameters in the numerical model to be considered and evaluated. The model was verified for real-lake conditions by applying it to Lake Erie.[21] Two uniform wind conditions were considered corresponding to winds of 11.8 mph and 22.7 mph. The numerical grid step used in the calculations was 2 miles in the open lake and 0.5 mile near the islands in the western basin. The numerical steady-state calculations of the wind-driven currents in Lake Erie were shown to compare favorably with current meter measurements made at middepth in the central and eastern basins. Many other features of the currents observed by other methods are predicted at least qualitatively by the calculations.

87. The agreement of calculations and measurements appears to indicate that the shallow-lake model that uses a constant eddy viscosity is capable of predicting accurately the local three-dimensional velocities at middepths. Additional prototype data near the surface and bottom of the lake in conjunction with measurements at middepths are needed to verify the model and the constant eddy viscosity assumption. The calculated results show that for a large percentage of Lake Erie the bottom stress is not in the direction of the horizontal mass flux. These results indicate that for Lake Erie and other shallow lakes there may be large errors in solutions obtained from models where the bottom stress is made proportional to the net horizontal mass flux.

Three-dimensional, time-dependent, constant-density model of A. Haq, W. Lick, and Y. P. Sheng

88. The basic formulation of this model[23] is an extension of the three-dimensional steady-state model of Gedney and Lick.[22] The method of solution of the model is, however, completely different. This model is time dependent, and irregular boundaries and variable bottom topography can be handled. It is, however, restricted to constant-density flow. The primary application of the model is for storm surge simulation where surface displacements rather than velocities are prime considerations. A free surface condition is imposed, rather than the rigid lid assumption used in the steady-state model in order that the details of the transient behavior are simulated. As with the steady-state model, the primary application is for shallow lakes with parameters in the program closely corresponding to those for Lake Erie.

89. Equations 63-66 and the boundary conditions given by Equations 67 and 68 form the basic system of equations for the model. These equations are put in a nondimensional form with some slight changes from the nondimensionalization process used by Gedney and Lick. The nondimensional variables are introduced as follows:

$$x^* = \frac{x}{L} , \quad y^* = \frac{y}{L} , \quad z^* = \frac{z}{H}$$

$$u^* = \frac{u}{U_R} , \quad v^* = \frac{v}{U_R} , \quad w^* = \frac{Lw}{HU_R}$$

$$p^* = \frac{p}{\rho f U_R L} , \quad \zeta^* = \frac{g\zeta}{fU_R L} , \quad t^* = ft \tag{90}$$

$$\tau_x^* = \frac{\tau_{wx}}{\tau_R} , \quad \tau_y^* = \frac{\tau_{wy}}{\tau_R} , \quad \tau_R^* = \frac{\rho A_V U_R}{H}$$

90. The nondimensionalized forms of the governing equations become

$$\frac{\partial u}{\partial x} + \frac{\partial v}{\partial y} + \frac{\partial w}{\partial z} = 0 \tag{91}$$

$$\frac{\partial u}{\partial t} - v = - \frac{\partial p}{\partial x} + E_V \frac{\partial^2 u}{\partial z^2} \tag{92}$$

$$\frac{\partial v}{\partial t} + u = - \frac{\partial p}{\partial y} + E_V \frac{\partial^2 v}{\partial z^2} \tag{93}$$

and

$$\frac{\partial p}{\partial z} = - \frac{gH}{fU_R L} \tag{94}$$

where the asterisks have been dropped for convenience.

91. The dimensionless boundary conditions are:

$$u,v,w = 0 \quad \text{at} \quad z = -\left(\frac{h}{H}\right)$$

$$\frac{\partial u}{\partial z} = \tau_x \qquad \text{at} \quad z = 0$$

$$\frac{\partial v}{\partial z} = \tau_y \qquad \text{at} \quad z = 0 \tag{95}$$

$$w = \frac{f^2 L^2}{gH} \frac{\partial \zeta}{\partial t} \qquad \text{at} \quad z = 0$$

92. The hydrostatic Equation 94 is integrated over the lake depth to obtain

$$p = p_o(x,y) + \zeta - \frac{gH}{fU_R L} z \tag{96}$$

Assuming that the atmospheric pressure is uniform results in

$$\frac{\partial p}{\partial x} = \frac{\partial \zeta}{\partial x}$$

$$\frac{\partial p}{\partial y} = \frac{\partial \zeta}{\partial y} \qquad (97)$$

Substituting into Equations 92 and 93 results in

$$\frac{\partial u}{\partial t} - v = - \frac{\partial \zeta}{\partial x} + E_V \frac{\partial^2 u}{\partial z^2} \qquad (98)$$

and

$$\frac{\partial v}{\partial t} + u = - \frac{\partial \zeta}{\partial y} + E_V \frac{\partial^2 v}{\partial z^2} \qquad (99)$$

93. Equation 91 is further modified by defining

$$U = \int_{-\frac{h}{H}}^{o} u \, dz \qquad (100)$$

and

$$V = \int_{-\frac{h}{H}}^{o} v \, dz \qquad (101)$$

The continuity equation is then integrated over the depth of the lake to obtain

$$\int_{\frac{-h}{H}}^{0} \frac{\partial u}{\partial x}\, dz + \int_{\frac{-h}{H}}^{0} \frac{\partial v}{\partial y}\, dz + \int_{\frac{-h}{H}}^{0} \frac{\partial w}{\partial z}\, dz = 0$$

$$w\Big|_{\frac{-h}{H}}^{0} + \int_{\frac{-h}{H}}^{0} \frac{\partial u}{\partial x}\, dz + \int_{\frac{-h}{H}}^{0} \frac{\partial v}{\partial y}\, dy = 0$$

For nondimensional variables the continuity equation becomes

$$\frac{f^2 L^2}{gH} \frac{\partial \zeta}{\partial t} + \frac{\partial U}{\partial x} + \frac{\partial V}{\partial y} = 0$$

or

$$\frac{\partial \zeta}{\partial t} + \frac{gH}{f^2 L^2} \left(\frac{\partial U}{\partial x} + \frac{\partial V}{\partial y} \right) = 0 \qquad (102)$$

94. Equations 98, 99, and 102 must be solved to obtain the velocity field and surface elevations, ζ, in the lake using this model. These equations are subjected to the boundary conditions given by Equation 95. The model as formulated does not provide for a mass flux inflow or outflow through the boundaries of the lake.

95. To insure no loss of accuracy in the numerical computation in the shallow regions of the lake, a more convenient coordinate system is introduced. The desired transformation maps the bottom of the lake onto a constant σ surface where σ is a transformed vertical coordinate. A uniform σ grid is then used in the (x,y,σ) system that corresponds to a nonuniform vertical grid in the (x,y,z) system. The new σ system is obtained by replacing the vertical coordinate in the (x,y,z) system by

$$\sigma = 1 + \frac{z}{h(x,y)}$$

where $h(x,y)$ is the dimensionless local depth.

96. The governing equations can then be written as

$$\frac{\partial u}{\partial t} - v = - \frac{\partial \zeta}{\partial x} + \frac{E_V}{h^2} \frac{\partial^2 u}{\partial \sigma^2} \tag{103}$$

$$\frac{\partial v}{\partial t} + u = - \frac{\partial \zeta}{\partial y} + \frac{E_V}{h^2} \frac{\partial^2 v}{\partial \sigma^2} \tag{104}$$

$$\frac{\partial \zeta}{\partial t} + \beta \left(\frac{\partial U}{\partial x} + \frac{\partial V}{\partial y} \right) = 0 \tag{105}$$

where

$$\beta = \frac{gH}{L^2 f^2}$$

and the horizontal mass fluxes U and V are defined by

$$U = h(x,y) \int_0^1 u \, d\sigma \tag{106}$$

$$V = h(x,y) \int_0^1 v \, d\sigma \tag{107}$$

The boundary conditions are

$$u = v = 0 \quad \text{at} \quad \sigma = 0$$

$$\frac{\partial u}{\partial \sigma} = h\tau_x \quad \text{at} \quad \sigma = 1 \tag{108}$$

$$\frac{\partial v}{\partial \sigma} = h\tau_y \quad \text{at} \quad \sigma = 1$$

and $\vec{V}_n = 0$ at the shoreline where $\vec{V}_n$ is velocity normal to shoreline.

97. The finite difference grid is set up using constant grid spacings Δx, Δy, and $\Delta\sigma$ and generally Δx equals Δy. The variables are defined as shown in Figure 24. The staggering of the variables simplifies the representation of the required derivatives. Centered differences in space and forward differences in time are used in the numerical calculations. Values for variables are sometimes needed at points at which they are not defined. These values are obtained by linearly interpolating from the values immediately adjacent to the point under consideration.

98. Equations 103-105 are written in a finite difference form using forward time and centered space differences and for stability consideration a modified DuFort-Frankel scheme for the vertical diffusion terms. The formulation is explicit. In addition, the mass fluxes U and V are evaluated by numerically integrating Equations 106 and 107 using Simpson's rule. The finite difference equations at time t_{n+1} can then be written as

$$u^{n+1}_{i,j+1/2,k} = \left(\frac{1}{1+\alpha}\right)\left\{u^{n}_{i,j+1/2,k} + \Delta t\left[v^{n}_{<i,j,+1/2,k>} - \left(\frac{\partial \zeta}{\partial x}\right)^{n}_{<i,j+1/2>}\right.\right.$$

$$\left.\left. + \frac{\alpha}{\Delta t}\left(u^{n}_{i,j+1/2,k+1} - u^{n-1}_{i,j+1/2,k} + u^{n}_{i,j+1/2,k-1}\right)\right]\right\}$$

$$\text{for } 1 < k < KM(\text{surface}) \tag{109}$$

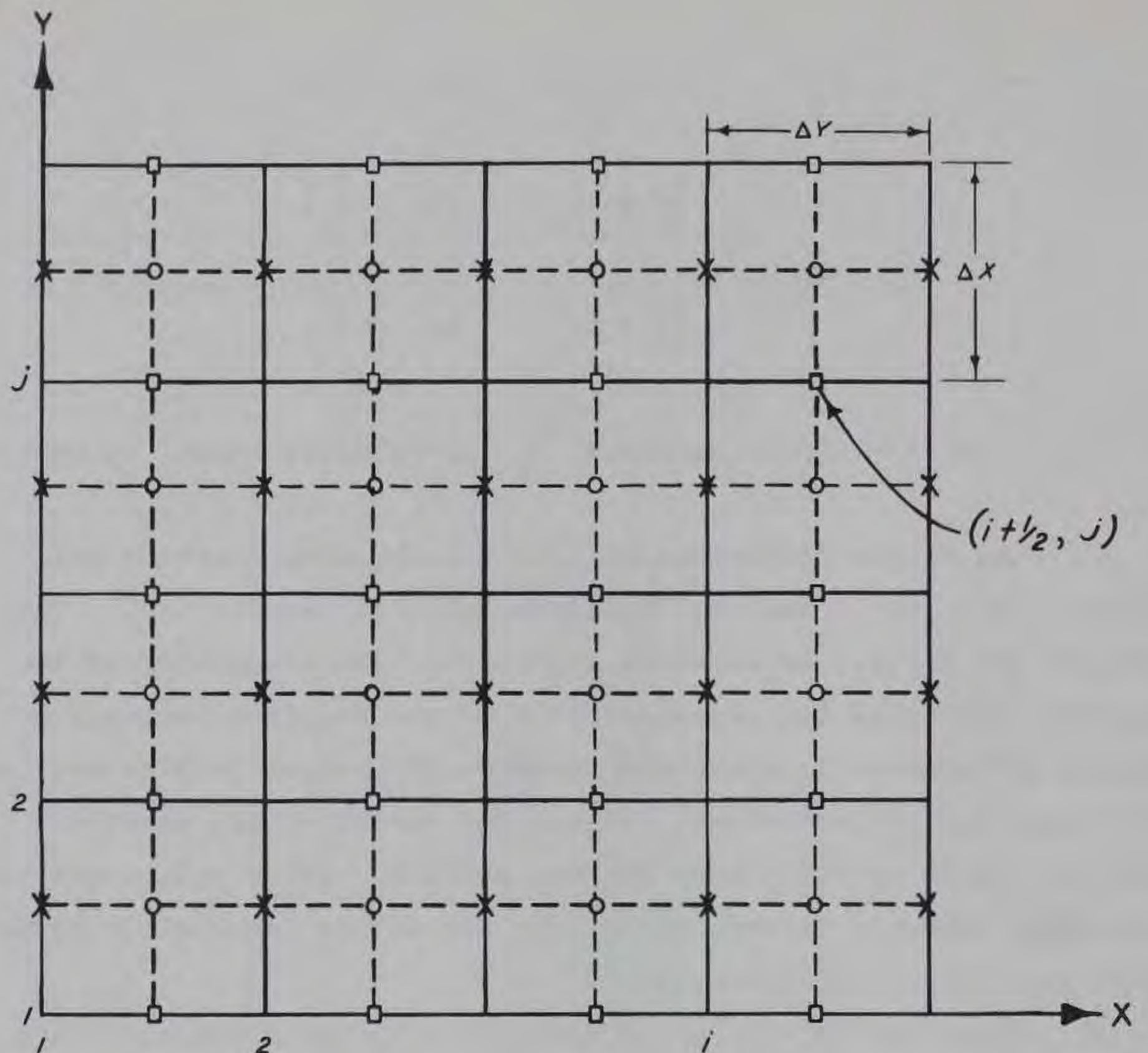

LEGEND

X POINTS DEFINING U, u (DEFINED AT i, J+½, k)
□ POINTS DEFINING V, v (DEFINED AT i+½, j, k)
O POINTS DEFINING ζ (DEFINED AT i+½, j+½, k)
▽ POINTS DEFINING u
△ POINTS DEFINING v

Figure 24. Spatial grid used in the numerical computations

$$u^{n+1}_{i,j+1/2,KM} = \left(\frac{1}{1+\alpha}\right)\left\{u^{n}_{i,j+1/2,KM} + \Delta t\left[v^{n}_{<i,j+1/2,KM>} - \left(\frac{\partial \zeta}{2x}\right)^{n}_{<i,j+1/2>}\right.\right.$$

$$\left.\left. + \frac{\alpha}{\Delta t}\left(2u^{n}_{i,j+1/2,KM-1} - u^{n-1}_{i,j+1/2,KM} + \frac{2\gamma\tau_x}{h\Delta\sigma}\right)\right]\right\} \qquad (110)$$

$$v^{n+1}_{i+1/2,j,k} = \left(\frac{1}{1+\alpha}\right)\left\{v^{n}_{i+1/2,j,k} + \Delta t\left[-u^{n}_{<i+1/2,j,k>} - \left(\frac{\partial \zeta}{\partial y}\right)^{n}_{<i+1/2,j>}\right.\right.$$

$$\left.\left. + \frac{\alpha}{\Delta t}\left(v^{n}_{i+1/2,j,k+1} - v^{n}_{i+1/2,j,k} + v^{n}_{i+1/2,j,k-1}\right)\right]\right\} \qquad (111)$$

for $1 < k < KM$ (surface)

$$v^{n+1}_{i+1/2,j,KM} = \left(\frac{1}{1+\alpha}\right)\left\{v^{n}_{i+1/2,j,KM} + \Delta t\left[-v^{n}_{<i+1/2,j,KM>} - \left(\frac{\partial \zeta}{\partial y}\right)^{n}_{<i+1/2,j>}\right.\right.$$

$$\left.\left. + \frac{\alpha}{\Delta t}\left(2v^{n}_{i+1/2,j,KM-1} - v^{n-1}_{i+1/2,j,KM} + \frac{2\gamma\tau_y}{h\Delta\sigma}\right)\right]\right\} \qquad (112)$$

$$\zeta^{n+1}_{i+1/2,j+1/2} = \zeta^{n}_{i+1/2,j+1/2} - \beta\Delta t$$

$$\left[\left(\frac{U^{n+1}_{i+1,j+1/2} - U^{n+1}_{i,j+1/2}}{\Delta x}\right) + \left(\frac{V^{n+1}_{i+1/2,j+1} - V^{n+1}_{i+1/2,j}}{\Delta y}\right)\right] \qquad (113)$$

where

$\alpha = E_V \Delta t/(h^2 \Delta\sigma^2)$

KM corresponds to $\sigma = 1$ (surface)

$\gamma = \tau_r/(\rho U_R H f)$

< > points at which variables must be interpreted since they are not evaluated in the staggered grid

99. Thus, the numerical procedure can be summarized as follows:

a. Assume that the values at time t_n are known (initially at t_1, $u = v = \zeta = 0$).

b. Use Equations 108 and 109 to calculate u^{n+1}.

c. Use Equations 111 and 112 to calculate v^{n+1}.

d. Evaluate U^{n+1} and V^{n+1} by numerically integrating Equations 106 and 107.

e. Set U and V equal to zero on appropriate boundary segments.

f. Evaluate ζ^{n+1} from Equation 113.

The calculation is completed at time t_{n+1} and the computation for the next time step can now be started with step a.

100. The numerical model consists of a system of five differential equations together with two numerical integrations. The stability of the system is found to be limited only by the well known limitation on surface gravity waves.

101. The model was initially verified by applying it to some simple lake geometries: an infinitely long lake, a square basin with constant depth, and a constant bottom slope basin. The numerical solutions were compared with analytical solutions to determine the effects of changes in the eddy diffusivity, lake geometry, and bottom topography.

102. The Wilson formulation[24] for the wind stress is used in the model:

$$\tau_w = \rho_a C_d |W_a| W_a \tag{114}$$

where ρ_a is the density of the air, C_d is the drag coefficient (C_d = 0.00273 for winds > 6 m/sec and C_d = 0.00166 for winds < 6 m/sec), and W_a is the wind velocity at 10 m above the water surface. For a spatially varying and time-varying wind stress, the stress at any point in the lake is obtained by interpolating from the known value at a few velocity measuring stations around the lake. The method of

interpolation is similar to that used by Platzman.[14]

103. The numerical model has been applied to Lake Erie for two cases.[22] The first case is for a uniform wind blowing along the long axis of the lake. The actual verification of the model is obtained by calculating the flow in the lake during storm Agnes. The calculated and measured values for the surface displacement at Cleveland and at Port Stanley are found to be in good agreement. Also, the spatial variation of the surface displacement is consistent with the limited amount of data that are available.

104. In applying the model to Lake Erie, it should be noted that much of the western basin and regions very close to shore become very shallow. In such regions, the assumption that the surface displacement is small compared with the depth may be inadequate, and the linearized theory is likely to be inaccurate. The minimum depth considered in the numerical model was 1.8 m. In addition, the islands separating the western and central basins of Lake Erie are neglected in the present model.

105. A uniform horizontal grid with $x = y = 6.4$ km is used in the entire lake for the Lake Erie calculations. In the vertical direction, the region from the top to the bottom ($\sigma = 0$ to $\sigma = 1$) is divided into five equal intervals of σ. In actual physical variables, the lengths of these intervals are smaller in shallow regions and larger in the deep regions of the lake. The time step used in the calculations for Lake Erie was 50 sec, and the results showed no evidence of instability.

106. Calculations were made for eddy diffusivity values of 25 cm^2/sec and 40 cm^2/sec. For $A_v = 25$ cm^2/sec the numerical results for surface displacement as a function of time for storm Agnes compare favorably with the measured values of the surface displacement. The surface displacement values for $A_v = 40$ cm^2/sec are indicated as being practically indistinguishable from those for $A_v = 25$ cm^2/sec indicating that the magnitude and direction of the wind velocity dominate the flow. This situation would not exist after the storm, as the surface oscillates and decays to an equilibrium position. The accuracy

of velocities predicted by the model cannot be properly evaluated because of a lack of appropriate prototype data.

107. The authors reference the numerical model study of storm Agnes on Lake Erie by Paskausky,[20] whose model is vertically integrated and contains a rigid lid assumption. Paskausky's values of setup at Cleveland and setdown at Port Stanley are indicated as being consistently lower than the measured values. The authors attribute this difference to the use of the rigid lid assumption combined with a greater minimum allowable depth (24 ft) in Paskausky's model. To verify their conclusions, the authors made several calculations with a vertically integrated model using a minimum allowable depth of 6 ft. This model predicted much better agreement with measured values than did that of Paskausky's.

Three-dimensional variable-density model by Jan J. Leendertse, Richard C. Alexander, and Shiao-Kung Liu

108. This model[25] lays the foundation for the development of a layered model to be used for numerical simulation of the fluid flow in water bodies with irregular boundaries and nonisotropic density distribution. Work on the model is not complete, and only very limited applications and attempts at model verification are reported. The model is intended for application to estuaries and coastal seas. Some of the assumptions and formulation procedures are not immediately adaptable to freshwater lakes, where density variations are due to temperature variations rather than to salinity variations. The general formulation procedures can be extended, however, to be applicable to freshwater lakes.

109. The conservation form of the governing equations is used to allow the preservation of certain integral conservative relations of the continuum equation in the finite difference formulation of the problem. This form insures that mass, momentum, or other variables are neither created nor destroyed as a result of the computational scheme. The fluid density is assumed to vary with salinity. The basic governing equations for the formulation are those given by Equations 59-62.

110. In addition, because the density is considered as a function of salinity, S, a constitutive equation and salinity transport and diffusion equation are required.

Salinity transport and diffusion

$$\frac{\partial S}{\partial t} + \frac{\partial (uS)}{\partial x} + \frac{\partial (vS)}{\partial y} + \frac{\partial (wS)}{\partial z} - \frac{\partial}{\partial x}\left(D_x \frac{\partial S}{\partial x}\right) - \frac{\partial}{\partial y}\left(D_y \frac{\partial S}{\partial y}\right) - \frac{\partial}{\partial z}\left(D_z \frac{\partial S}{\partial z}\right) = 0 \qquad (115)$$

Constitutive equation

$$\rho = \bar{\rho} + \rho'(S) \qquad (116)$$

where

S = salinity

D_x, D_y, D_z = eddy diffusion coefficients of salinity in x, y, and z directions

$\bar{\rho}$ = constant reference density

ρ' = departure from $\bar{\rho}$ depending on salinity

111. For a more general constitutive equation, a density dependence on temperature as well as on salinity would be required. This more general formulation would require an additional equation governing the energy balance for the system. Diffusion equations for the various other substances of interest would also be required. The actual numerical simulation of the three-dimensional flow problem in this model is considerably more complex than for the previous models that have been considered. Fewer simplifications of the basic equations are made, and the resulting model is highly nonlinear with the accompanying difficulties of formulating the nonlinear terms.

112. The basic approach in the layered model is to visualize the fluid motion in horizontal slices. Within each horizontal slice the equations are integrated over the height of the layer to obtain at any

horizontal position depth-averaged fluid properties for the slice. For any slice, this approach is essentially identical with the two-dimensional depth-averaged model formulation. The layers are not independent, however, since there is an exchange of mass, momentum, and salinity between layers. The air-water interface is the boundary for the system's upper layer, and the bottom defines the boundary condition for the bottom layer. At these boundaries the mass and salinity fluxes are zero. Only momentum is transferred, at the surface as a driving force by wind and at the bottom as a dissipative effect due to friction.

113. Figure 25 shows a sample layout of the vertical grid. The surfaces $z = z_k$ = constant are levels separating the various layers of thickness h_k. The thickness h_1 will generally vary in space and time due to wave action. The intermediate thicknesses are constant over the region while the bottom layer will vary with x and y according to the prescribed bottom topography. The number of layers will vary from one position in the horizontal plane to another depending on the depth.

114. The governing equations are integrated over the thickness of the layer in the same manner as was worked out in detail previously for the two-dimensional depth-averaged models. The momentum equations for the k_{th} layer become

$$\int_{k+1/2}^{k-1/2} \frac{\partial u}{\partial t}\, dz + \int_{k+1/2}^{k-1/2} \frac{\partial}{\partial x}(uu)\, dz + \int_{k+1/2}^{k-1/2} \frac{\partial}{\partial y}(uv)\, dz + \int_{k+1/2}^{k-1/2} \frac{\partial}{\partial z}(uw)$$

$$dz - \int_{k+1/2}^{k-1/2} fv\, dz + \int_{k+1/2}^{k-1/2} \frac{1}{\rho}\frac{\partial p}{\partial x}\, dz - \int_{k+1/2}^{k-1/2} \frac{1}{\rho}\left(\frac{\partial \tau_{xx}}{\partial x} + \frac{\partial \tau_{xy}}{\partial y} + \frac{\partial \tau_{xz}}{\partial z}\right) dz = 0$$

and

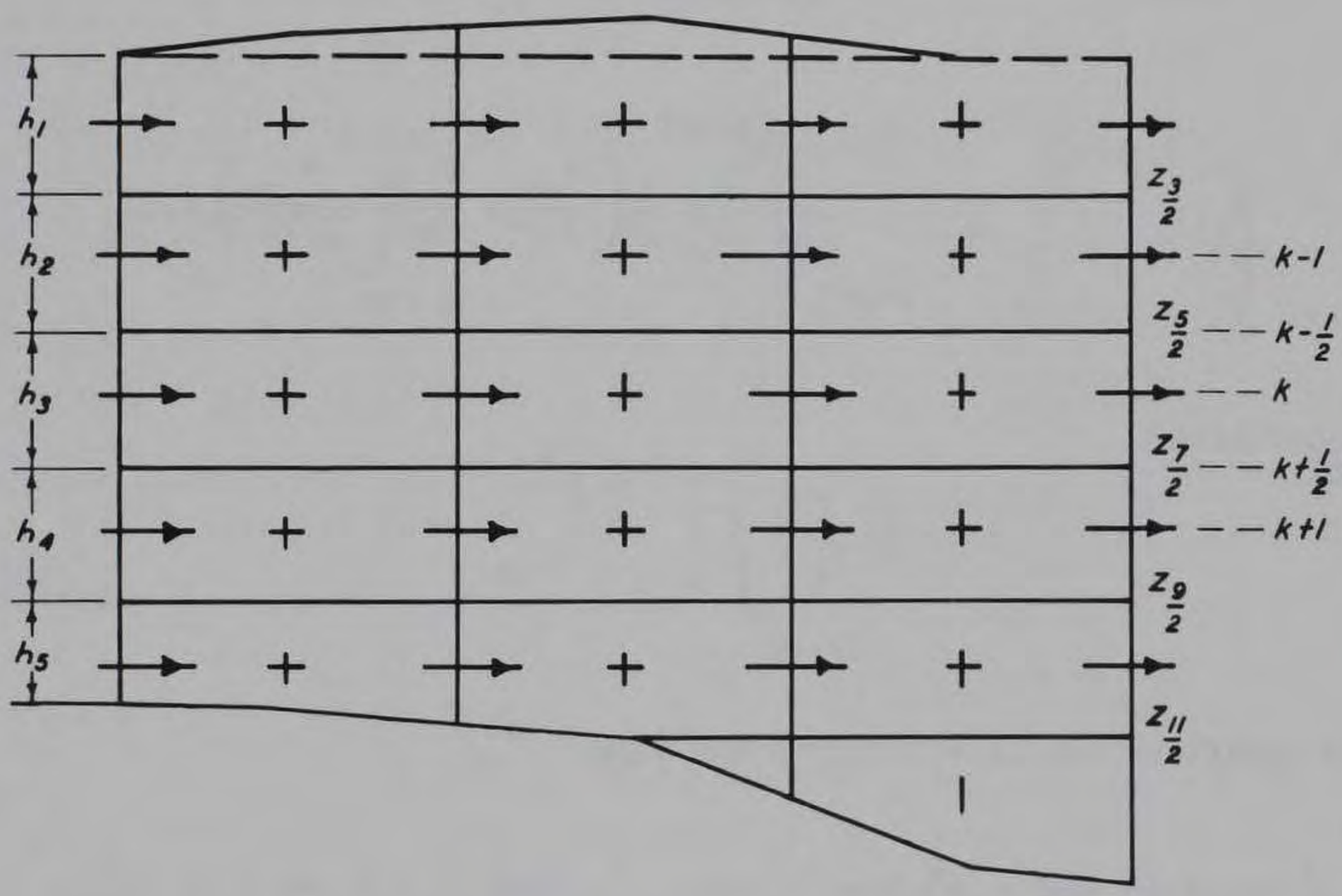

Figure 25. Location of variables of the vertical grid

$$\int_{k+1/2}^{k-1/2} \frac{\partial v}{\partial t}\, dz + \int_{k+1/2}^{k-1/2} \frac{\partial}{\partial x}(uv)\, dz + \int_{k+1/2}^{k-1/2} \frac{\partial}{\partial y}(vu)\, dz$$

$$+ \int_{k+1/2}^{k-1/2} \frac{\partial}{\partial z}(vw)\, dz + \int_{k+1/2}^{k-1/2} fu\, dz + \int_{k+1/2}^{k-1/2} \frac{1}{\rho}\frac{\partial p}{\partial y}\, dz$$

$$- \int_{k+1/2}^{k-1/2} \frac{1}{\rho}\left(\frac{\partial \tau_{yx}}{\partial x} + \frac{\partial \tau_{yy}}{\partial y} + \frac{\partial \tau_{yz}}{\partial z}\right) = 0$$

or defining

$$\langle\ \rangle_k = \int_{k+1/2}^{k-1/2} (\ )\, dz \qquad (117)$$

The equations can be written in the form:

$$\frac{\partial}{\partial t}\langle u\rangle + \frac{\partial}{\partial x}\langle uu\rangle + \frac{\partial}{\partial y}\langle uv\rangle + (uw)_{k+1/2} - (uw)_{k+1/2} - f\langle v\rangle + \frac{1}{\hat{\rho}_k}\left\langle\frac{\partial p}{\partial x}\right\rangle$$

$$- \frac{1}{\hat{\rho}_k}\left\langle\frac{\partial \tau_{xx}}{\partial x}\right\rangle - \frac{1}{\hat{\rho}_k}\left\langle\frac{\partial \tau_{xy}}{\partial y}\right\rangle - \frac{1}{\hat{\rho}_k}\left(\tau^{xz}_{k-1/2} - \tau^{xz}_{k+1/2}\right) = 0$$

and

$$\frac{\partial}{\partial t}\langle v\rangle + \frac{\partial}{\partial x}\langle uv\rangle + \frac{\partial}{\partial y}\langle vv\rangle + (vw)_{k-1/2} - (vw)_{k+1/2} + f\langle u\rangle$$

$$+ \frac{1}{\hat{\rho}_k}\left\langle\frac{\partial p}{\partial y}\right\rangle - \frac{1}{\hat{\rho}_k}\left\langle\frac{\partial \tau_{yy}}{\partial y}\right\rangle - \frac{1}{\hat{\rho}_k}\left\langle\frac{\partial \tau_{yx}}{\partial x}\right\rangle - \frac{1}{\hat{\rho}_k}\left(\tau^{yz}_{k-1/2} - \tau^{yz}_{k+1/2}\right) = 0$$

where $\hat{\rho}_k$ is the depth-averaged density for the K^{th} layer.

115. Some approximations are necessary at this point. The second and third terms represent integrals of products of velocities. These terms are replaced by products of integrals.

$$\frac{\partial}{\partial x}\langle uu\rangle = \frac{\partial}{\partial x}\int_{k+1/2}^{k-1/2} uu\,dz \approx \frac{\partial}{\partial x}\left[\frac{1}{h}\int_{k+1/2}^{k-1/2} u\,dz \int_{k+1/2}^{k-1/2} u\,dz\right]$$

$$\approx \frac{\partial}{\partial x}\left[\frac{1}{h}\langle u\rangle\langle u\rangle\right] \tag{118}$$

Similarly

$$\frac{\partial(uv)}{\partial y} \approx \frac{\partial}{\partial y}\left(\frac{1}{h}\langle u\rangle\langle v\rangle\right)$$

$$\frac{\partial(uv)}{\partial x} \approx \frac{\partial}{\partial x}\left(\frac{1}{h}\langle u\rangle\langle v\rangle\right)$$

and

$$\frac{\partial(vv)}{\partial y} \approx \frac{\partial}{\partial y}\left(\frac{1}{h}\langle v\rangle\langle v\rangle\right)$$

The density is considered to vary only with horizontal position <u>within each layer</u>. The differentiation and integration processes are taken

as interchangeable in the momentum diffusion terms and are approximated by:

$$\left\langle \frac{\partial \tau_{xx}}{\partial x} \right\rangle \approx \frac{\partial}{\partial x} \langle \tau_{xx} \rangle$$

$$\left\langle \frac{\partial \tau_{xy}}{\partial y} \right\rangle \approx \frac{\partial}{\partial y} \langle \tau_{xy} \rangle \qquad (119)$$

$$\left\langle \frac{\partial \tau_{yx}}{\partial x} \right\rangle \approx \frac{\partial}{\partial x} \langle \tau_{yx} \rangle$$

$$\left\langle \frac{\partial \tau_{yy}}{\partial y} \right\rangle \approx \frac{\partial}{\partial y} \langle \tau_{yy} \rangle$$

116. In integrating the hydrostatic pressure variation across the layer

$$\int_{k+1/2}^{k-1/2} \frac{\partial p}{\partial z}\, dz + \int_{k+1/2}^{k-1/2} \rho g\, dz = 0$$

approximations must be introduced since p and ρ are not defined at the interface between elements but at the center of the elements. Therefore

$$\int_{k+1/2}^{k-1/2} \frac{\partial p}{\partial z}\, dz$$

can be approximated by:

$$\underline{P}_k - \underline{P}_{k-1}$$

where P_k is the layer-averaged pressure of the k^{th} layer and

$$\int_{k+1/2}^{k-1/2} \rho g \, dz$$

is approximated by

$$\frac{1}{2}\left(\hat{\rho}_k + \hat{\rho}_{k+1}\right)\left[\frac{1}{2}\left(h_k + h_{k+1}\right)\right]$$

The same principle is extended to represent all the interface values of dependent variables as the two point averages of the adjacent layer values for the same variable; for example,

$$U_{k+1/2} = \frac{1}{2}\left(V_k + V_{k+1}\right) \tag{120}$$

where U_k is the layer-averaged U-component of velocity.

117. From the hydrostatic pressure variation an expression for p can be obtained:

$$\frac{\partial p}{\partial z} + \rho g = 0$$

$$p = \int \rho g \, dz + f(x,y)$$

or simply

$$p = \int \rho g \, dz$$

if the variation in atmospheric pressure over the water body is neglected. A change in pressure at a particular location can therefore occur as a result of an effective change in depth (change in ζ) or as a result of a variation in density.

118. The horizontal pressure gradient term for the upper layer can then be approximated by:

$$\frac{\partial \underline{P}_1}{\partial x} = g\hat{\rho}_1 \frac{\partial \zeta}{\partial x} + \frac{1}{2} gh_1 \frac{\partial \hat{\rho}_1}{\partial x}$$

$$\frac{\partial \underline{P}_1}{\partial y} = g\hat{\rho}_1 \frac{\partial \zeta}{\partial y} + \frac{1}{2} gh_1 \frac{\partial \hat{\rho}_1}{\partial y} \tag{121}$$

The pressure gradient for the other layers is given by

$$\frac{\partial \underline{P}_k}{\partial x} = \frac{\partial \underline{P}_{k-1}}{\partial x} + gh_{k-1/2} \frac{\partial \hat{\rho}_{k-1/2}}{\partial x}$$

$$\frac{\partial P_k}{\partial y} = \frac{\partial \underline{P}_{k-1}}{\partial y} + gh_{k-1/2} \frac{\partial \hat{\rho}_{k-1/2}}{\partial y} \qquad k = 2,3,\cdots,\bar{B} \tag{122}$$

where the total number of layers $\bar{B}$ is a function of local depth.

119. When the continuity equation is integrated over layer k,

$$\int_{k+1/2}^{k-1/2} \left(\frac{\partial w}{\partial z} + \frac{\partial u}{\partial x} + \frac{\partial v}{\partial y} \right) dz = 0$$

or

$$w_{k-1/2} - w_{k+1/2} + \int_{k+1/2}^{k-1/2} \left(\frac{\partial u}{\partial x} + \frac{\partial v}{\partial y} \right) dz = 0$$

Interchanging the differential and integral operators

$$W_{k-1/2} - W_{k+1/2} + \frac{\partial}{\partial x} \int_{k+1/2}^{k-1/2} u \, dz + \frac{\partial}{\partial y} \int_{k+1/2}^{k-1/2} v \, dz = 0$$

for a particular layer gives

$$W_{k-1/2} - W_{k+1/2} + \frac{\partial}{\partial x} \langle u_k h_k \rangle + \frac{\partial}{\partial y} \langle v_k h_k \rangle = 0 \qquad (123)$$

At the bottom $w = 0$; therefore

$$W_{k-1/2} = - \sum_{l=k}^{\bar{B}} \left[\frac{\partial}{\partial x} (u_l h_l) + \frac{\partial}{\partial y} (v_l h_l) \right] \qquad (124)$$

At the water surface $w = \partial\zeta/\partial t$ and therefore

$$\frac{\partial \zeta}{\partial t} + \sum_{l=1}^{\bar{B}} \left[\frac{\partial (h_l u_l)}{\partial x} + \frac{\partial (h_l v_l)}{\partial y} \right] = 0 \qquad (125)$$

reflects the free-surface conditions.

120. Horizontal momentum diffusion terms are expressed as gradients of Reynolds stresses evaluated by means of eddy viscosity coefficients

$$\tau_{xx} = A_{xx} \frac{\partial u}{\partial x}$$

$$\tau_{xy} = A_{xy} \frac{\partial u}{\partial y}$$

$$\tau_{yy} = A_{yy} \frac{\partial v}{\partial y}$$

$$\tau_{yx} = A_{yx} \frac{\partial v}{\partial x} \qquad (126)$$

These terms are further approximated by assuming only a single eddy viscosity coefficient characteristic of the u and v components of velocity, i.e.,

$$\tau_{xx} = A_x \frac{\partial u}{\partial x}$$

$$\tau_{xy} = A_x \frac{\partial u}{\partial y} \qquad (127)$$

$$\tau_{yx} = A_y \frac{\partial v}{\partial x}$$

$$\tau_{yy} = A_y \frac{\partial v}{\partial y}$$

121. The final governing equations for the k^{th} layer are

$$\frac{\partial}{\partial t}(hu) + \frac{\partial(huu)}{\partial x} + \frac{\partial(hvu)}{\partial y} + (wu)_{k-1/2} - (wu)_{k+1/2} - fhv + \frac{h}{\rho}\frac{\partial p}{\partial x}$$

$$+\left(\frac{1}{\hat{\rho}}\tau_{xz}\right)_{k+1/2} - \left(\frac{1}{\hat{\rho}}\tau_{xz}\right)_{k-1/2} - \frac{1}{\hat{\rho}}\frac{\partial(hA_x\frac{\partial u}{\partial x})}{\partial x} - \frac{1}{\hat{\rho}}\frac{\partial(hA_y\frac{\partial u}{\partial y})}{\partial y} = 0 \qquad (128)$$

$$\frac{\partial}{\partial t}(hv) + \frac{\partial(huv)}{\partial x} + \frac{\partial(hvv)}{\partial y} + (wv)_{k-1/2} - (wv)_{k+1/2} + fhu + \frac{h}{\rho}\frac{\partial p}{\partial y}$$

$$+\left(\frac{1}{\hat{\rho}}\tau_{yz}\right)_{k+1/2} - \left(\frac{1}{\hat{\rho}}\tau_{yz}\right)_{k-1/2} - \frac{1}{\hat{\rho}}\frac{\partial(hA_x\frac{\partial v}{\partial x})}{\partial x} - \frac{1}{\hat{\rho}}\frac{\partial(hA_y\frac{\partial v}{\partial y})}{\partial y} = 0 \qquad (129)$$

$$\frac{\partial}{\partial t}(hS) + \frac{\partial(huS)}{\partial x} + \frac{\partial(hvS)}{\partial y} + (wS)_{k-1/2} - (wS)_{k+1/2} - \frac{\partial(hD_x \frac{\partial S}{\partial x})}{\partial x}$$

$$- \frac{\partial(hD_y \frac{\partial S}{\partial y})}{\partial y} + \left[K\left(\frac{\partial S}{\partial z}\right)\right]_{k+1/2} - K\left(\frac{\partial S}{\partial z}\right)_{k-1/2} = 0 \qquad (130)$$

where τ_{xz} and τ_{yz} are the x- and y- components of interfacial shear stress. At the bottom

$$W_{k-1/2} = -\sum_{l=k}^{\bar{B}} \left[\frac{\partial(h_l u_l)}{\partial x} + \frac{\partial(h_l v_l)}{\partial y}\right] \qquad (131)$$

and at the surface

$$\frac{\partial \zeta}{\partial t} + \sum_{l=1}^{\bar{B}} \left[\frac{\partial(h_l u_l)}{\partial x} + \frac{\partial(h_l v_l)}{\partial y}\right] = 0 \qquad (132)$$

122. The boundary stresses are handled in a conventional manner. At the bottom the stress is related to the Chezy coefficient C.

$$\tau_{Bx} = \frac{\rho_B g u \sqrt{u^2 + v^2}}{C^2} \qquad (133)$$

$$\tau_{By} = \frac{\rho_B g v \sqrt{u^2 + v^2}}{C^2}$$

At the surface the shear stress is formulated in terms of the quadratic law,

$$\tau = \rho C_d \bar{u}^2 \tag{134}$$

where $\bar{u}$ = mean wind speed

123. The equation of state is taken as

$$\rho = \frac{p_o}{\lambda' - \alpha_o p_o} \tag{135}$$

While λ' can be expressed as a function of both temperature and salinity, ρ is considered to vary only with salinity within this particular problem formulation.

124. A space-staggered grid was selected for the finite difference representation of Equations 128-132. The grid structure is shown in Figures 26 and 27.

125. Because of the nonlinear nature of the problem, the finite difference formulation is complex and cumbersome. Sum and difference operations are introduced as an aid in formulating the finite difference scheme. For an arbitrary variable

$$F \equiv F\ (i\Delta x,\ j\Delta y,\ k\Delta z,\ n\Delta t)$$

The following sum and difference operators are adapted for representing the function at (i, j, k, n) :

$$\bar{F}^x = \frac{1}{2}\left\{F[(i + \tfrac{1}{2})\Delta x,\ j\Delta y,\ k\Delta z,\ n\Delta t] + F[(i - \tfrac{1}{2})\Delta x,\ j\Delta y,\ k\Delta z,\ n\Delta t]\right\} \tag{136}$$

$$\delta_x F = \frac{1}{\Delta x}\left\{F[(i + \tfrac{1}{2})\Delta x,\ j\Delta y,\ k\Delta z,\ n\Delta t] - F[(i - \tfrac{1}{2})\Delta x,\ j\Delta y,\ k\Delta z,\ n\Delta t]\right\} \tag{137}$$

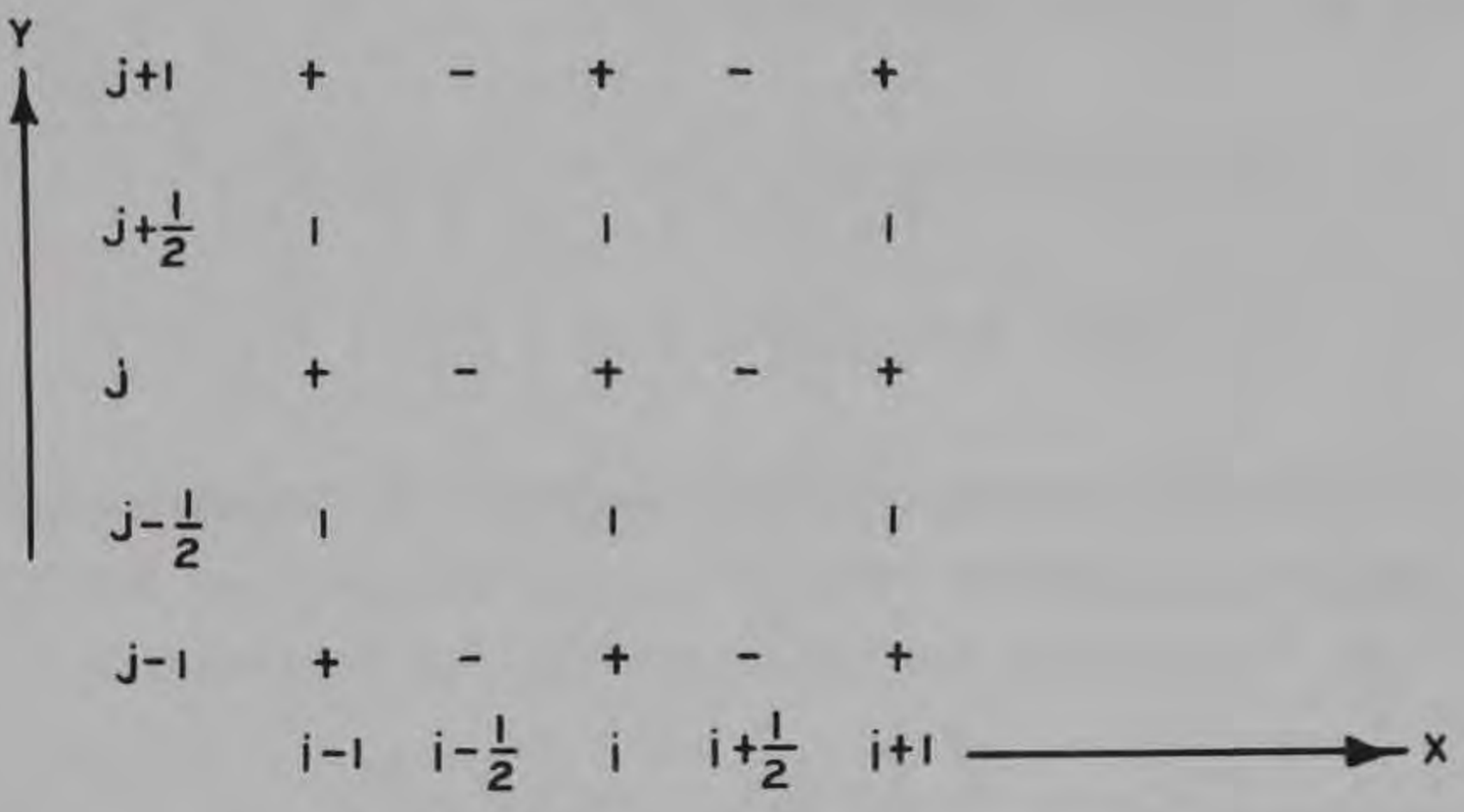

Figure 26. The location of u (-), v (1), and other parameters (+) in the space-staggered grid

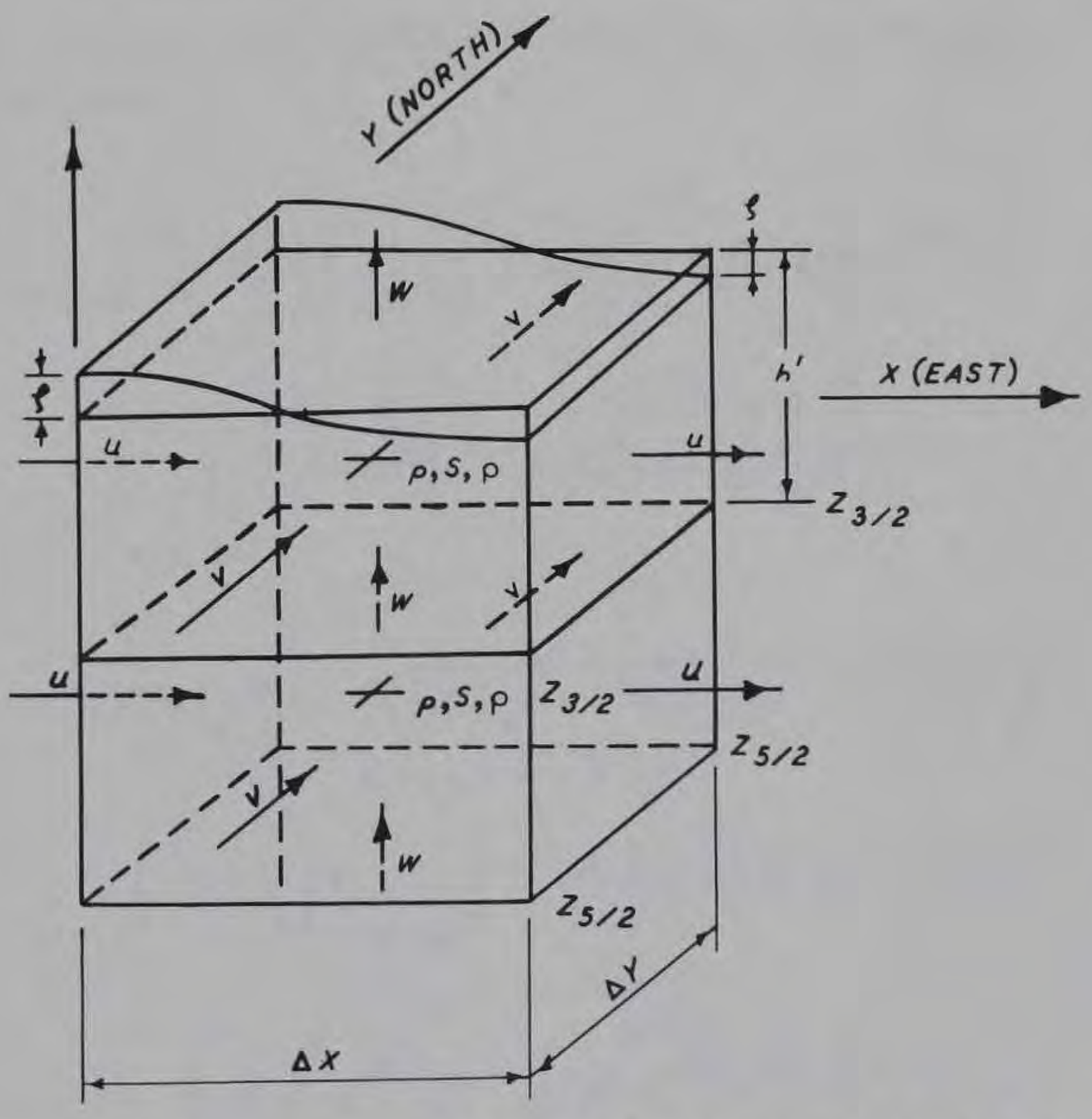

Figure 27. Relative position of the variables in the model

Similar operations are defined for y , z and t . The special notation used for shifting time levels is

$$F_+ = F\,[i\,\Delta x\ ,\ j\,\Delta y\ ,\ k\,\Delta z\ ,\ (n+1)\,\Delta t]$$

$$F_- = F\,[i\,\Delta x\ ,\ j\,\Delta y\ ,\ k\,\Delta z\ ,\ (n-1)\,\Delta t] \qquad (138)$$

126. The finite difference approximations of Equations 128-132 used for integration become

$$\overline{\delta_t \zeta}^t = -\sum_k \left[\delta_x(\bar{h}^x u) + \delta_y(\bar{h}^y v)\right]_{\text{at } i,\ j,\ n} \qquad (139)$$

$$\overline{\delta_t(\bar{h}^x u)}^t = -\delta_x(\overline{\bar{h}^x u\,\bar{u}^x}^x) - \delta_y(\overline{\bar{h}^y v\,\bar{u}^y}^x) - \bar{h}^z \delta_z(\bar{u}^z \bar{w}^x)$$
$$+ f\bar{h}^{x-xy} v - \frac{1}{\bar{\rho}^x}\bar{h}^x \delta_x p - \left(\frac{1}{\bar{\rho}^{xz}}\tau^{xz}_-\right)_{k+1/2} + \left(\frac{1}{\bar{\rho}^{xz}}\tau^{xz}_-\right)_{k-1/2}$$
$$+ \frac{1}{\bar{\rho}^x}\left[\delta_x\left(\overline{\bar{h}^x A_x}^x\,\delta_x u\right)_- + \delta_y\left(\overline{\bar{h}^x A_y}^y\,\delta_y u\right)_-\right] \qquad (140)$$
$$\text{at } i + 1/2,\ j,\ k,\ n$$

$$\overline{\delta_t(\bar{h}^y v)}^t = -\delta_x(\overline{\bar{h}^x u\,\bar{v}^x}^y) - \delta_y(\overline{\bar{h}^y v\,\bar{v}^y}^y) - \bar{h}^y \delta_z(\bar{v}^z \bar{w}^y)$$
$$- f\bar{h}^{y-xy} u - \frac{1}{\bar{\rho}^y}\bar{h}^y \delta_y p - \left(\frac{1}{\bar{\rho}^{yz}}\tau^{yz}_-\right)_{k+1/2} + \left(\frac{1}{\bar{\rho}^{yz}}\tau^{yz}_-\right)_{k+1/2}$$
$$+ \frac{1}{\bar{\rho}^y}\left[\delta_x\left(\overline{\bar{h}^y A_x}^x\,\delta_x v\right)_- + \delta_y\left(\overline{\bar{h}^y A_y}^y\,\delta_y v\right)_-\right] \qquad (141)$$
$$\text{at } i,\ j + p,\ k,\ n$$

$$\overline{\delta_t(hS)}^t = -\delta_x(\bar{h}^x u\bar{S}^x) - \delta_y(\bar{h}^y v\bar{S}^y) - \bar{h}^z\delta_z(w\bar{S}^z)$$

$$+ \delta_x\left(\bar{h}^x D_x\delta_x S\right)_- + \delta_y\left(\bar{h}^y D_y\delta_y S\right) + \bar{h}^z\delta_z(k\delta_z S)_- \qquad (142)$$

at i, j, k, n

These finite difference equations in the compact notation, which was used, have the same appearance as the differential equations.

127. The density is computed with the equation of state as follows:

$$\rho = \frac{p_o}{(\lambda + \alpha_o p_o)} \quad \text{at i, j, k, n + 1} \qquad (143)$$

128. The following finite difference equations are used to compute derived variables:

$$\delta_z w = -\delta(\bar{h}^x u) - \delta(\bar{h}^y v)$$

at i, j, k, n + 1 (144)

$$\delta_x p = g(\bar{\rho}^x\delta_x\zeta) + 1/2\ (\bar{h}^x\delta_x\rho)$$

at i + 1/2, j, 1, n + 1 (145)

$$\delta_y p = g(\bar{\rho}^y\delta_y\zeta) + 1/2\ (\bar{h}^y\delta_y\rho)$$

at i, j + 1/2, 1, n + 1 (146)

$$\delta_z(\delta_x p) - g\,\bar{h}^z\delta_x\bar{\rho}^z$$

at i + 1/2, j, k + 1/2, n + 1 (147)

$$\delta_z(\delta_y p) = g\,\bar{h}^z\delta_y\bar{\rho}^z$$

at i, j + 1/2, k + 1/2, n + 1 (148)

Boundary stress and interfacial stress term formulations

129. At the surface, the stress term can be computed from

$$\left(\frac{1}{\bar{\rho}^{xz}}\,\tau^{xz}_{-}\right)_{k-1/2} = C^{*}\,\frac{\rho_a}{\bar{\rho}^{x}}\,w_a^2\,\sin\phi \quad \text{at } i+1/2,\ j,\ 1,\ n \tag{149}$$

$$\left(\frac{1}{\bar{\rho}^{yz}}\,\tau^{yz}_{-}\right)_{k-1/2} = C^{*}\,\frac{\rho_a}{\bar{\rho}^{y}}\,w_a^2\,\cos\phi \quad \text{at } i,\ j+1/2,\ 1,\ n \tag{150}$$

where

C^{*} = resistance coefficient

ρ_a = atmospheric density

w_a = wind speed at 10-m level

ϕ = angle between wind direction and y-axis

Similarly, the stress term at the bottom (in layer B) can be computed from Equation 133.

$$\left(\frac{1}{\bar{\rho}^{xz}}\,\tau^{xz}_{-}\right)_{k+1/2} = \frac{g u_{-}\left[u_{-}^2 + (\bar{v}^{xy}_{-})^2\right]^{1/2}}{(\bar{C}^{x})^2} \tag{151}$$

at $i+1/2,\ j,\ B,\ n$

$$\left(\frac{1}{\bar{\rho}^{yz}}\,\tau^{yz}_{-}\right)_{k+1/2} = \frac{g v_{-}\left[(\bar{u}^{xy}_{-})^2 + v_{-}^2\right]^{1/2}}{(\bar{C}^{y})^2} \tag{152}$$

at $i,\ j+1/2,\ B,\ n$

130. Since estuary motions are mostly turbulent, the effects of eddy viscosity play a significant part in controlling stresses between adjacent layers with different velocities. Mass and momentum transfers are the result, and these transfers tend to equalize relative velocity differences in both the lateral and the vertical directions. If the

quadratic relationship between the interlayer stresses and the velocity differences is assumed applicable, the following expressions for the interlayer stresses can be used.

$$\left(\frac{1}{\bar{\rho}^{xz}}\,\tau^{xz}_{-}\right)_{k+1/2} = \nu(\delta_z u_-)\left[(\delta_z u_-)^2 + (\delta_z \bar{v}^{xy})^2\right]^{1/2} \qquad (153)$$

at i + 1/2, j, k + 1/2, n

$$\left(\frac{1}{\bar{\rho}^{yz}}\,\tau^{yz}_{-}\right)_{k+1/2} = \nu(\delta_z v_-)\left[(\delta_z \bar{u}^{xy})^2 + (\delta_z v_-)^2\right]^{1/2} \qquad (154)$$

at i, j + 1/2, k + 1/2, n

where ν is the coefficient of interfacial friction.

131. The equations used in the numerical integrations are second-order approximations in time and space, except that the evaluation of the momentum diffusion by use of Equations 153 and 154 in Equations 140 and 141 is not central in time, but at a lower time level, since otherwise the computation would become unstable. For the same reason the dispersion terms in Equation 142 are taken at the lower time level.

132. In describing the progress of the computation, it is assumed that the computation has progressed to a time level n. At this time the velocity components u and v, the salinity S, and the pressure p are all determined for each point of the grid and available for computation. These variables are also available at the previous time step $n - 1$. The water levels are available for computation at time level n and $n - 1$.

133. At the boundaries of the water body to be computed, all diffusion coefficients are zero, as are the velocities perpendicular to the boundary. In this manner, no mass fluxes or diffusive transports of salt will result. The boundaries of the horizontal layers also satisfy a no-slip boundary condition.

134. With this information, the prediction equations 139-142 are

used to advance the computational field of ζ , u , v , and S . For the evaluation of the boundary and interfacial stress terms in these equations, Equations 149-154 are used. These are all explicit operations for each of the variables resulting in computed values of ζ , u , v , and S at time level $n + 1$.

135. Subsequently, the vertical velocities, the densities, and the pressures required for the next step of the integration are computed. For the vertical velocity, Equation 143 is used, starting at the bottom layer and proceeding upward with the computation. In this manner the vertical velocity at the lower interface is known, and the other vertical velocities can be determined explicitly.

136. The density for each grid point can be computed by using Equation 135 from the salinity data now available at time $n + 1$. As water levels and densities are known at time level $n + 1$, the pressure gradients in the x and y directions can now be computed by using Equations 145-148. In this case, the gradients at the surface layer, and subsequently the other layers, proceeding downward, are computed by using Equations 145 and 148. In this manner the horizontal pressure gradient in the upper layer of the two layers involved in Equations 147 and 148 is known, and the horizontal pressure gradient in the lower layer can be determined explicitly.

137. The computational cycle is now ready to be reported, and ζ , u , v , and S can be computed for time level $n + 2$, as all variables are now determined for time level $n + 1$. To start a computation, information at two time levels is required.

138. The model was initially applied to several simple cases to test the computational procedure. These test cases were characterized by an increasing complexity in both boundary geometry and hydrodynamic behavior of the process. These test cases included

a. A seiche oscillation in a rectangular basin (density constant).

b. Wind-driven circulation in a rectangular basin with wind direction along the axis of the rectangle (density constant).

c. Wind-driven circulation is a rectangular basin with a diagonal wind stress (density constant).

d. Wind-driven circulation in a rectangular basin with a density gradient.

e. Wind-driven circulation in Lake Michigan with a constant density.

The model results for the test case appear reasonable and verify the general operating principles of the model. No attempt has been made however to simulate real events using observed field data. It should also be noted that no model results are indicated for the general problem of variable geometry, variable topography, and variable density. Work on this model is still progressing. To make the model applicable to engineering investigations, the following development work is recommended:

a. Formulate and develop the computational code for boundaries, such as those that occur at the bottom, sides, and the seaward ends of the model, based upon realistic formulations of the local physical processes and conditions.

b. Investigate the transfer of energy from one frequency range to another in the model by analyzing properties of the finite difference scheme and by experimenting with different formulations of the advective terms in the equations of motion.

c. Develop methods for graphically representing results.

d. Incorporate the transport of heat in the model, together with the interaction of temperature distribution with the fluid flow.

139. This model presently provides for a variation of density only with salinity and thus is not directly applicable to Lake Erie as a variable density model. It could be applied to Lake Erie as a three-dimensional constant density model. The other alternative, as far as application to Lake Erie, is to introduce the energy equation and convert the model to treating density as a function of temperature if a variable density lake model is desired. The author indicates that this modification is presently being investigated.

Model of J. Paul,
W. Lick, and R. T. Gedney

140. A time-dependent, three-dimensional, viscous, variable-density, heat-conducting model is presently being developed by J. Paul and W. Lick of Case Western Reserve University and R. T. Gedney at National Aeronautics and Space Administration (NASA) Lewis Research Center. This model is not yet completely operational; however, it is an extension of an operational model for thermal plumes and river discharges developed by Paul and Lick.[26] The thermal plume and river discharge model was developed for studying the near field surrounding the point of discharge of a river or power plant discharging into a body of water. Application of the thermal plume model required establishing computational limits in the body of water to which the plume is being discharged and appropriate boundary conditions on the computational boundaries. In the new model, the plume model will be coupled with a variable density model for a freshwater lake to allow the entire lake and the plume to interact. Changing lake conditions will then be reflected in an appropriate change in the plume.

141. The formulation for the lake model is not available at present; it must, however, be consistent with the thermal plume model where the two solutions are meshed together. The actual model formulation is more involved than any model discussed previously in this report due to the introduction of an energy balance equation.

142. While the complete formulation of the model is not available at present, the plume model will be discussed as illustrating some of the methods and techniques required in the model. The governing equations for the plume model are derived from the time-dependent, three-dimensional equations of motion for a viscous, compressible, heat-conducting fluid with a linear stress-strain relationship.

143. The time-dependent, three-dimensional equations of motion for a viscous, compressible, heat-conduting fluid with a linear stress-strain relationship are as follows:

$$\bar{\rho}\left(\frac{\partial \bar{u}}{\partial t} + \bar{u}\frac{\partial \bar{u}}{\partial x} + \bar{v}\frac{\partial \bar{u}}{\partial y} + \bar{w}\frac{\partial \bar{u}}{\partial z}\right) = -\frac{\partial \bar{P}}{\partial x} + \frac{\partial}{\partial x}\left(\bar{\mu}\frac{\partial \bar{u}}{\partial x}\right) + \frac{\partial}{\partial y}\left(\bar{\mu}\frac{\partial \bar{u}}{\partial y}\right) + \frac{\partial}{\partial z}\left(\bar{\mu}\frac{\partial \bar{u}}{\partial z}\right) \tag{155a}$$

$$\bar{\rho}\left(\frac{\partial \bar{v}}{\partial t} + \bar{u}\frac{\partial \bar{v}}{\partial x} + \bar{v}\frac{\partial \bar{v}}{\partial y} + \bar{w}\frac{\partial \bar{v}}{\partial z}\right) = -\frac{\partial \bar{P}}{\partial y} + \frac{\partial}{\partial x}\left(\bar{\mu}\frac{\partial \bar{v}}{\partial x}\right) + \frac{\partial}{\partial y}\left(\bar{\mu}\frac{\partial \bar{v}}{\partial y}\right) + \frac{\partial}{\partial z}\left(\bar{\mu}\frac{\partial \bar{v}}{\partial z}\right) \tag{155b}$$

$$\bar{\rho}\left(\frac{\partial \bar{w}}{\partial t} + \bar{u}\frac{\partial \bar{w}}{\partial x} + \bar{v}\frac{\partial \bar{w}}{\partial y} + \bar{w}\frac{\partial \bar{w}}{\partial z}\right) = -\frac{\partial \bar{P}}{\partial z} + \frac{\partial}{\partial x}\left(\bar{\mu}\frac{\partial \bar{w}}{\partial x}\right) + \frac{\partial}{\partial y}\left(\bar{\mu}\frac{\partial \bar{w}}{\partial y}\right) + \frac{\partial}{\partial z}\left(\bar{\mu}\frac{\partial \bar{w}}{\partial z}\right) \tag{155c}$$

$$\frac{\partial \bar{\rho}}{\partial t} + \frac{\partial}{\partial x}\left(\bar{\rho}\bar{u}\right) + \frac{\partial}{\partial y}\left(\bar{\rho}\bar{v}\right) + \frac{\partial}{\partial z}\left(\bar{\rho}\bar{w}\right) = 0 \tag{156}$$

$$\bar{\rho}C_p\left(\frac{\partial \bar{T}}{\partial t} + \bar{u}\frac{\partial \bar{T}}{\partial x} + \bar{v}\frac{\partial \bar{T}}{\partial y} + \bar{w}\frac{\partial \bar{T}}{\partial z}\right) = -\frac{\bar{T}}{e}\left(\frac{\partial \bar{\rho}}{\partial \bar{T}}\right)\bar{P}\left(\frac{\partial \bar{P}}{\partial t} + \bar{u}\frac{\partial \bar{P}}{\partial x} + \bar{v}\frac{\partial \bar{P}}{\partial y} + \bar{w}\frac{\partial \bar{P}}{\partial z}\right)$$

$$+ \frac{\partial}{\partial x}\left(\bar{k}\frac{\partial \bar{T}}{\partial x}\right) + \frac{\partial}{\partial y}\left(\bar{k}\frac{\partial \bar{T}}{\partial y}\right) + \frac{\partial}{\partial z}\left(\bar{k}\frac{\partial \bar{T}}{\partial z}\right) + \Phi + Q^* \tag{157}$$

$$\bar{\rho} = B'(\bar{T}) \tag{158}$$

where

$\bar{\rho}$ = density

$\bar{\mu}$ = absolute viscosity

C_p = specific heat at constant pressure

$\bar{T}$ = absolute temperature

$\bar{k}$ = thermal conductivity

Φ = heat dissipation

Q^* = heat source and/or sink

$B'(\bar{T})$ = equation of state

Note that

$$\Phi = \bar{\mu}\left[\frac{\partial ui}{\partial xj}\left(\frac{\partial ui}{\partial xj} + \frac{\partial uj}{\partial xi}\right) - \frac{2}{3}\left(\frac{\partial ui}{\partial xj}\right)^2\right] \quad i, j = 1, 2, 3$$

where

$$u_1 = \bar{u}$$
$$u_2 = \bar{v}$$
$$u_3 = \bar{w}$$
$$x_1 = \bar{x}$$
$$x_2 = \bar{y}$$
$$x_3 = \bar{z}$$

The density is taken to be dependent only upon the temperature.

144. The geometry of the plume is shown in Figure 28 where b_o and h_o are width and depth, respectively, of river discharging the plume. In obtaining the governing equations for the plume model, the following assumptions are made:

a. The pressure is assumed to vary hydrostatically, and therefore

$$\frac{\partial \bar{P}}{\partial z} = \rho g$$

b. The rigid lid approximation is made, i.e., $w(z=0) = 0$.

c. The Boussinesq approximation is made. This approximation assumes that the density variations are small and can be neglected except in the gravity term.

d. Heat sources and/or sinks in the fluid are neglected.

e. Eddy coefficients are used to account for the turbulent and molecular diffusion effects in both the momentum and energy equations. The horizontal coefficient is assumed to be constant, but the vertical coefficient is assumed to be dependent on the local vertical temperature gradient.

f. The variations in the bottom topography are assumed to be gradual.

All of these assumptions except d and f along with their consequences have been discussed previously in connection with other models. All heat inputs and outputs to the model are assumed to occur at the boundaries of the model. As a consequence, heat transfer by radiation to the water is treated as a surface heat flux.

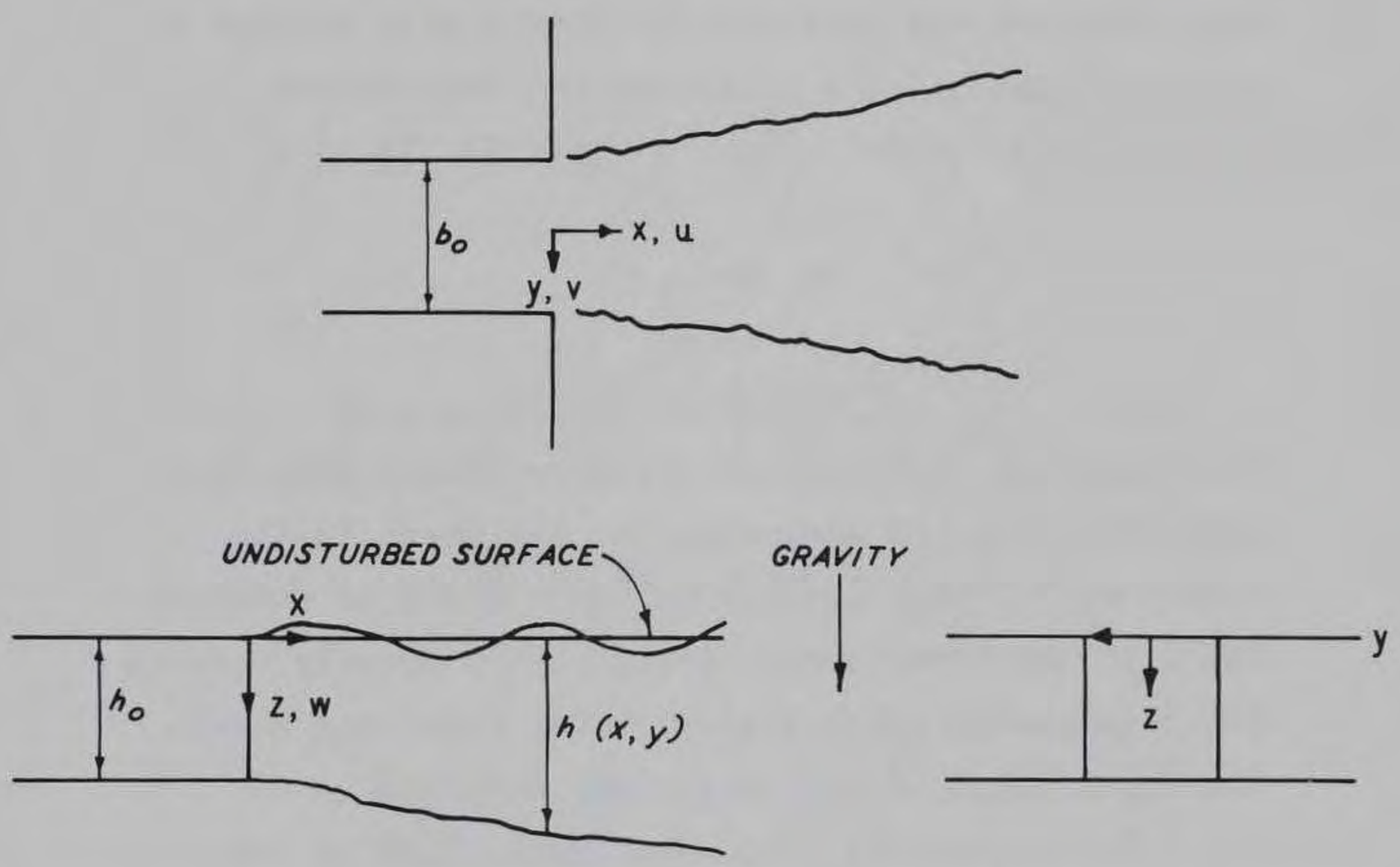

Figure 28. Geometry for three-dimensional jet

145. Paul and Lick presented in a previous study[27] the following detailed mathematical description of their plume model.

> The present numerical model allows variations in the depth of the basin which the outfall discharges into. A standard numerical procedure to fit the variable depth into a model is to vary the number of vertical points in the computational mesh according to the local depth.[28] A seemingly more complicated procedure, although a lot simpler in many aspects, is to stretch the vertical coordinate with respect to the local depth. The equations are transformed according to
>
> $$x \leftrightarrow x,$$
> $$y \leftrightarrow y,$$
> $$\sigma \leftrightarrow z/h(x,y).$$
>
> The equations to be solved are more complicated looking because of the appearance of the depth in the equation, but they are solved for a basin of constant depth in the transformed system. This greatly reduces the programming complexities of the model and makes the inclusion of depth variations simpler.
>
> The assumption of gradual variations in the depth allows a reduced form for the transformed diffusion terms to be used. The transformation used is not conformal and so the transformed diffusion terms involve cross-derivatives of the spatial coordinates. The terms containing derivatives of the depth are neglected with respect to those terms containing only the depth. This approximation is used in meteorological problems when topographic variations are included.[29,30]
>
> The resulting system of transformed equations, in nondimensional form, are the following:

$$\frac{1}{h}\frac{\partial(hu)}{\partial x} + \frac{1}{h}\frac{\partial(hv)}{\partial y} + \frac{\partial \Omega}{\partial \sigma} = 0,$$

$$\frac{\partial u}{\partial t} + Re\left[\frac{1}{h}\frac{\partial(hu^2)}{\partial x} + \frac{1}{h}\frac{\partial(huv)}{\partial y} + \frac{\partial \Omega u}{\partial \sigma}\right]$$

$$+ Rov = -\frac{\partial P}{\partial x} + \frac{1}{h}\left[\frac{1}{h}\frac{\partial}{\partial x}\left(h\frac{\partial u}{\partial x}\right) + \frac{\partial}{\partial y}\left(h\frac{\partial u}{\partial y}\right)\right]$$

$$-\frac{Re}{Fr^2}\left[h\int_o^\sigma \frac{\partial \Delta\rho}{\partial x}\,d\sigma + \frac{\partial h}{\partial x}\left(\int_o^\sigma \Delta\rho\,d\sigma - \sigma\Delta\rho\right)\right] + \left(\frac{b_o}{h_o}\right)^2 \frac{1}{h^2}\frac{\partial}{\partial \sigma}\left(\gamma\frac{\partial u}{\partial \sigma}\right)$$

$$\frac{\partial v}{\partial t} + Re\left[\frac{1}{h}\frac{\partial(huv)}{\partial x} + \frac{1}{h}\frac{\partial(hv^2)}{\partial y} + \frac{\partial \Omega v}{\partial \sigma}\right] - Rou$$

$$= -\frac{\partial P}{\partial y} + \frac{1}{h}\left[\frac{\partial}{\partial x}\left(h\frac{\partial v}{\partial x}\right) + \frac{\partial}{\partial y}\left(h\frac{\partial v}{\partial y}\right)\right]$$

$$-\frac{Re}{Fr^2}\left[h\int_o^\sigma \frac{\partial \Delta\rho}{\partial y}\,d\sigma + \frac{\partial h}{\partial y}\left(\int_o^\sigma \Delta\rho\,d\sigma - \sigma\Delta\rho\right)\right]$$

$$+\left(\frac{b_o}{h_o}\right)^2 \frac{1}{h^2}\frac{\partial}{\partial \sigma}\left(\gamma\frac{\partial v}{\partial \sigma}\right)$$

$$Pr\left(\frac{\partial \Delta T}{\partial t}\right) + Re\left[\frac{1}{h}\frac{\partial(hu\Delta T)}{\partial x} + \frac{1}{h}\frac{\partial(hv\Delta T)}{\partial y} + \frac{\partial \Omega \Delta T}{\partial \sigma}\right]$$

$$= \frac{1}{h}\left[\frac{\partial}{\partial x}\left(h\frac{\partial \Delta T}{\partial y}\right) + \frac{\partial}{\partial y}\left(h\frac{\partial \Delta T}{\partial y}\right)\right] + \left(\frac{b_o}{h_o}\right)^2 \frac{1}{h^2}\frac{\partial}{\partial \sigma}\left(\beta\frac{\partial \Delta T}{\partial \sigma}\right)$$

$$\frac{1}{h}\frac{\partial P}{\partial \sigma} = \frac{Re}{Fr^2}(1 + \Delta\rho)$$

$$\Delta\rho = f(\Delta T)$$

$$\sigma = z/h(x,y)$$

$$\Omega = \frac{1}{h}\left[w - \sigma\left(u\,\frac{\partial h}{\partial x} + v\,\frac{\partial h}{\partial y}\right)\right] = \frac{d\sigma}{dt}$$

where

$$u = \frac{\bar{u}}{u_o}, \qquad v = \frac{\bar{v}}{u_o},$$

$$w = \frac{\bar{w} b_o}{u_o h_o}, \qquad x = \frac{\bar{x}}{b_o},$$

$$y = \frac{\bar{y}}{b_o}, \qquad z = \frac{\bar{z}}{h_o},$$

$$P = \frac{\bar{P}Re}{\rho_o g h_o Fr^2}, \qquad \Delta\rho = \frac{\bar{\rho} - \rho_o}{\rho_o},$$

$$\Delta T = \frac{\bar{T} - T_E}{T_E}, \qquad t = \frac{\bar{t} A_H}{b_o^2},$$

$$\gamma = \frac{A_V}{A_H}, \qquad \beta = \frac{B_V}{B_H}$$

$$Ro = \frac{k b_o^2}{A_H}, \qquad Fr = \frac{u_o}{\sqrt{g h_o}},$$

$$Pr = \frac{A_H}{B_H}, \qquad Re = \frac{u_o b_o}{A_H},$$

$\rho_o = \bar{\rho}(T_E)$ and
u_o = reference velocity,
b_o = horizontal reference length,
h_o = vertical reference length,
A_H = horizontal eddy viscosity,
A_V = vertical eddy viscosity,
B_H = horizontal eddy diffusivity,
B_V = vertical eddy diffusivity,

T_E = equilibrium temperature

k = Coriolis parameter,

$f(\Delta T)$ = equation of state and

$(\bar{\ })$ = refers to dimensional quantity.

The equilibrium temperature is defined as the temperature at the surface for which there is no heat transfer.

The conservative form of the convective terms is used as this has been found by Arakawa[31] to be advantageous for numerical computations. The density is taken as only a function of temperature. The energy equation is nondimensionalized in terms of temperature differences. The effect of round-off error will be less in the evaluation of the derivatives if the differences are used.

The rigid-lid condition is difficult to apply in a numerical solution of the above system of equations. To alleviate this difficulty, an additional equation, a Poisson equation for the pressure, which contains the rigid-lid condition, can be derived. This is accomplished by taking the divergence of the vertically integrated horizontal momentum equations and using the vertically integrated continuity and hydrostatic pressure equations. The Poisson equation is:

$$\frac{\partial}{\partial x} h \frac{\partial P_s}{\partial x} + \frac{\partial}{\partial y} h \frac{\partial P_s}{\partial y} = - h \frac{\partial}{\partial t} \quad \Omega(\sigma=0)$$

$$+\left(\frac{b_o}{h_o}\right)^2 \frac{\partial}{\partial x}\left(\frac{1}{h} \gamma \frac{\partial u}{\partial \sigma}\right)_{\sigma=1} - \left(\frac{1}{h} \gamma \frac{\partial u}{\partial \sigma}\right)_{\sigma=0}$$

$$+\left(\frac{b_o}{h_o}\right)^2 \frac{\partial}{\partial y}\left(\frac{1}{h} \gamma \frac{\partial v}{\partial \sigma}\right)_{\sigma=1} - \left(\frac{1}{h} \gamma \frac{\partial v}{\partial \sigma}\right)_{\sigma=0}$$

$$- \frac{\partial}{\partial x} h \int_o^1 \left[Re\left(\frac{1}{h} \frac{\partial hu^2}{\partial x} + \frac{1}{h} \frac{\partial huv}{\partial y} + \frac{\partial \Omega u}{\partial \sigma} \right) + Rov - \frac{1}{h} \frac{\partial}{\partial x} h \frac{\partial u}{\partial x} \right.$$

$$\left. - \frac{1}{h} \frac{\partial}{\partial y} h \frac{\partial u}{\partial y} + \frac{Re}{fr^2} \left(\frac{\partial}{\partial x} h \int_o^\sigma \Delta\rho d\sigma - \sigma \frac{\partial h}{\partial x} \Delta\rho \right) \right] d\sigma$$

$$- \frac{\partial}{\partial y} h \int_o^1 \left[Re\left(\frac{1}{h} \frac{\partial huv}{\partial x} + \frac{1}{h} \frac{\partial hv^2}{\partial y} + \frac{\partial \Omega v}{\partial \sigma} \right) - Rou - \frac{1}{h} \frac{\partial}{\partial x} h \frac{\partial v}{\partial x} \right.$$

$$\left. - \frac{1}{h} \frac{\partial}{\partial y} h \frac{\partial v}{\partial y} + \frac{Re}{fr^2} \left(\frac{\partial}{\partial y} h \int_o^\sigma \Delta\rho d\sigma - \sigma \frac{\partial h}{\partial y} \Delta\rho \right) \right] d\sigma$$

The term P_s is the integration constant resulting from the vertical integration of the hydrostatic pressure equation and is the surface pressure, i.e., the pressure at the surface $z = 0$. It is a function of both x and y. This surface pressure can be interpreted in terms of the equivalent height of water above or below the surface $z = 0$ required to provide the prescribed pressure. In this way, surface displacements of water, neglecting gravity waves, can be compared between this rigid-lid model and the equivalent free surface model.

The vertical velocity at the surface $z = 0$ has not been set to zero in the right-hand-side of the Poisson equation for the surface pressure. This is because a corrective procedure[32] is used in the

numerical solution to eliminate accumulative error in the satisfaction of the continuity equation.

The following boundary conditions are used with the above system of equations:

River outflow

$$u = g_1(y,z)$$
$$v = g_2(y,z)$$
$$\Delta T = g_3(y,z)$$

Shore

$$u = 0$$
$$v = 0$$
$$\frac{\partial \Delta T}{\partial n} = 0$$

Bottom

$$u = 0$$
$$v = 0$$
$$w = 0$$
$$\frac{\partial \Delta T}{\partial z} = 0$$

Surface

$$\frac{\partial u}{\partial z} = \tau_{wx}$$
$$\frac{\partial v}{\partial z} = \tau_{wy}$$
$$\frac{\partial \Delta T}{\partial z} = K\Delta T$$
$$w = 0$$

Outer Boundary

either $\frac{\partial u}{\partial n} = 0$ or $u = f_1$

$$\frac{\partial v}{\partial n} = 0 \quad \text{or} \quad v = f_2$$

$$\frac{\partial \Delta T}{\partial n} = 0 \quad \text{or} \quad \Delta T = f_3$$

Pressure Conditions

$\frac{\partial p}{\partial n}$ = integrated x or y momentum equation, specify pressure level at one point.

The functional forms g_1, g_2, and g_3 are the specified velocity and temperature profiles across the river outfall. The bottom and shore are taken as no-slip, impermeable, insulated surfaces. A heat transfer condition proportional to the temperature difference[32] and a wind-dependent stress are imposed at the surface. The normal derivative pressure boundary conditions are derived from the appropriate vertically integrated momentum equation. The pressure must be specified at one point to make its solution unique. The boundary conditions applied at the outer x and y boundaries are either that the normal derivatives of the velocity and temperature are zero, or that the velocity and temperature are specified.

146. The general arrangement of variables in the grid system for the plume model is almost identical with that used previously by Paul and Lick.[26] The horizontal velocities are defined at integral nodal points, the vertical velocity is defined at half-integral nodal points, the temperature is defined at half-integral nodal points in the horizontal and integral nodal points in the vertical, and the surface pressure is defined at half-integral nodal points in the horizontal. Figure 29 indicates typical horizontal and vertical grid sections and shows the relative positions of the various variables. For the derivation of the finite difference equations, variables are sometimes

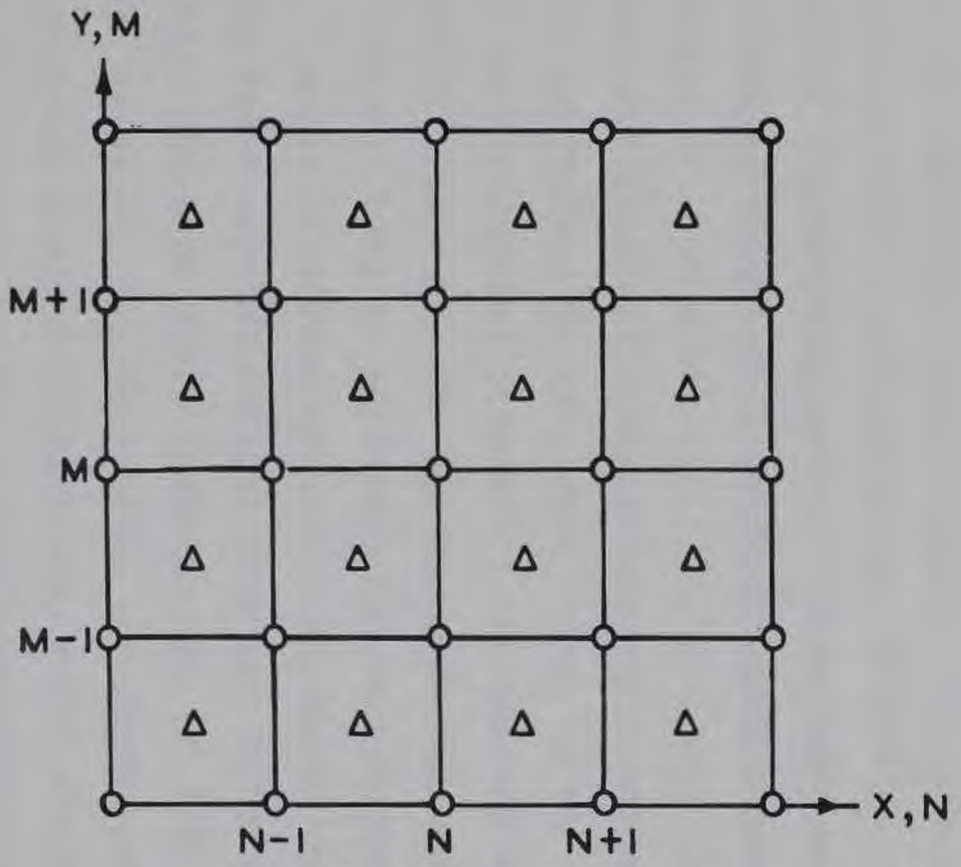

HORIZONTAL PLANE

VARIABLES

○ u, v
△ T, ρ, P_s
□ w

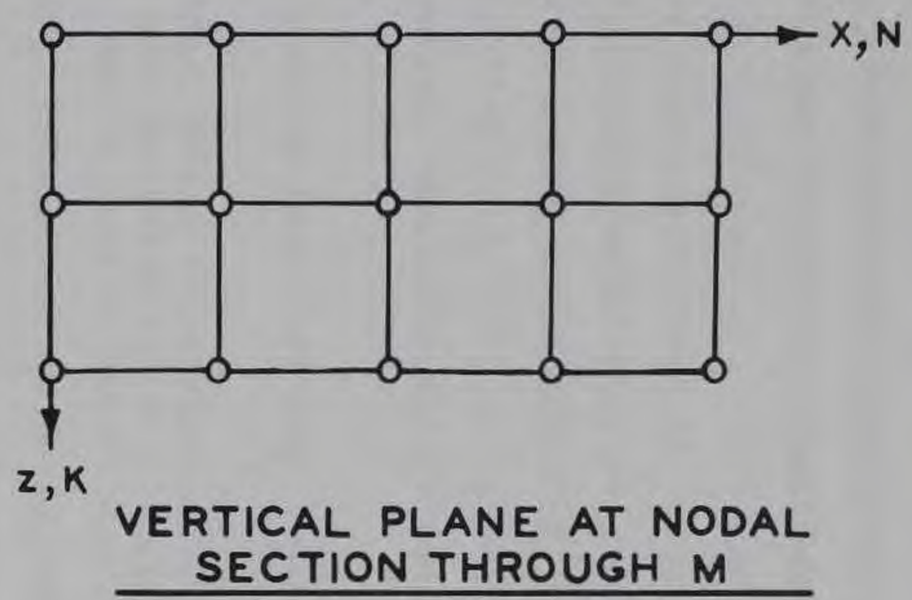

VERTICAL PLANE AT NODAL SECTION THROUGH M

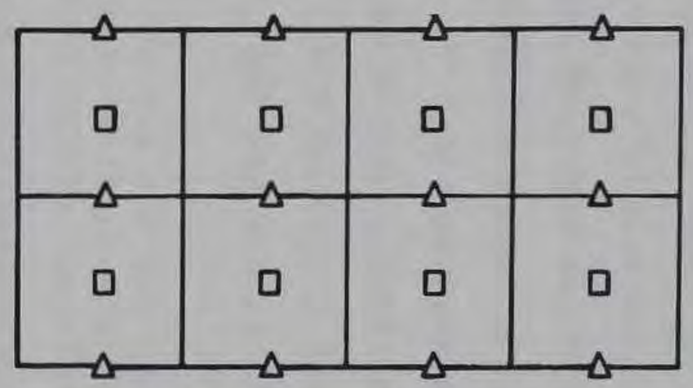

VERTICAL PLANE AT HALF-NODAL SECTION THROUGH M+1/2

Figure 29. Arrangement of variables in grid sections

required at points where they are not defined. In these circumstances, the undefined quantity is taken as the simple average of the neighboring values.

147. The Euler explicit time scheme is used exclusively in the present model in which the time derivative is written as a simple forward time difference and the rest of the equation is evaluated with the previously calculated values.

148. The following scheme is used for the solution of the difference equations for the plume model:

a. It is assumed that values from the previous time step are available.

b. The surface pressure is calculated with the right side of the equation evaluated from the previous time step values.

c. The temperature is calculated by the explicit time scheme.

d. The density is calculated from the equation of state.

e. The horizontal velocities are calculated by the explicit time scheme.

f. The vertical velocity is calculated by vertically integrating the continuity equation from the bottom.

g. The present time step is now complete.

At each time step the Poisson equation in the surface pressure has been solved. This is solved by the alternating-direction-implicit (ADI) method.[33,34]

149. After the temperatures are calculated by the explicit time scheme, they are checked to see if static stability is satisfied, i.e., if the temperatures decrease monotonically downward (assuming that density increases with decreasing temperature). When a static instability is encountered, an infinite mixing procedure is used. This procedure merely averages the temperature over an unstable region.

150. The thermal plume model has been applied for the Point Beach Power Plant thermal outfall and for the Cuyahoga River entering Lake Erie. In the vicinity of the inlet, the grid spacing is constant, then increases with distance from the inlet, and finally becomes constant in each direction. Such a grid system is used to pick up details of the

flow near the inlet where quantities change rapidly and to avoid an excessive number of points away from the inlet where quantities are changing much more slowly. Constant spacing is used in the vertical direction.

151. The vertical eddy coefficient is taken as dependent on the local vertical temperature gradient ($\partial T/\partial z$). The actual form used is similar to that used in an application of the numerical model to the wind-driven and thermally driven circulation in a small pond.[35]

$$A_v = \alpha - \beta \frac{\partial T}{\partial z}$$

where α and β are constants dependent on the local conditions of the problem. The constant α is chosen so that in the absence of temperature gradients, the eddy coefficient is equal to that which would be used in a constant eddy coefficient model.

152. The stress acting on the water surface due to the wind is calculated by the formulae developed by Wilson.[24] These formulae have been used successfully in numerical calculations of wind-driven circulations in lakes and small ponds.[22,23,35]

153. The results obtained from the plume model for these two indicated applications appear reasonable; however, no comparison with prototype data is available. The complete lake and plume model has not as yet been applied to any actual physical geometries.

PART V: RECOMMENDED HYDRODYNAMIC MODELS

Storm Surge

154. From a review of available literature, accurate storm surge surface elevations in lakes apparently can be obtained from the two-dimensional depth-averaged models if a free surface boundary condition is used. If hydrodynamic quantities other than surface elevations are desired, however, the two-dimensional storm surge model is of little use and three-dimensional models must be used. The changes in circulation patterns produced by structures can be obtained only from three-dimensional models.

155. The three-dimensional models are usually more expensive to operate than the two-dimensional models. This expense suggests the use of two-dimensional models in the preliminary storm surge calculations followed by application of the three-dimensional models for final detailed analyses.

156. Several satisfactory two-dimensional storm surge models with a free surface condition are available. The three-dimensional storm surge model developed by Haq, Lick, and Sheng[23] appears the most promising of a limited number of three-dimensional models and should be available in a matter of months with initial application to Lake Erie for storm Agnes.

Wind-Driven Circulation

157. The two-dimensional models provide very little useful information relative to lake circulation. The velocity predictions obtained from the two-dimensional models are interesting only in a rough, qualitative manner. The detailed hydrodynamic variables required to determine the complex velocity structure in a lake can be obtained only from a three-dimensional model.

158. The three-dimensional numerical models presently available and in the development stage by Dr. Wilbert Lick and associates at

Case Western Reserve University appear to be the most promising models for wind-driven circulation in freshwater lakes. These models are particularly appropriate for Lake Erie applications since the models have previously been applied to Lake Erie and much lake information is already available in a convenient format for input into the model.

159. A three-dimensional steady-state circulation model is presently operational at Case Western Reserve University.[22] This model has been applied to Lake Erie with some degree of verification based on prototype data. A three-dimensional stratified circulation model is presently under development and should be operational in the near future.

PART VI: MODEL VERIFICATION

General Verification Procedures

160. A hydrodynamic mathematical model is a discretization of the actual physical system. As such, the mathematical model is somewhat limited in the resolution of actual physical details. In a mathematical model based upon finite difference techniques, any physical detail smaller than the grid size cannot be directly represented. In a similar manner, the results of the mathematical model cannot resolve small-scale local circulation patterns or eddies unless the condition extends over an area covering several grid points. In addition, since the depths are indicated in a discrete manner, the numerical model tends to smooth or average the bottom topography and eliminate local undulations. At the same time, changes in the boundary configuration are made in a step manner rather than a gradual change.

161. The mathematical modeler must therefore select a grid size and orientation of the coordinate system that will allow the desired phenomena to be resolved. He must also use judgment and experience in the selection of system boundaries and the representation of the topography. These details represent part of the "art" as opposed to "science" of mathematical modeling and must be accomplished prior to actually "running" the model. Unfortunately, although very important, these details are some of the lesser problems associated with mathematical models.

162. The mathematical model formulation contains parameters that are not well defined quantities. Bottom friction, the horizontal eddy viscosity, the vertical eddy viscosity coefficient, and the wind speed-surface stress relationship are examples of model input that are very much dependent upon the specific model application. The bottom friction is basically a function of the bottom surface, i.e. sand, mud, rubble, grass, etc. The eddy viscosity coefficients are functions of the degree of turbulence, the density variations, the wind condition, the local ship traffic, etc. The wind speed-surface stress relationship presents

problems primarily due to difficulties associated with extrapolating known wind conditions at some fixed land site to obtain a wind speed at some location in the lake.

163. The nature of the parameters in the mathematical model are such that model verification is required prior to using the model as a predictive tool. Order of magnitude values of the parameters are known; however, these values are not sufficient for the model applications. The model parameters must be adjusted in such a manner that the numerical model results agree with existing prototype conditions. Once agreement with existing prototype condition has been obtained, the values of the parameters required to obtain the agreement are considered to be the appropriate values of the parameters. These values of the parameters are then used when the model is applied to predict changes resulting from some proposed modification of the existing condition.

164. Sufficient prototype data for existing conditions must be known to allow the mathematical model to be verified. The degree of verification, and hence confidence, in the model results depend upon the amount of prototype data available for verification of the model. For complete model verification, prototype data should exist for all hydrodynamic variables under investigation, and the data should be available at a number of locations extending over the area to which the model will be applied. If less than this amount of prototype data is available for model verification, a corresponding decrease in confidence in the model results must be accepted.

Verification Status of Recommended Models

Storm surge

165. The two-dimensional storm surge models are the most extensively verified of the recommended models. While there are some differences between the various models, the basic formulation procedure is the same and similar results are obtained from all the models. The surface elevations predicted by the two-dimensional models have been compared with measured values for several actual storm systems. For

example, Platzman[14] has investigated several extreme storm surge conditions on Lake Erie; Paskausky[20] has investigated the Lake Erie storm surge associated with storm Agnes; and Reid and Bodine[18] have investigated storm surge in Galveston Bay during hurricanes Carla (1961) and Cindy (1963). The surface elevations predicted by the two-dimensional models display a reasonable agreement with measured tidal elevations.

166. The recommended three-dimensional storm surge model has been partially verified by application to Lake Erie during storm Agnes.[23] The calculated and measured values for the surface displacement at Cleveland and at Port Stanley were found to be in good agreement. There has been no known effort to verify the calculated velocities, due primarily to a lack of reliable prototype velocity data.

Wind-driven circulation

167. The recommended three-dimensional, steady-state, constant-density model of Gedney and Lick[22] has been verified to a limited extent. The model has been applied to Lake Erie for a constant wind condition and the calculated velocities compared with measured velocities observed whenever the wind was fairly steady for two or more days. The results show that the velocities vary greatly from position to position and depend strongly on the bottom topography and boundary geometry. The calculated velocities are compared with a limited number of continuous current meter measurements at 10 and 15 m below the surface. Good quantitative agreement between the meter measurements and calculations were found to exist whenever the wind was fairly steady for two or more days. Qualitative agreement with lakebed drifter and surface drift measurements has also been observed.

168. The three-dimensional, variable-density model, which is recommended, is not yet completely operational; and no model verification efforts have been conducted. This model is, however, an extension of a thermal plume model to which some verification efforts have been directed.

169. The recommended models have not been verified to the extent needed for detailed quantitative results. This situation is particularly true for the velocity fields predicted by the three-dimensional

models. Additional Lake Erie prototype data, especially for the region near Cleveland, are required to verify the models and to enhance their operational mode as a predictive tool.

PART VII: RECOMMENDED PROTOTYPE DATA ACQUISITION SYSTEM

Prototype Data Requirements

170. A review of available data by WES as a part of the Lake Erie International Jetport Model Feasibility Investigation indicated that sufficient prototype data near Cleveland were not available to verify either a physical or analytical lake mass circulation model. Other areas where insufficient data exist include wave regime definition, littoral transport, and harbor flushing. Limited current data are available at four stations near Cleveland for several months during the summer of 1965, from a 1964-65 Environmental Protection Agency (formerly the Federal Water Pollution Control Agency) current metering program. The data from these stations are not continuous over the recording period and, for three of the stations, are available for one depth only.

171. A prototype data acquisition and analysis program is proposed by WES to obtain sufficient prototype data for verification of analytical and physical circulation models of the effects of a jetport on the hydrodynamics of Lake Erie near Cleveland, Ohio. This program has two modes: (a) time-series data in the lake proper and (b) synoptic data near and in the commerical harbor and river navigation channel. For the time-series mode, water velocity, water temperature, mean water level, wave height, wind velocity, and air temperature will be monitored; and in the synoptic survey, water velocity, water temperature, and dye concentration will be monitored.

Proposed Time-Series Data Acquisition System

172. In the time-series mode of data acquisition, the hydrological parameters to be recorded are the x-y components of water and wind velocities, water and air temperature, wave height, water elevation, and barometric pressure. A data acquisition system to collect these data can be subdivided into the transducer conditioner, transmitter, receiver, conditioner for recording, and recorder subsystems.

173. Four instrument towers are proposed to be installed in Lake Erie near Cleveland. The transducer, conditioner, and transmitter subsystems are to be mounted on these towers and shall be capable of operating at rated specifications in the ambient environmental conditions. Location of the towers and the instrumentation to be attached to each tower are shown in Figures 30 and 31. The towers will be similar in configuration and bracing to triangular communication towers mounted on land. They will be 80 ft in height and installed in a water depth of about 60 ft. Two sets of guy wires will be included as shown in Figure 32. The power requirements shall be kept at a minimum to ensure the longest battery life possible. The analog output of the velocities and temperature transducers shall be digitized and conditioned for radio transmission.

174. The receiver, conditioner for recording, and recording subsystems shall be located in an office area where air conditioning, regulated power, and general laboratory conditions are available. These subsystems need meet only laboratory type specifications.

Specifications for transducers

175. The transducer subsystem will require various sensors that are specialized to collect the required data at specified sampling rates. Such instruments are highly specialized and will be discussed below as to the required data types.

176. Water velocity. A magnetic current meter capable of measuring the x-y components of the water velocity shall be used. This type meter was selected because of its small size, accuracy, and no moving parts, which would require constant attention. The meter range is 0 to $\pm$ 10 fps $\pm$ 0.07 fps or 2 percent of reading. Increased accuracy to $\pm$ 0.02 fps can be obtained at additional cost. The resolution shall be $0.03/\sqrt{T}$ fps where T is the time constant. The standard time constant is 1 sec with optional values from 0.2 sec to 20 sec. There shall be a recorder output of $\pm$ 5 v full scale. The current meter sensor, which will be mounted vertically, is approximately 10-1/2 in. long and 1 in. in diameter.

177. Wind velocity. The wind velocity shall be measured with two

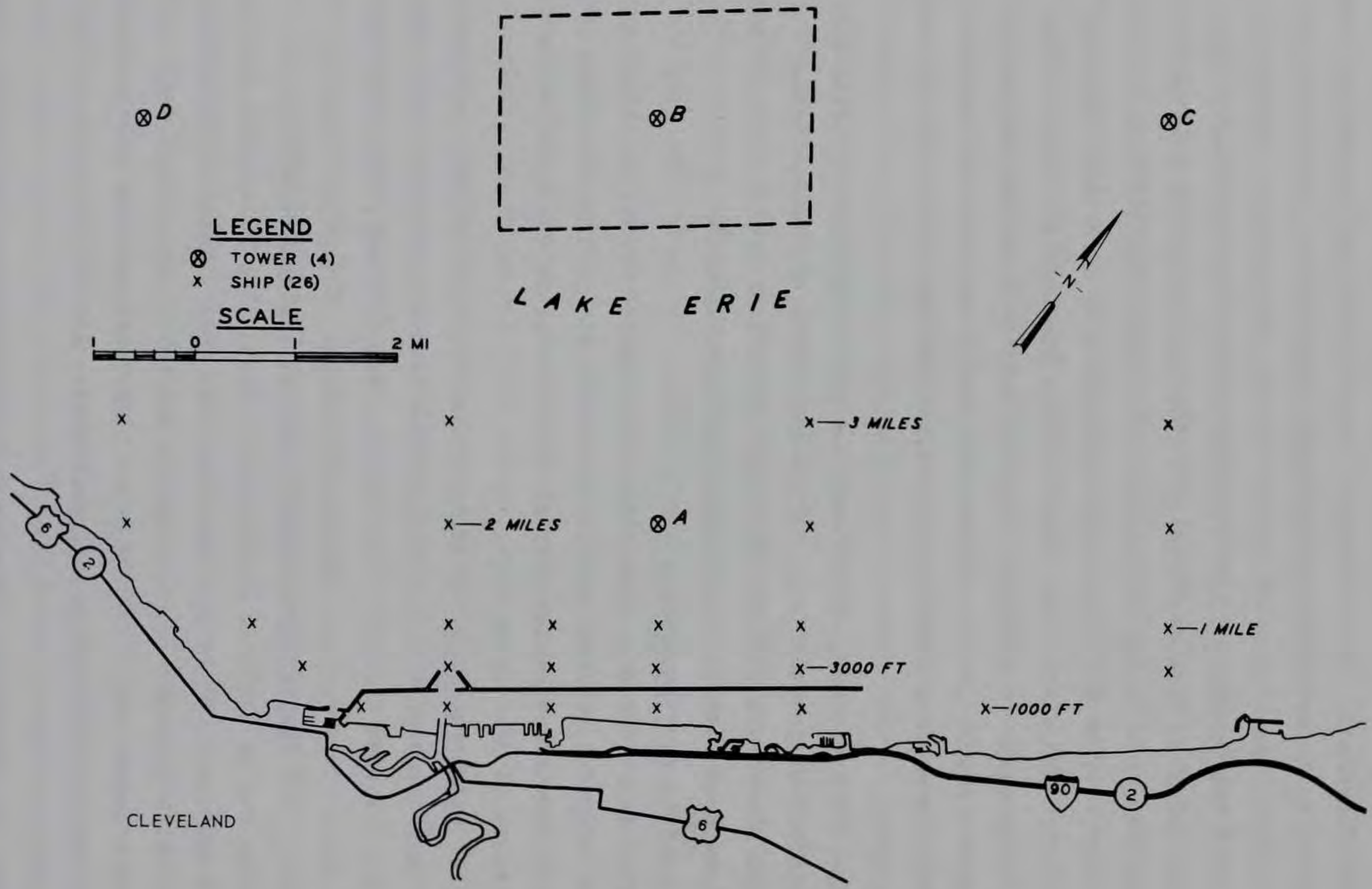

Figure 30. Location of time-series survey stations

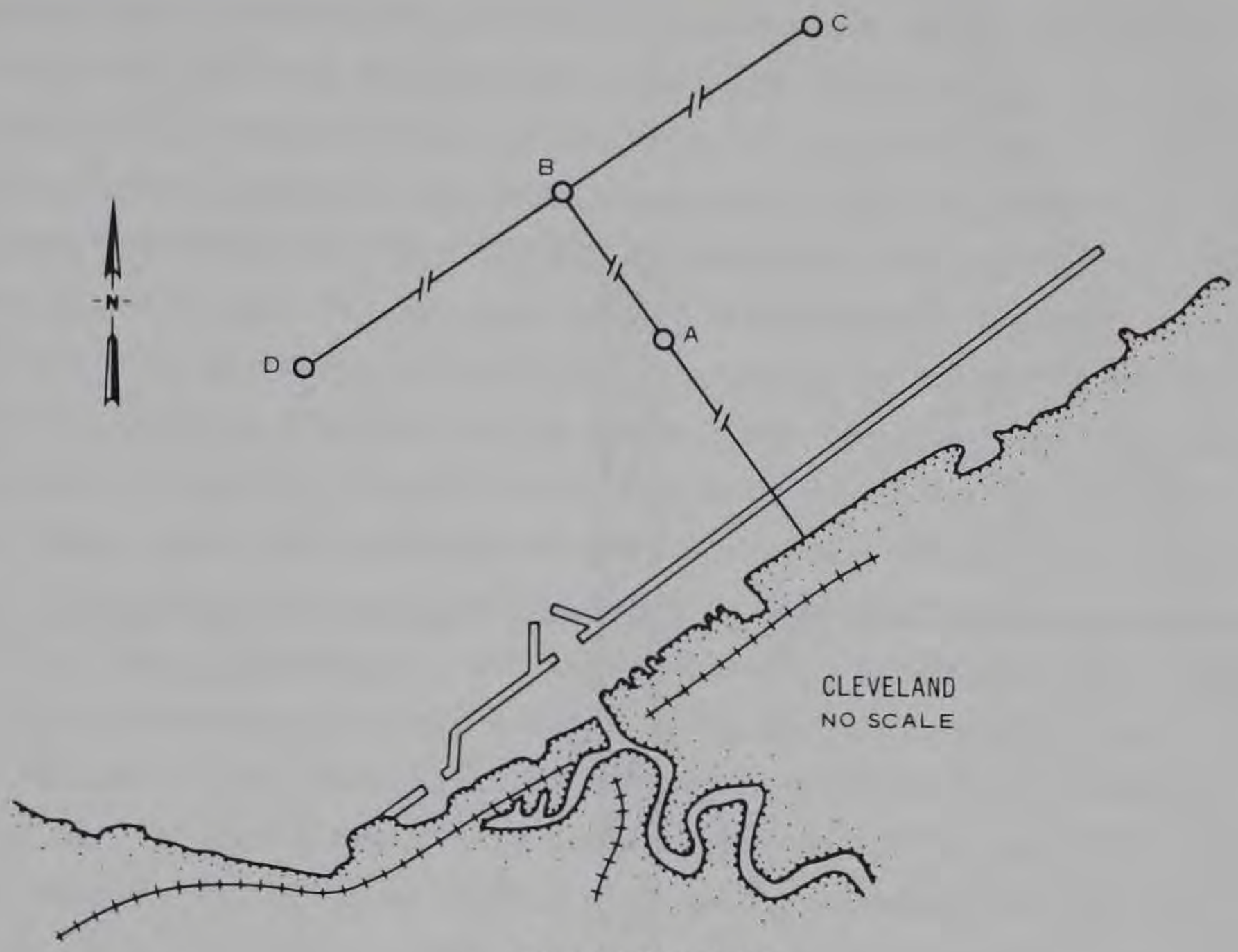

a. TOWER LOCATIONS

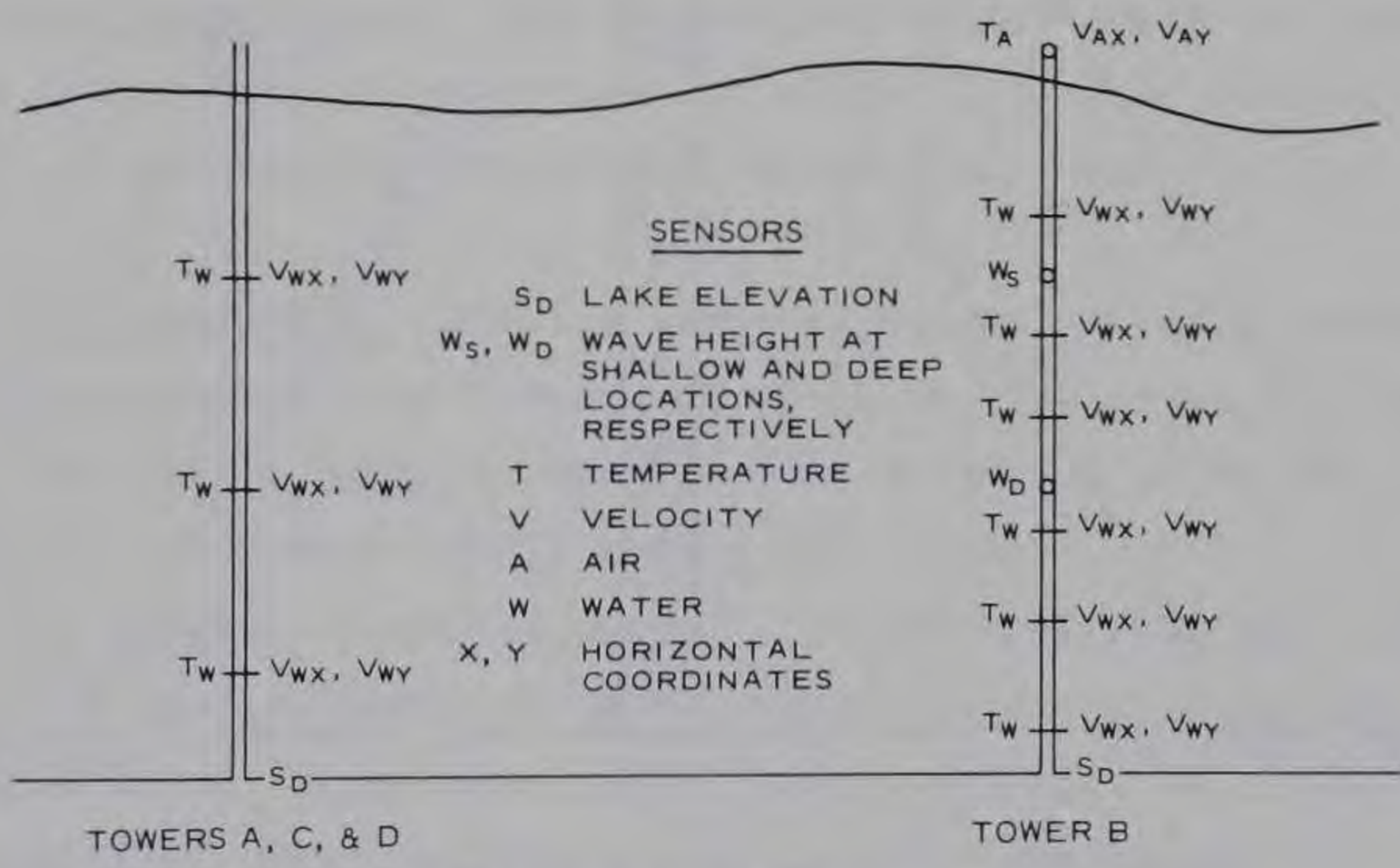

b. INSTRUMENTATION LOCATIONS

Figure 31. Location of towers and instruments for time-series survey

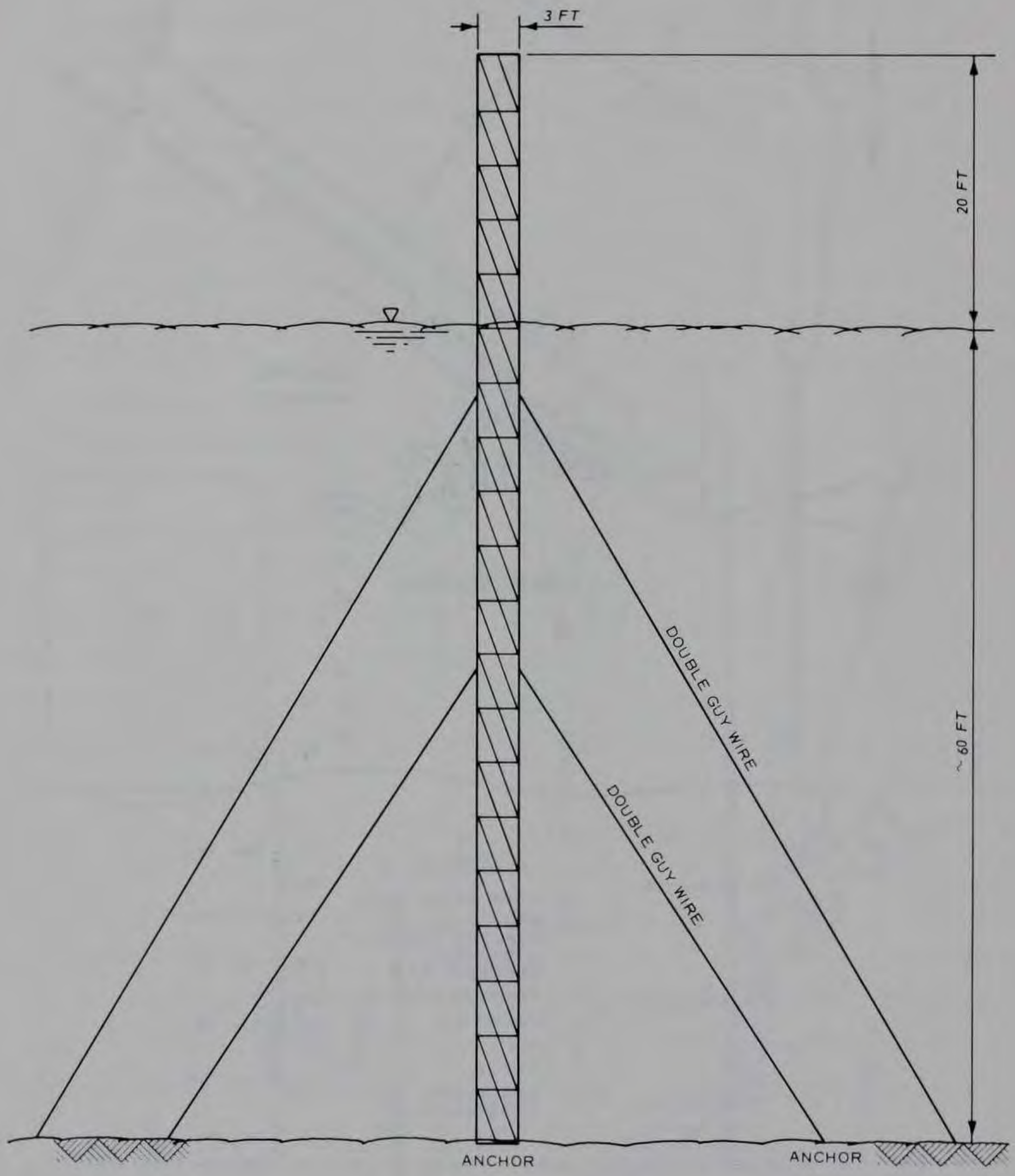

Figure 32. Schematic of instrumentation towers

perpendicularly mounted propeller-type anemometers that respond only to that component of wind parallel with its axis of rotation. When the wind is exactly perpendicular to the axis of the propeller, it will stop rotating. The propeller responds as a function of its orientation to the wind; this response very closely approximates the cosine law. Each sensor measures both forward and reverse air movement, providing a signal whose magnitude is proportional to propeller speed and whose polarity indicates direction. The range shall be 90 mph head on and 70 mph at all angles. The threshold shall be 0.3-0.5 mph. The propeller shall have 0.96 revolutions per foot of air movement. The $d_o = c_o$ tachometer output shall be $\pm$500 mv DC at $\pm$1800 rpm.

178. Water elevation. The water elevation transducer shall consist of a mechanically driven encoder, a float, tape, pulley, and counterweight. The float shall operate in a cylinder that is vented to the lake through a small hole near the bottom of the cylinder. The water level in the cylinder is the mean water elevation of the lake and will not vary with wave action. As the water level changes, the float system rotates the encoder input shaft. The encoder shall have binary coded decimal output with a resolution and accuracy of one part in 10,000. Full range shall be 99.99 ft.

179. Water temperature. The temperature sensor shall be capable of measuring temperature over a range of $0^{\circ}C$ to $40^{\circ}C$ to an accuracy of $\pm 0.15^{\circ}C$. The output of the device shall be no less than 1 v full scale.

180. Air temperature. The air temperature sensor shall be capable of measuring temperature over a range of $-10^{\circ}C$ to $30^{\circ}C$ to an accuracy of $\pm 0.25^{\circ}C$. The sensor shall be mounted in a structure to shield it from direct sun. The output shall be 5 v full scale.

181. Wave height. Wave heights will be measured with two transducers, one at a shallow depth for small waves and one at a greater depth for large waves. Each wave height transducer will be an absolute pressure transducer. This transducer will have no moving parts exposed to the lake water. The pressure transducer will be encased in a container 6.5 in. OD and 15 in. long. The pressure port will be in the

top of this container, and the case will be made of plastic or some noncorrosive, nonmetallic material. The shallow-depth pressure transducer range will be 58 ft absolute, from which the barometric pressure must be subtracted, leaving about 25 ft for wave variations. The greater-depth transducer range will be 116 ft absolute, with about 80 ft for wave variations. The operating temperature will be 35°F to 75°F. The output will be 0.28 to 7.5 MHz with linearity and hysteresis being 0.05 percent of full scale from best straight line between 15 psia and full scale. The repeatability will be 0.02 percent full scale with a long-term accuracy of 0.25 percent. The frequency analog output will be connected to an above-the-surface unit that will convert the frequency to a 12-bit natural binary output.

182. Sampling rates. The sampling rates of each instrument will vary depending upon the phenomena to be sampled. The anticipated sampling rates are as follow:

a. Temperature.

(1) Air: instantaneous value every 20 min.

(2) Water: instantaneous value every 20 min.

b. Velocity.

(1) Air: 20-min average of 1-sec digital valves.

(2) Water: 20-min average of 1-sec digital valves.

c. Waves.

(1) Deep: four per second for 20 min every 3 hr.

(2) Shallow: four per second for 20 min every 3 hr.

d. Lake level. Instantaneous value every 20 min.

183. Analog-to-digital converter (ADC). The ADC converts the analog voltage outputs of the various transducers to a 2's complement binary code. A 16-channel analog multiplexer will be an integral part of the ADC unit. The analog input levels are ±5 v. The input impedance will be 10^9 ohms. The transfer characteristics will have an accuracy and linearity of 0.023 percent full scale ± least significant bit. The temperature coefficient will be no greater than 0.044 percent/°C. The acquisition time will be no greater than 150 μsec. The system throughput rate will be no greater than 450 μsec. The ADC unit

will operate from a 12-v storage battery. The binary output will be positive true logic and be transistor-true-logic compatible.

184. Conditioning and transmission. The output of the ADC will be connected to shift registers where it will be stored until ready for radio telemetry. The average values of velocity could be made at the transducer location and then conditioned and transmitted by radio telemetry to the central station. Alternatively, the average velocity values could be made after transmission, if determined to be more feasible and economical. The radio telemetry network shall have the capability of multiplexing all data channels, either parallel or serial. Block diagrams of these systems are shown in Figures 33 and 34.

185. Central station. The telemetry signals are received and converted to a digital format compatible with a 1/2-in. magnetic tape recorder. These magnetic tapes will, in turn, be compatible with a large General Electric computer at WES and will be shipped to Vicksburg, Mississippi, at regular intervals for analysis and data reduction. All of the parameters shall be recorded on the magnetic tape. There shall be a digital clock which shall keep time in day of the year, hour, minute, and second. This clock shall have a binary coded decimal output compatible with the magnetic tape recorder. The clock shall keep time for the entire system. From its output, timed sync signals shall be transmitted to the remote stations. These sync signals shall time the acquisition and transmission of data.

186. The velocity, temperature, water elevation, barometric pressure, and time data shall be printed out on paper for a "quick look" to determine if these channels are working. The water wave data will be recorded on a strip chart recorder. The strip chart recorder shall be turned on and off with the systems clock. A block diagram of the central station is shown in Figure 35.

Summary

187. The transducers have been given more time and consideration because it is felt that methods of detection and sensors are of prime importance. The technique and hardware for the conversion, handling, transmission, reception, and recording of these data can be designed

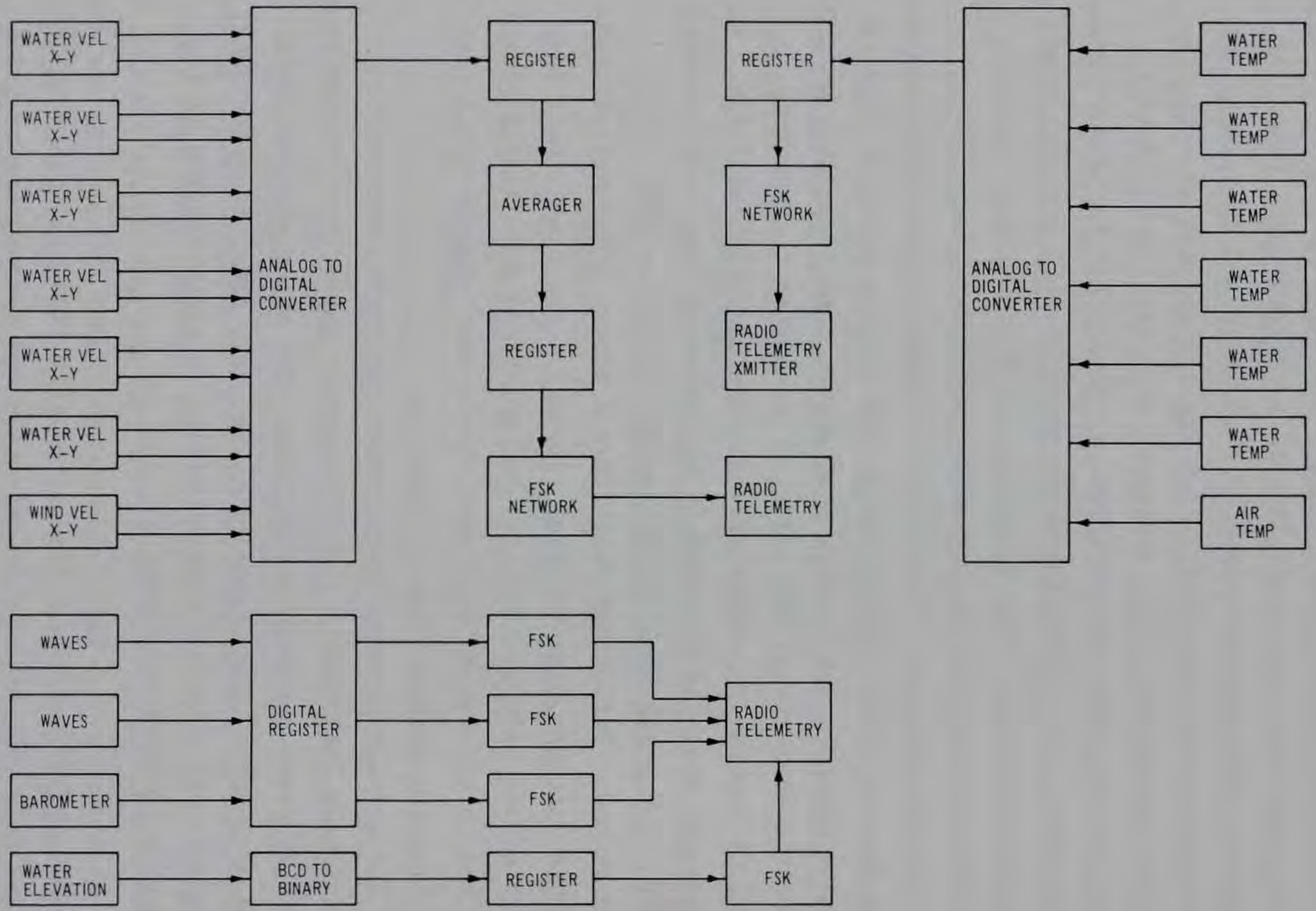

Figure 33. Block diagram, location B

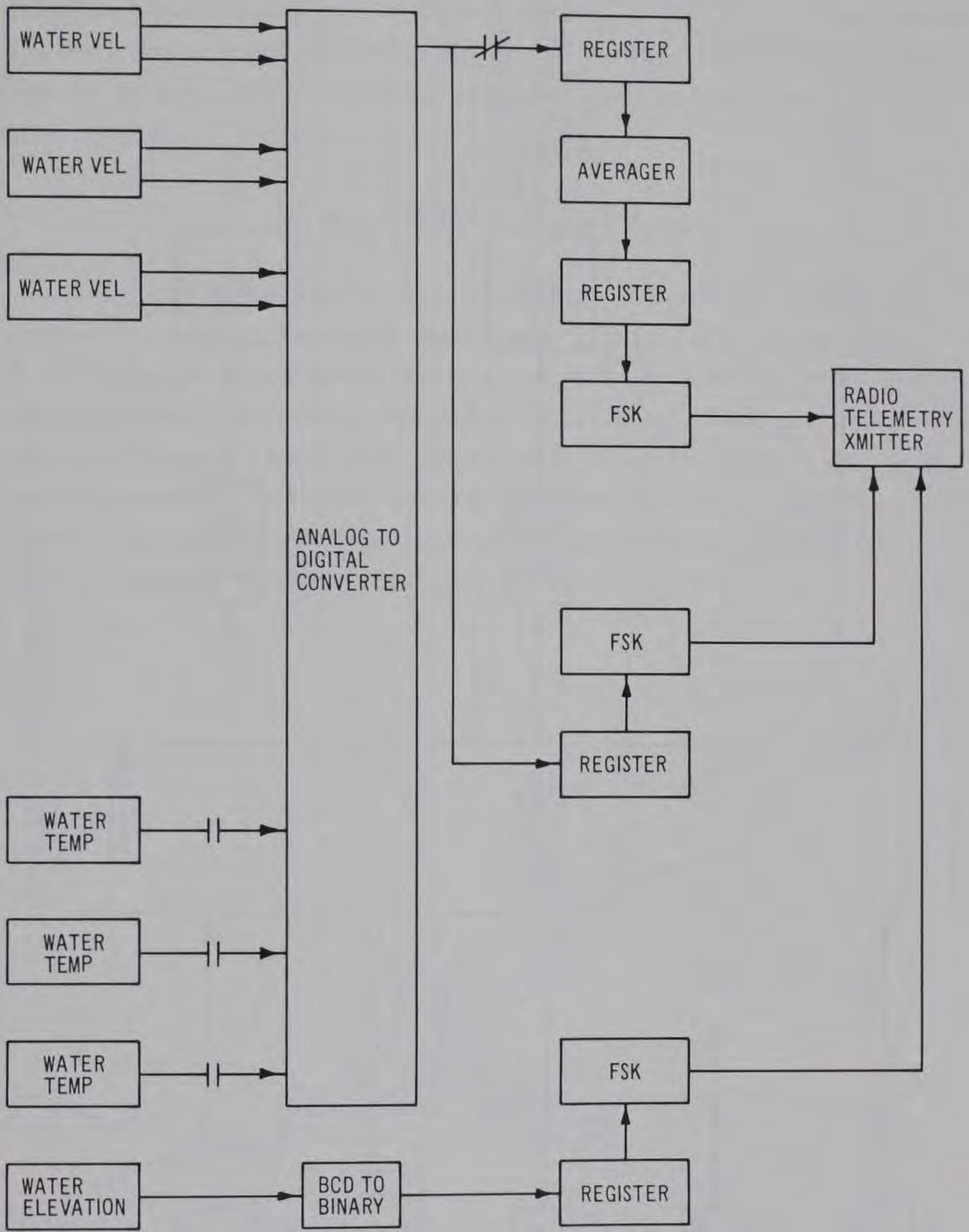

Figure 34. Block diagram locations A, C, and D

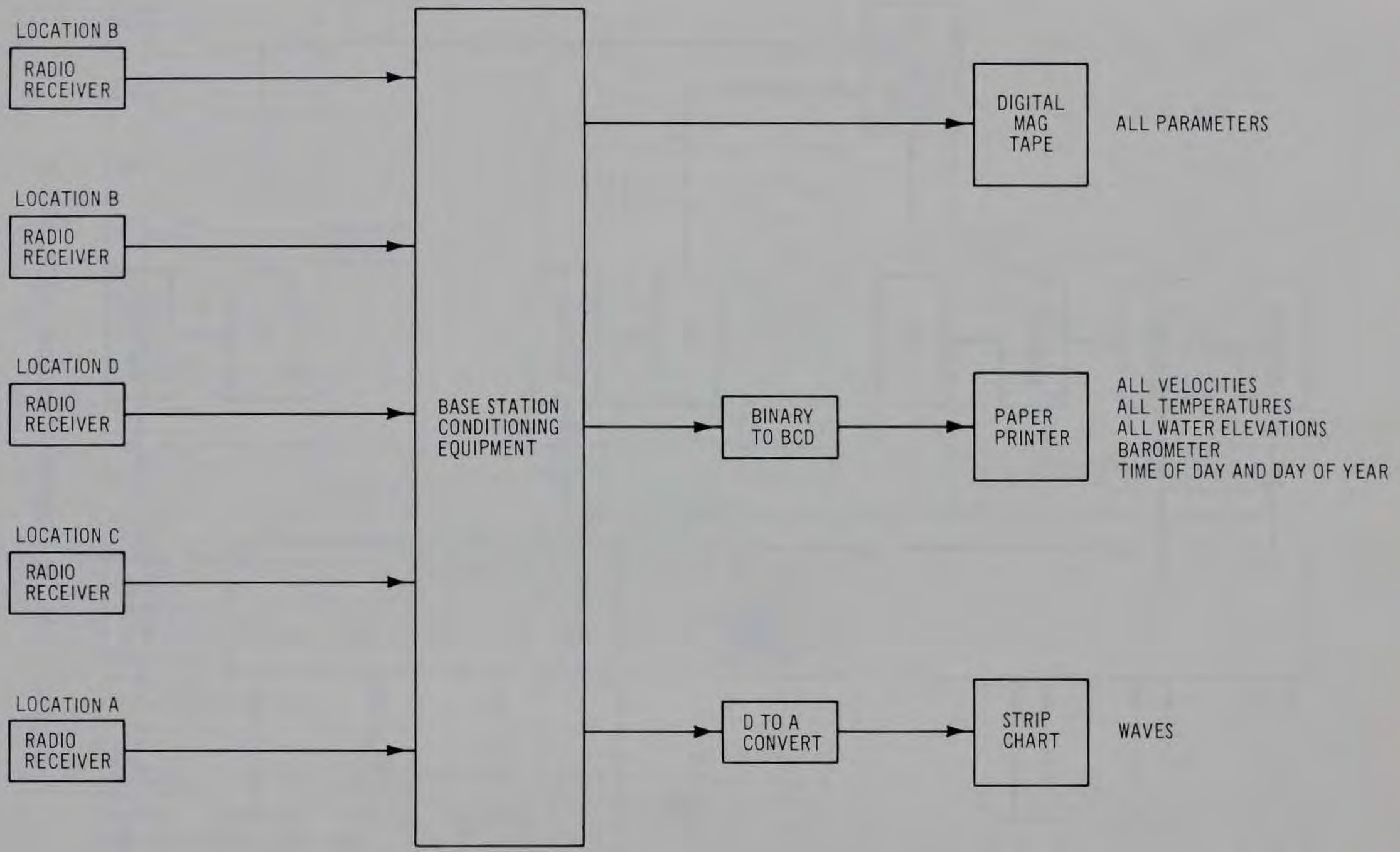

Figure 35. Block diagram base station

fully after a prototype study has been authorized. The block diagrams (Figures 33-35) depicting the initial concept of the acquisition system and the receiving and recording system at the base station are illustrative in purpose, are preliminary in nature, and do not constitute the final design of the systems.

Proposed Synoptic Survey

188. The parameters to be monitored in each of the two synoptic surveys are current velocity, water temperature, and dye concentration. Observations of these parameters will be taken at 2-hr intervals over a 12-hr period for 8 days. These data will be monitored at three depths for 32 stations. Location of these stations is indicated in Figure 36. The stations will be marked by buoys anchored to the lake bottom. The surveys will be made during a typical spring or fall condition and during a typical summer stratified condition.

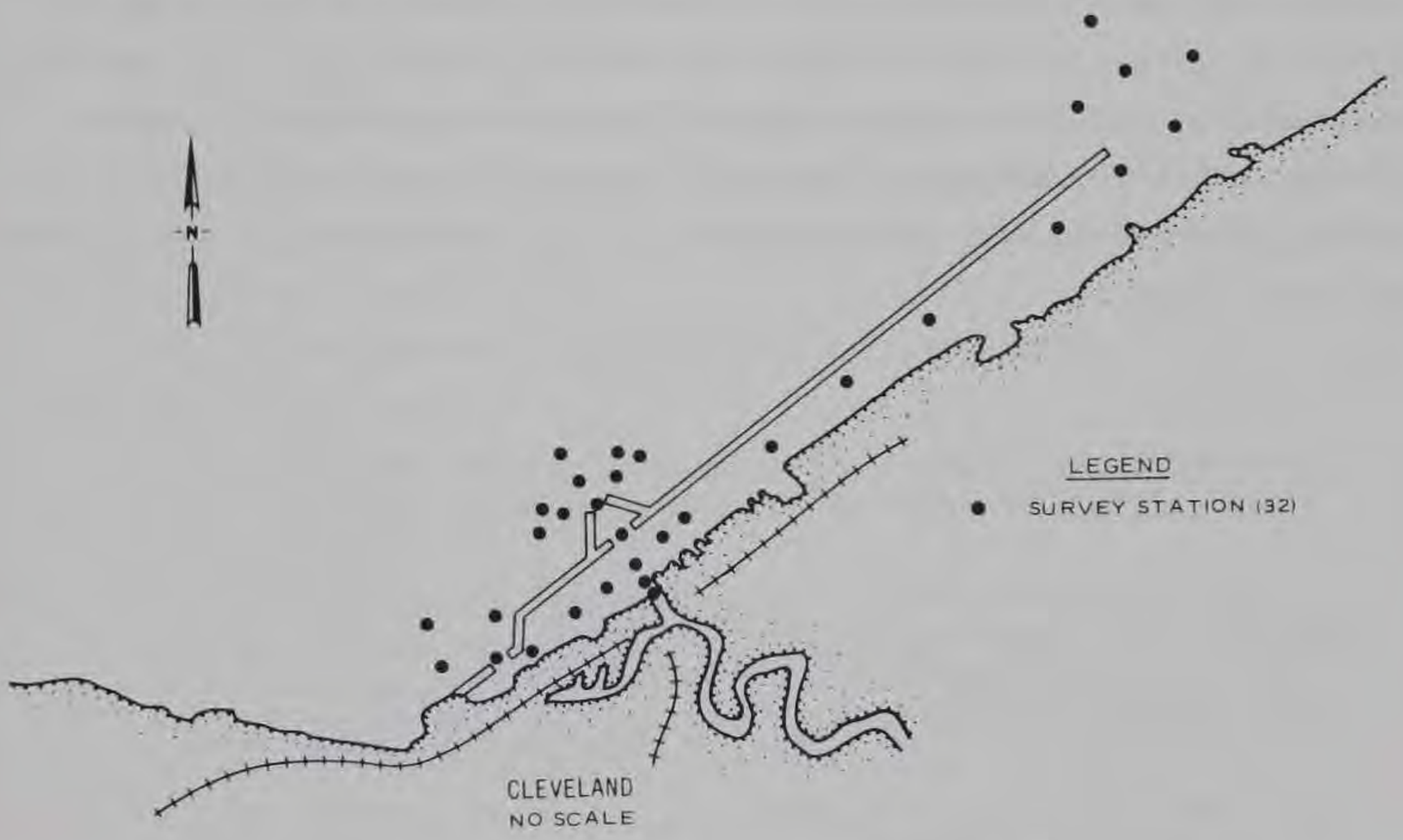

Figure 36. Location of synoptic survey stations

189. Dye concentrations during the survey will be obtained after point release of a known quantity of dye in the Cuyahoga River near its outflow into the harbor. The concentrations in water samples from each station will be determined using a fluorometer. Current velocity will be measured using low-threshold electromagnetic current meters (required for the low magnitudes of currents typical of the lake circulation).

190. The prototype data monitored during the survey will be transcribed from field observations to a format compatible with the WES computer prior to analysis of the data. Analyses of these data basically consist of determining the flushing rate and/or time required for conservative constitutents to move out of the present harbor, estimating local horizontal and vertical eddy diffusivity coefficients, and obtaining statistical information on the movement of the outflow plume of the Cuyahoga River.

191. As a part of the survey, surface temperature patterns and, if present, the location of the Cuyahoga River sediment plume, could be obtained by overflights conducted by the NASA Lewis Research Center. Initial inquiries by WES have been conducted with NASA to define WES's requirements and NASA's support capabilities for this survey. Initial efforts indicated an existing potential for cooperative efforts, but further study definition and coordination will be required in advance of any field study.

PART VIII: CONCLUSIONS AND RECOMMENDATIONS

192. Current state-of-the-art numerical models and numerical models that may become available in the time frame necessary for application to the Lake Erie Jetport study can provide much useful hydrodynamic information. The presently available seiche models and two-dimensional wind-driven circulation models have been operational for several years and within their recognized limitations appear to yield valid information. A three-dimensional, constant-density, steady-flow model for Lake Erie was reported in the literature in 1972 by Gedney and Lick.[22] Dr. Wilbert Lick and associates at Case Western Reserve University are working on three-dimensional storm surge models[23] and three-dimensional variable-density models.[26,32] The three-dimensional storm surge models should be available in an operational form in a matter of months. The time schedule on the three-dimensional, variable-density model is less well defined due to the complexity of the model; however, it can hopefully be made available within the time frame when application to the jetport study will be possible.

193. In general, the numerical models have not been verified to the extent desirable. If they are applied to the jetport study, additional model verification will be necessary for which sufficient prototype data are not available.

194. The following recommendations are the result of the numerical model feasibility study:

a. Obtain for the jetport study operational mathematical models which have been recommended earlier in this report.

b. Insure the expedient development of needed three-dimensional models, which are presently in a development state, by contracting with Case Western Reserve University to provide these models with preliminary application to the jetport study.

c. Provide the necessary prototype data for proper verification of numerical models (and/or future physical models) by initiating the prototype data acquisition program outlined earlier in this report.

d. Estimate the effects of a proposed offshore jetport on

storm surge and lake circulation in Lake Erie, particularly in the vicinity of Cleveland, Ohio, by conducting the following recommended numerical studies:

(1) Investigate the near-field and far-field effects of a jetport island on the steady-state wind-driven circulation in Lake Erie for well mixed (nonstratified) lake conditions. Circulation patterns with and without a jetport should be defined for average and extreme winter wind speeds and several wind directions.

(2) Investigate the effects of a jetport island on the storm surge along the shoreline from Fairport to Lorain, Ohio. Time-dependent wind fields for at least two severe storms on Lake Erie should be used to estimate surge elevation and velocity fields for well mixed lake conditions.

(3) Investigate the effects of a jetport island on the stratified lake circulation (epilimnion and hypolimnion) around the jetport and in the Cleveland Harbor with typical Cuyahoga River outflows and steady-state, summer wind fields.

REFERENCES

1. Durham, D. L. and Outlaw, D. G., "Lake Erie International Jetport Model Feasibility Investigation; Scope of Study and Review of Available Data," Technical Report H-74-6, Report 1, Jul 1974, U. S. Army Engineer Waterways Experiment Station, CE, Vicksburg, Miss.

2. Welander, P., "Wind Action on a Shallow Sea: Some Generalizations of Ekman's Theory," Tellus, Vol 9, No. 1, 1975.

3. Stoker, J. J., Water Waves, the Mathematical Theory with Applications, Interscience, New York, 1957.

4. Desai, C. S. and Abel, J. F., Introduction to Finite-Element Method; A Numerical Method for Engineering Analysis, Van Nostrand, New York, 1972.

5. Weinstock, R., Calculus of Variations, with Applications to Physics and Engineering, McGraw-Hill, New York, 1952.

6. Taylor, C., Patil, B. S., and Zienkiewicz, O. C., "Harbour Oscillation: A Numerical Treatment for Undamped Natural Modes," Proceedings, Institution of Civil Engineering, Vol 43, Jun 1969, pp 141-155.

7. Patil, B. S., Harbor Resonance, Ph. D. Dissertation, University of Wales, Cardiff, England, 1970.

8. Felippa, C. A., Refined Finite Element Analysis of Linear and Nonlinear Two-Dimensional Structures, Ph. D. Dissertation, University of California, Berkeley, Calif., 1966.

9. Platzman, G. W. and Rao, D. B., "Spectra of Lake Erie Water Levels," Journal, Geophysical Research, Vol 69, No. 12, Jun 1964, pp 2525-2535.

10. _____, "The Free Oscillations of Lake Erie," Technical Report No. 8, Sep 1963, Department of Geophysical Sciences, University of Chicago, Chicago, Ill.

11. Lamb, H., Hydrodynamics, Dover Publications, New York, 1932.

12. Roache, P. J., Computational Fluid Dynamics, Hermosa Publishers, Albuquerque, 1972.

13. Simons, T. J., "Development of Numerical Models of Lake Ontario," Proceedings, Fourteenth Conference on Great Lakes Research, International Association of Great Lakes Research, 1971, pp 654-669.

14. Platzman, G. W., "The Dynamic Predictional of Wind Tides on Lake Erie," Meteorological Monographs, Vol 4, No. 26, 1963, pp 1-44.

15. Ekman, W. V., "On the Influence of Earth's Rotation on Ocean Currents," Arkiv f. Matem. Astr. o. Fysik, Vol 2, No. 11, 1905.

16. Leendertse, J. J., "Aspects of a Computational Model for Long-Period Water-Wave Propagation," RM-5294-PR, May 1967, The Rand Corporation, Santa Monica, Calif.

17. Masch, F. D., Brandes, R. W., and Reagan, J. D., "Simulation of Hydrodynamics in a Tidal Inlet," Contract Report No. DACW72-C-0028, 1973, U. S. Army Coastal Engineering Research Center, Fort Belvoir, Va.

18. Reid, R. O. and Bodine, B. R., "Numerical Model for Storm Surges in Galveston Bay," Journal, Waterways and Harbor Division, American Society of Civil Engineers, Vol 94, WW1, Feb 1968, pp 33-57.

19. Paskausky, D. F., "Winter Circulation in Lake Ontario," Proceedings, Fourteenth Conference on Great Lakes Research, International Association of Great Lakes Research, 1971, pp 593-606.

20. Paskausky, D. F. and Murphy, D. L., "Two Dimensional Numerical Prediction of Wind Surge in Lake Erie," Proceedings, Sixteenth Conference on Great Lakes Research, International Association of Great Lakes Research, 1973, pp 808-817.

21. Gedney, R. T., "Numerical Calculations of the Wind-Driven Currents in Lake Erie," TM-X-52985, 1971, National Aeronautics and Space Administration, Washington, D. C.

22. Gedney, R. T. and Lick, W., "Wind-Driven Currents in Lake Erie," Journal, Geophysical Research, Vol 77, No. 15, May 1972, pp 2714-2723.

23. Haq, A., Lick, W., and Sheng, Y. P., "The Time-Dependent Flow in Large Lakes with Applications to Lake Erie," Jul 1974, Department of Earth Sciences and Division of Fluid, Thermal and Aerospace Sciences, Case Western Reserve University, Cleveland, Ohio.

24. Wilson, B. W., "Note on Surface Wind Stress over Water at Low and High Wind Speeds," Journal, Geophysical Research, Vol 65, No. 10, 1960, pp 3377-3382.

25. Leendertse, J. J., Alexander, R. C., and Liu, S. -K., "A Three Dimensional Model for Estuaries and Coastal Seas; Principles of Computation," R1417-OWRR, Vol 1, Dec 1973, The Rand Corporation, Santa Monica, Calif.

26. Paul, J. F. and Lick, W. J., "A Numerical Model for Thermal Plumes and River Discharges," Proceedings, Seventeenth Conference on Great Lakes Research, International Association of Great Lakes Research, 1974, pp 445-455.

27. _____, "Report to Argonne National Laboratory on the Application of the Paul-Lick Model to Point Beach Unit 1 Outfall. Appendix A of Temperature and Velocity Measurements and Predictive Model Comparisons in the Near-Field Region of Surface Thermal Discharges," 1974, Argonne National Laboratory, Argonne, Ill.

28. Bennett, J. R., "Thermally Driven Lake Currents During the Spring and Fall Transition Periods," Proceedings, Fourteenth Conference on Great Lakes Research, International Association of Great Lakes Research, 1971, pp 535-544.

29. Phillips, N. A., "A Coordinate System Having Some Special Advantages for Numerical Forecasting," Journal, Meteorology, Vol 14, 1957.

30. Smagorinsky, J., Manabe, S., and Holloway, J. L., "Numerical Results from a Nine-Level General Circulation Model of the Atmosphere," Monthly Weather Review, Vol 93, 1965, pp 727-768.

31. Arakawa, A., "Computational Design for Long-Term Numerical Integration of the Equations of Fluid Motion: Two-Dimensional Flow," Journal, Computational Physics, Vol 1, Part I, 1966, pp 119-143.

32. Paul, J. F. and Lick, W. J., "A Numerical Model for a Three-Dimensional Variable-Density Jet," 1973, Department of Earth Sciences and Division of Fluid, Thermal and Aerospace Sciences, Case Western Reserve University, Cleveland, Ohio.

33. Varga, R. S., Matrix Iterative Analysis, Prentice-Hall, Englewood Cliffs, 1962.

34. Wachspress, E. L., Iterative Solutions of Elliptic Systems, and Applications to the Neutron Diffusion Equations of Reactor Physics, Prentice-Hall, Englewood Cliffs, 1966.

35. Sengupta, S. and Lick, W., "A Numerical Model for Wind Driven Circulation and Temperature Fields in Lakes and Ponds," 1974, Department of Earth Sciences and Division of Fluid, Thermal and Aerospace Sciences, Case Western Reserve University, Cleveland, Ohio.

Table 1

Relative Amplitude Comparison

Location	Observed Relative Amplitude*	Computed Relative Amplitude
Buffalo	-0.70	-0.72
Port Colborne	-0.66	-0.69
Dunkirk	-0.66	-0.66
Port Dover	-0.60	-0.63
Erie	-0.50	-0.48
Port Stanley	-0.19	-0.09
Fairport	0.13	0.09
Erieau	0.27	0.21
Cleveland	0.25	0.27
Huron	0.49	0.54
Port Clinton	0.52	0.86
Toledo	1.00	1.00
Monroe	0.95	0.99

* Based on results of spectral analysis of observed lake level variations (Reference 9).

Table 2

Periods for First Five Modes of Oscillation for Different Jetport Configurations

	Period, hr				
	Mode of Oscillation				
Configuration*	1	2	3	4	5
No Jetport--Observed	14.38	9.14	5.93	4.15	--
No Jetport--Calculated	14.43	9.22	6.01	4.31	3.87
A	14.50	9.28	6.06	4.32	3.87
B	14.51	9.28	6.05	4.33	3.87
C	14.52	9.28	6.07	4.33	3.87
D	14.52	9.27	6.06	4.33	3.87

* Letters refer to configurations shown in Figure 5.

APPENDIX A: NOTATION

A	Surface area of Lake Erie
$[A]$	Square matrix whose order is equal to the number N of the interior grid points
A^e	A divided into N subregions (elements)
A_H	Horizontal eddy diffusion coefficient
A_V	Vertical eddy diffusion coefficient
b_o	Horizontal reference width of river discharging the plume
B	Bottom stress coefficient
C	Chezy coefficient
$[C]$	Vector column matrix containing the nonhomogeneous portion of the difference equations
C^*	Resistance coefficient
C_d	Drag coefficient
C_p	Specific heat at constant pressure
D	Frictional depth; water depth in Paskausky's model
D_x, D_y, D_z	Eddy diffusion coefficients of salinity in x, y, and z direction
E_H	Horizontal Ekman number
E_V	Vertical Ekman number
f	Coriolis parameter
$f'(\bar{T})$	Equation of state
f_o	Coriolis parameter evaluated to mean latitude of Lake Erie
g	Acceleration due to gravity
G_w	Element slope matrix
h	H/H_n, dimensionless depth
$h(x,y)$	Water depth

$\bar{h}^e$	Mean depth for each element
h_o	Vertical reference depth of river discharging the flume
H	Characteristic length in the vertical direction
[H]	M × M square matrix of coefficients
H_m	Mean depth of Lake Erie
i	Imaginary number
$\vec{i}$	Unit vector in x direction
i,j,k	Indices of nodes of each element
$\vec{j}$	Unit vector in y direction
$\bar{k}$	Thermal conductivity
K	Coefficient of eddy viscosity or diffusivity
[K]	Element of stiffness matrix
K_h	Horizontal diffusion coefficient
K_v	Vertical diffusion coefficient
L	Characteristic horizontal scale; characteristic length in the horizontal direction
m	Nodal point
M	Total number of node points
[M]	Lumped mass matrix
M_T	Horizontal mass flux
M_x	x-component of horizontal mass flux
M_y	y-component of horizontal mass flux
n	Unit normal to boundary
$\bar{n}$	Manning friction factor
[N]	Interpolation or shape function

N_i Value of interpolation function at element node with index i and is equal to $[(x_k y_j - x_j y_k) + (y_k - y_j)x + (x_j - x_k)y]/2\Delta$ where Δ is the area of the element A^e.

N_j, N_k Similar expressions obtained by the cyclical permutation of i, j, and k

p Pressure

P Volumetric flow in the x direction

P_k Layer-averaged pressure of the k^{th} layer

Q Volumetric flow in y direction

Q* Heat source and/or sink

Re Real number

R_o Rossby number

S Salinity

t Time

t_R Reference time value

T Period of oscillation

$\bar{T}$ Absolute temperature

T_s Period of time during which intensity of wind stress increases linearly across the stress band

u Velocity in x direction

$\bar{u}$ Mean wind speed

u' Depth-dependent perturbations in horizontal velocity in x direction

U x-component of depth-averaged, horizontal velocity

U_k Layer-averaged u-component of horizontal velocity

U_R Characteristic velocity in Lake Erie

v Velocity in y direction

v'	Depth-dependent perturbations in horizontal velocity in y direction
V	y-component of depth-averaged, horizontal velocity
$\vec{V}_n$	Velocity normal to shoreline
V_s	Constant translation speed of wind field
w	Velocity in z direction
W_R	Reference vertical velocity
W_a	Wind velocity at a certain height above the water surface
x,y,z	Cartesian coordinates
$[Z]$	Modal matrix, where columns are eigenvectors $\{Z_i\}$ of $[H]$
$\alpha_1,\alpha_2,\alpha_3$	Coefficients of Taylor's expansion
Γ	$u + iv$, a complex variable representing horizontal velocity
ζ	Surface displacement as a function of x and y
$\hat{\zeta}$	Vertical component of vorticity
ζ_R	Reference surface displacement
$\eta(x,y,t)$	Surface displacement as a function of time and space
λ	An eigenvalue expressed as ω^2/g; $\pi H/D$ a constant which is proportional to the ratio of water depth to frictional depth
λ'	Function of both temperature and salinity
$[\Lambda]$	Diagonal matrix of eigenvalues
$\bar{\mu}$	Absolute viscosity
ν	Coefficient of interfacial friction
ξ	Wave amplitude
ρ	Density
$\bar{\rho}$	Constant reference density
ρ'	Departure from $\bar{\rho}$ depending on salinity

ρ_a	Density of the air; atmospheric density
$\hat{\rho}_k$	Depth-averaged density for the k^{th} layer
σ	Transformed vertical coordinate
$\bar{\sigma}$	Bottom friction coefficient
τ_{Bx}, τ_{By}	x- and y- components, respectively, of bottom friction
τ_{wR}	Reference wind shear stress
τ_{wx}, τ_{wy}	x- and y- components, respectively, of wind stress at the water surface
τ_x, τ_y	x and y components of shear stress
τ_{xz}, τ_{yz}	x- and z- components of shear stress interfacial
χ	Functional integral
ψ	Volume transport stream function
$[\psi]$	Vector column matrix for the stream function
$\psi(x,y)$	Mass flux stream function
ϕ	Angle between wind direction and y-axis
Φ	Heat dissipation
ω	$2\pi/T$
$< >$	Points at which variables must be interpreted since they are not in the staggered grid